

**BIOMARKERS OF CELL STRESS AND CELL DEATH  
DETECTED BY PROTON HIGH RESOLUTION MAGIC  
ANGLE SPINNING (<sup>1</sup>H HR-MAS) NUCLEAR MAGNETIC  
RESONANCE (NMR) SPECTROSCOPY IN A RAT GLIOMA  
CELL LINE**

by

**LADAN MIRBAHAI**

A thesis submitted to

The University of Birmingham

for the degree of DOCTOR OF PHILOSOPHY

School of Sport and Exercise Sciences

The University of Birmingham

October 2009

UNIVERSITY OF  
BIRMINGHAM

**University of Birmingham Research Archive**

**e-theses repository**

This unpublished thesis/dissertation is copyright of the author and/or third parties. The intellectual property rights of the author or third parties in respect of this work are as defined by The Copyright Designs and Patents Act 1988 or as modified by any successor legislation.

Any use made of information contained in this thesis/dissertation must be in accordance with that legislation and must be properly acknowledged. Further distribution or reproduction in any format is prohibited without the permission of the copyright holder.

## Abstract

Early detection of biomarkers of tumour treatment response improves clinical management, *in vivo*. Magnetic resonance spectroscopy (MRS) has demonstrated potential for identifying early biomarkers of effective treatment. However, more detailed *in vitro* studies are required to improve our understanding and facilitate its use.

The aim of this study is to determine  $^1\text{H}$  high-resolution magic angle spinning (HR-MAS) nuclear magnetic resonance (NMR) biomarkers of cytostasis and cell death in a rat glioma BT4C cell line.

Cytostasis and cell death were induced in BT4C cells using cisplatin and substrate free medium, respectively. Cell viability was examined by various techniques. The lipid and metabolite alterations in whole cells were investigated by  $^1\text{H}$  HR-MAS NMR.

Significant alterations in lipids and metabolites were detected in response to cytostasis or necrosis. NMR lipid accumulation was associated with an increase in cytoplasmic lipid droplets seen prior to morphological and molecular markers of cell death. Significant differences were detected in individual choline containing metabolites (CCMs), emphasising the importance of identifying CCMs separately. Alterations were also detected in lactate, alanine, glycine, glutamate, and succinate levels, suggesting changes in the energy metabolism pathways which may provide novel biomarkers *in vivo*.

$^1\text{H}$  HR-MAS NMR reveals alterations in lipids and metabolites during cytostasis and cell death which may provide early markers of treatment efficacy.

## Declaration

I confirm that this work is my own and that I have been involved in the design and conduct of this study, analysis of data and preparation of this thesis. The following aspects of this study were undertaken as part of collaboration with:

1. Martin Wilson assisted with performing  $^1\text{H}$  high-resolution magic angle spinning on the prepared samples. Martin and Greg Reynolds developed the TARQUIN algorithm. The  $^1\text{H}$  HR-MAS data were assigned and quantitated by Martin using the TARQUIN algorithm and I further analysed and interpreted the findings. Also principal component analysis of the metabolite data (described in chapters 3 and 5) was carried out by Martin using the MATLAB statistics Toolbox implementation of PCA.

The HR-MAS experiments were carried out in the Henry Wellcome Building for Biomolecular NMR Spectroscopy at the University of Birmingham.

2. Matthew Wakeman at the Histopathology Department of the Birmingham Children's Hospital contributed to transmission electron microscopy sample preparation and image capturing (described in chapters 4 and 5).
3. Roger Malcomson additionally counted and confirmed the number of viable, apoptotic and necrotic cells detected by H&E (described in chapters 3 and 5) and DAPI (described in chapters 4 and 5) staining.

## **Acknowledgements**

I would like to thank my supervisor Dr Andrew Peet for his continued support and guidance throughout the period of my study.

I also wish to thank Professor Risto Kauppinen for giving me the chance to study such a vast research area and for his support and input during my PhD studies.

I am grateful for the assistance and guidance that I have been given by Dr Martin Wilson, Dr Carmel McConville, and the staff of the Histopathology Department of the Birmingham Children's Hospital, especially Dr Roger Malcomson and Mr Matthew Wakeman.

I would like to thank the staff and postgraduate members of the School of Sport and Exercise Sciences for all their support during my time at the University of Birmingham. In particular, I wish to thank Dr Jos Bosch, Dr Chris Shaw, Professor Anton Wagenmakers, and Mrs Hazel Robinson. I would also like to thank Rob Wheeler for saving my laptop and PhD data from a potentially hazardous computer virus.

Many thanks to Leila and Stephen my office room-mates for all the long hours spent together in the office, thank you both for all your support and those many happy memories.

Importantly, I am forever grateful to my mum and dad, Sandra and Farrokh. Thank you ever so much for supporting me in so many different ways. Thank you for all your guidance, encouragement and love that you have given me. Lastly, thanks for believing in me.

Furthermore, I would like to extend a special thank you to my Aunty Sue and Uncle Tony for their support during the early stages of my studies when everything was a big maze for me.

A special thanks also goes to my sister, Leda. Your energy, passion and dedication have always inspired me. Thank you for being there and picking me up when I needed it. Also thanks for saving me from the e-mails! You are my little star and I am very proud of you.

# Table of Contents

<b>Chapter One: Introduction .....</b>	<b>1</b>
1.1. Introduction .....	2
1.2. Aim of This Thesis .....	5
1.3. Basic Principles of Magnetic Resonance Spectroscopy .....	5
1.4. Magnetic Resonance Spectroscopy of Tumours.....	10
1.5. Role of MRS in Monitoring Treatment Response .....	11
1.6. Treatment induced MRS alterations .....	12
1.6.1. MRS Lipid Alterations .....	13
1.6.2. Low Molecular Weight Metabolite Alterations .....	16
1.6.2.1. Choline Containing Metabolites .....	16
1.6.2.2. Glycolytic Metabolites .....	18
1.6.2.3. Other Low Molecular Weight Metabolites .....	19
1.7. MRS alterations associated to Cell Death .....	20
1.8. Features of Cell Death .....	22
1.8.1. Necrosis .....	24
1.8.2. Apoptosis .....	26
1.8.3. Autophagy .....	28
1.8.4. Cell Cycle and Cell Cycle Control .....	32
1.9. Cell Death Assessment .....	35
1.9.1. Light and Electron Microscopy .....	35
1.9.2. Light Microscopy Analysis of Haematoxylin and Eosin stained Cells .....	35
1.9.3. 4', 6-diamino-2-phenylindole Staining .....	36
1.9.4. Trypan Blue Exclusion .....	36
1.9.5. Detection of Nucleosomal DNA Fragments on Agarose Gel Electrophoresis .....	37
1.9.6. Flow cytometry Analysis of AnnexinV-FITC Labelled and Propidium Iodide Stained Cells .....	38

1.10. The Use of Cisplatin to Induce Cell Cycle Arrest and Cell Death .....	39
1.11. Objective of the Thesis .....	42
<b>Chapter Two: Materials and Methods .....</b>	<b>43</b>
2.1. Rat Glioma Cells .....	44
2.1.1. Cell Culture .....	44
2.1.2. Detachment of Confluent Cells .....	44
2.1.3. Cell Counting .....	45
2.1.4. Cell Cryopreservation .....	45
2.1.5. Cell Culture from Frozen Samples .....	46
2.1.6. Cytospin Preparation and Cytocentrifuge .....	47
2.2. Cell Stress Stimuli .....	49
2.2.1. Cisplatin .....	49
2.2.1.1. Preparing Cisplatin for Cell Treatment .....	49
2.2.1.2. Adding Cisplatin to the Cells .....	49
2.2.2. Culture in Phosphate Buffered Saline .....	50
2.3. Harvesting Cells for Morphological and Molecular Assays .....	50
2.4. <sup>1</sup> H HR-MAS NMR Spectroscopy.....	51
2.4.1. Harvesting Cells for <sup>1</sup> H HR-MAS NMR Spectroscopy .....	51
2.4.2. <sup>1</sup> H HR-MAS NMR Spectroscopy Sample Preparation .....	51
2.4.3. Performing <sup>1</sup> H HR-MAS NMR Spectroscopy .....	52
2.4.4. Assigning and Quantitating <sup>1</sup> H HR-MAS NMR Signals .....	53
2.5. Assessing Cell Viability and Cell Death .....	58
2.5.1. Trypan Blue Staining .....	58
2.5.2. Haematoxylin and Eosin Staining .....	59
2.5.2.1. Preparing Cells for H&E Staining .....	59
2.5.2.2. H&E staining of the prepared slides .....	59
2.5.3. Transmission Electron Microscopy .....	60

2.5.3.1. Sample Preparation for Transmission Electron Microscopy.....	60
2.5.3.2. Cutting the Samples and observing with Transmission Electron Microscopy .....	61
2.5.4. Flow Cytometry Analysis of Annexin V-FITC labelled and Propidium Iodide stained Cells .....	61
2.5.5. Detecting DNA Fragmentation .....	62
2.5.5.1. Preparing Buffers .....	62
2.5.5.2. Preparing the Sample and Running the Agarose Gel .....	63
2.6. Assessing Cell Cycle Phase Distribution .....	64
2.6.1. Preparing Buffers and Solutions .....	64
2.6.2. Preparing Untreated Samples for Flow Cytometry Analysis .....	65
2.6.3. Preparing Cisplatin Exposed Cells for Flow Cytometry Analysis .....	66
2.6.4. Flow cytometry analysis .....	66
2.7. Nile Red and DAPI Co-Staining .....	68
2.7.1. Preparing Nile Red and DAPI Stock Solutions .....	68
2.7.2. Nile Red and DAPI Staining Procedures .....	69
2.7.3. Fluorescence Microscopy and Image Capture .....	69
2.7.4. Image Processing .....	70
2.8. Statistical Tests .....	74
2.9. Principal Component Analysis .....	74
<b>Chapter Three: <sup>1</sup>H HR-MAS NMR Metabolite Alterations of Cisplatin Induced Growth Arrest in Rat BT4C Glioma Cells .....</b>	<b>76</b>
3.1. Introduction .....	77
3.2. Methods.....	79
3.3. Results .....	81
3.3.1. Preliminary work.....	81
3.3.2. Morphological Analysis of Cell Death: Trypan Blue and H&E Staining.....	82
3.3.3. Molecular Analysis of Cell Death: Flow cytometry Analysis of Annexin V- FITC Labelled and PI Stained Cells and Detection of DNA Laddering .....	85

3.3.4. Cell Cycle Phase Distribution .....	88
3.3.5. <sup>1</sup> H HR-MAS NMR Metabolite Alterations .....	89
3.4. Discussion .....	96
3.4.1. Choline Containing Metabolite Alterations .....	97
3.4.2. Energy Related Metabolite Alterations .....	100
3.4.3. Taurine Alterations .....	104
3.5. Conclusion .....	106
<b>Chapter Four: <sup>1</sup>H HR-MAS NMR Lipid Alterations of Cisplatin Induced Growth Arrest in Rat BT4C Glioma Cells and the Source of the NMR Visible Lipids .....</b>	<b>108</b>
4.1. Introduction .....	109
4.2. Methods.....	111
4.3. Results .....	112
4.3.1. Nile red and DAPI staining .....	112
4.3.2. Transmission Electron Microscopy Images .....	120
4.3.3. <sup>1</sup> H HR-MAS NMR Visible Lipid Alterations .....	122
4.4. Discussion .....	126
4.5. Conclusions .....	133
<b>Chapter Five: <sup>1</sup>H HR-MAS NMR Metabolite and Lipid Alterations of Starvation Induced Necrosis in Rat BT4C Cells .....</b>	<b>135</b>
5.1. Introduction .....	136
5.2. Methods.....	138
5.3. Results .....	140
5.3.1. Trypan Blue and Haematoxylin and Eosin Staining .....	140
5.3.2. Nile red and DAPI staining .....	143
5.3.3. Transmission Electron Microscopy Images .....	149
5.3.4. <sup>1</sup> H HR-MAS NMR alterations .....	151
5.3.4.1. <sup>1</sup> H HR-MAS NMR Visible Lipid Alterations .....	154

5.3.4.2. $^1\text{H}$ HR-MAS NMR Metabolite Alterations .....	156
5.3.5. Principal Component Analysis of Cisplatin Exposed and Substrate Deprived Metabolite Data of BT4C cells .....	162
5.4. Discussion .....	164
5.4.1. Cell Growth Arrest Leading to Apoptosis vs. Necrosis .....	170
5.5. Conclusion .....	172
<b>Chapter Six: Conclusions .....</b>	<b>173</b>
6.1. Summary and Conclusions .....	174
6.2. Future Work .....	181
<b>References .....</b>	<b>184</b>
<b>List of Conference Abstracts.....</b>	<b>211</b>

## List of Figures

	<b>Page</b>
Figure 1.1.	7
<p>Schematic image of the magnetic resonance spectroscopy (MRS) effect. (A and B). A specific radiofrequency causes the nuclei to move to the other magnetic state. In absence of radiofrequency, the nuclei return to equilibrium. The resonant waves are registered and presented as peaks. (C). Radiofrequencies are applied during MRS and the waves resonate according to the nuclei and the surrounding environment.</p>	
Figure 1.2.	26
<p>Schematic image of the events occurring in cells during apoptosis and necrosis cell death. During apoptosis chromatin condenses and cell shrinks and membrane blebbing occurs. During the final stages, cell breaks up to cluster of apoptotic bodies. During necrosis, cell swells and blebbing and vacuolisation occur. Cell membrane becomes permeable and at final stages cell shrinkage and lysis occur.</p>	
Figure 1.3.	31
<p>Autophagy pathway and its many functions. Autophagy is stimulated by metabolic stress or cancer therapies. Autophagosome sequesters cytoplasmic material and fuses with lysosome, forming an autolysosome. Degradation of cytoplasmic material generates free fatty acids and amino acids, which can result in energy production, protein synthesis, or removal of harmful proteins. Autophagy can cause cell death by self- cannibalism and/or apoptosis.</p>	
Figure 1.4.	34
<p>Cell cycle process and cell check points. Cell cycle is controlled by G1, S-phase, and mitotic cyclin-dependent kinase complexes (Green). Ubiquitin ligase complexes SCF and APC polyubiquitinate S phase inhibitors, securing, and mitotic cyclins for degradation by proteasomes. Proteolysis of these substrates activates the relevant cyclin-CDK complexes, leading to cell cycle progression.</p>	
Figure 1.5.	37
<p>The biochemistry of DNA fragmentation during apoptosis and the appearance of 180-200 bp DNA</p>	

fragments as ladder pattern on gel electrophoresis.

Figure 1.6.	Schematic representation of loss of cell membrane asymmetry during early stages of apoptosis. PS molecules are located in the inner layer of the cell membrane (orange circles). During apoptosis they are translocated to the outer membrane. FITC labelled annexin V has high affinity to the exposed PS.	38
Figure 1.7.	Cisplatin interaction with DNA. (a) inter-strand cross-link. (b) 1,2-intra-strand cross-link. (c) 1,3-intra-strand cross-link. (d) protein-DNA cross-link	41
Figure 2.1.	A schematic image of a Neubauer haemocytometer slide and the grids used to count the cells.	46
Figure 2.2.	A Shandon cytopsin.	48
Figure 2.3.	Image of assembled filter card, cytofunnel, and cytoclip.	48
Figure 2.4.	A Varian 600 MHz spectrometer at the Henry Wellcome Building, The University of Birmingham.	53
Figure 2.5.	A typical spectrum of BT4C cells. The TARQUIN algorithm was used to identify and quantitate metabolite and lipids in the spectrum. The residual spectrum is shown at the top section of the image.	56
Figure 2.6.	Trypan blue staining of BT4C cells. Dead cells appear darker and viable cells are identified as brighter, unstained cells. Only a few of the dead cells are labelled in this image.	58
Figure 2.7.	Haematoxylin and eosin staining of BT4C cells. Morphological characteristics of the cell nuclei help in identifying necrotic and apoptotic cells. Apoptotic cells contain fragmented nuclei and necrotic cells have dispersed nucleus.	60
Figure 2.8.	Cell cycle analysis platform of multicycle software version 3. A control sample is used to define the G1 and G2 ranges. The defined regions are used to fit the treated samples and the optimal fits are presented as fraction of cells in each phase of the cell cycle.	67

Figure 2.9.	ImageJ 1.38X platform for threshold detection. The threshold of the lipid droplet and the whole cell were selected based on where they were identified. The selected areas were then measured and the percentage of the cell area covered by lipid droplets was calculated.	72
Figure 2.10.	ImageJ 1.38X platform for image measurements. The diameter of a lipid droplet is measured by drawing a line across the droplet and measuring the length of the line.	73
Figure 3.1	Flow chart of the methods used in chapter 3 and 4.	80
Figure 3.2.	Images of control and cisplatin treated cells after various time intervals (12, 24, 48, 72 hrs), stained with H&E. The arrows are pointing to apoptotic cells and the arrow heads are showing the necrotic cells. The scale bars represent 20 micrometer.	83
Figure 3.3.	Percentages of dead cells revealed by H&E (◆) and trypan blue (■) staining in untreated and after 12, 24, 48, or 72 hrs cisplatin exposure in BT4C cells. The error bars are SEM and the significant differences are identified by comparing each time point with the control, untreated samples (n=3 for each time point, * $p$ <0.05, ** $p$ <0.001).	84
Figure 3.4.	Percentages of apoptotic and necrotic cells revealed by annexin V-FITC flow cytometry. To confirm the high percentages of viable cells detected by trypan blue and H&E staining after 12, 24, or 48 hrs cisplatin exposure, cells were labelled and stained with annexin V-FITC and PI. The cells were then analysed with flow cytometer and the data were processed with FlowJo (n=3 for each time point).	86
Figure 3.5.	Detecting DNA fragmentation. DNA was harvested from untreated and cisplatin treated BT4C cells (12, 24, 48, or 72 hrs) according to the procedures described in the method section. The DNA harvested from the cells was ran on gel electrophoresis to determine presence of the ladder pattern, a typical late stage marker of apoptosis (A. 1: negative control, 2,9: positive	87

	control, 3,6: untreated cells, 4,7: 48 hrs cisplatin exposed cells, 5,8: 72 hrs cisplatin exposed cells; B.1: negative control, 2: positive control, 3,6: untreated cells, 4,7: 24 hrs cisplatin exposed cells, 5,8: 48 hrs cisplatin exposed cells).	
Figure 3.6.	<sup>1</sup> H HR-MAS NMR spectra of BT4C cells following cisplatin exposure. (A) 0.5 to 4.5 ppm region. Metabolites labelled are as follows: <b>1</b> - lactate, <b>2</b> -alanine, <b>3</b> - glutamate, <b>4</b> - succinate, <b>5</b> - glutamine and aspartate, <b>6</b> - creatine, <b>7</b> - choline, <b>8</b> - GPC and PC, <b>9</b> - taurine, <b>10</b> - scyllo-inositol, <b>11</b> - glycine, <b>12</b> - myo-inositol, <b>13</b> - Guanidinoacetate.	90
Figure 3.7.	Choline containing region. Metabolites labelled on the control spectrum are as follows: <b>1</b> - choline, <b>2</b> - phosphocholine, <b>3</b> - glycerophosphocholine, <b>4</b> - taurine, <b>5</b> - phosphatidylcholine <b>6</b> - glycine).	91
Figure 3.8.	PCA of the 19 fitted metabolite quantities of cisplatin exposed cells. (A) Scores plot. (B) Loadings for principal component 1. (C) Loadings for principal 2.	95
Figure 3.9.	Phospholipid metabolism. The activities of phospholipase A2 and lysophospholipase result in production of GPC and fatty acids and phospholipase C activity results in degradation of phosphatidylcholine and production of phosphocholine.	99
Figure 3.10.	The metabolite pathways relevant to metabolite alterations in cisplatin exposed BT4C cells. Damaged DNA may activate poly (ADP-ribose) polymerase (PARP), a DNA repair enzyme which results in consumption of NAD and inhibition of glyceraldehyde-3-phosphate dehydrogenase (GAPDH) activity (indicated by a red circle). Hence glucose dependent ATP production is inhibited. In this diagram the metabolites with red arrows altered significantly with longer exposure to cisplatin in BT4C cells.	102
Figure 4.1.1.	Nile red and DAPI images of cisplatin exposed cells for various times of 12, 24, 48 or 72 hrs. Cells were stained with Nile red and DAPI and images were captured by a Nikon E600 microscope coupled to a SPOT RT KE colour 3 shot CCD camera. Gray scale images were	113-114

acquired and then images were pseudocoloured red and blue to represent Nile red and DAPI, respectively. Coloured Nile red and DAPI images were then merged (The scale bars represent 20 micrometers).

Figure 4.1.2.	Representative images of mitotic, viable, apoptotic and necrotic cells detected by Nile red and DAPI co-staining (The scale bars represent 5 micrometers).	115
Figure 4.2.	Mean percentage of cell area covered by lipid droplets in untreated and cisplatin treated samples (12, 24, 48, or 72 hrs) (* $p$ <0.05, ** $p$ <0.001; the error bars are SEM).	110
Figure 4.3.	Lipid droplet diameter of untreated and cisplatin exposed cells (12, 24, 48 or 72 hrs). The results are presented as micrometer ( $\mu$ m) (* $p$ <0.05, ** $p$ <0.001; the error bars are SEM).	117
Figure 4.4.	Percentages of dead cells revealed by DAPI staining in untreated and cisplatin exposed samples of different time points of 12, 24, 48 or 72 hrs (the sum of apoptotic and necrotic cells $\blacklozenge$ , apoptotic $\blacksquare$ , and necrotic $\blacktriangle$ cells) (* $p$ <0.05, ** $p$ <0.001; the error bars represent SEM).	119
Figure 4.5.	TEM images of control and 24 hrs cisplatin treated cells (LD- lipid droplets; SM- swollen mitochondria; V- vacuoles; IM- intact mitochondria).	121
Figure 4.6.	$^1\text{H}$ HR-MAS NMR spectra of untreated and cisplatin exposed cells of various time points of 12, 24, 48, or 72 hrs (Lipid signals labelled on the control spectrum are as follows: 1- 0.89 ppm, 2- 1.3 ppm, 3- 1.58 ppm, 4- 2.02 ppm, 5- 2.2 ppm, 6- 2.8 ppm, 7- 5.4 ppm).	122
Figure 4.7.	Ratio of the signals $-\text{CH}_2-\text{CH}_2-\text{CH}_2-/-\text{CH}_3$ did not alter by longer exposure to cisplatin showing that the mean chain length remains unchanged.	125
Figure 4.8.	Phospholipid metabolism. Phospholipase A2 and lysophospholipase activity result in production of GPC and fatty acids. Fatty acids can be used in production of phospholipids and triglycerides.	130

Figure 5.1.	Flow chart of the methods used in chapter 5.	139
Figure 5.2.	The percentages of necrotic cells detected by different methods of staining, trypan blue (◆), H&E (■), and DAPI (▲). The error bars are SEM. (* $p$ <0.05, ** $p$ <0.001).	141
Figure 5.3.	Images of control and starved cells after various time intervals (4, 6, 12, 18, or 24 hrs), stained with H&E. The arrows are pointing to necrotic cells and the scale bars represent 20 micrometers.	142
Figure 5.4.	Nile red and DAPI images of starved cells. Control and starved cells for various times of 4, 6, 12, 18 or 24 hrs were stained with Nile red and DAPI. A Nikon E600 microscope coupled to a SPOT RT KE colour 3 shot CCD camera was used to visualise and capture gray scale images. The images were merged after they were pseudocoloured red and blue to represent Nile red and DAPI, respectively (The scale bars represent 20 micrometer).	144-145
Figure 5.5.	The mean percentages of cell area covered by lipid droplets in starved cells. The error bars are SEM (* $p$ <0.05).	147
Figure 5.6.	The diameter of cytoplasmic lipid droplets of starved cells. The error bars are SEM (* $p$ <0.05, ** $p$ <0.001).	148
Figure 5.7.	TEM images of control and starved cells after 6, 12, and 24 hrs (LD- lipid droplets; A- autophagic bodies; SM- swollen mitochondria; M- myelinoid bodies; V- vacuoles; IM- intact mitochondria).	150
Figure 5.8.	<sup>1</sup> H HR-MAS NMR spectra of BT4C cells following substrate starvation. (A) 0.5 to 4.5 ppm region. Metabolites labelled are as follows: <b>1</b> - lactate, <b>2</b> -alanine, <b>3</b> - glutamate, <b>4</b> - succinate, <b>5</b> - glutamine and aspartate, <b>6</b> - creatine, <b>7</b> - choline, <b>8</b> - GPC and PC, <b>9</b> - taurine, <b>10</b> - scyllo-inositol, <b>11</b> - glycine, <b>12</b> - myo-inositol, <b>13</b> - guanidinoacetate.	152
Figure 5.9.	<sup>1</sup> H HR-MAS NMR spectra of BT4C cells following substrate starvation. (A) 0.5 to 4.5 ppm region. (B) Choline containing region (metabolites	153

labelled on the control spectrum are as follows: 1- choline, 2- phosphocholine, 3- glycerophosphocholine, 4- taurine, 5- phosphatidylcholine 6- glycine).

- Figure 5.10. PCA of  $^1\text{H}$  HR-MAS NMR metabolite profiles for substrate starved cells. (A) Scores plot, (B) Loadings for principal component 1, (C) Loadings for principal component 2. 161
- Figure 5.11. PCA of  $^1\text{H}$  HR-MAS NMR metabolite profiles for cisplatin exposed and substrate starved cells (A) scores plot, (B) loadings for principal component 1, (C) loadings for principal component 2. 163
- Figure 5.12. The relevant metabolite pathways in starved BT4C cells. In this diagram, the metabolites with red arrows altered significantly with longer substrate deprivation. 167

## List of Tables

		<b>Page</b>
Table 1.1.	Morphological and biological features of apoptosis, necrosis, and autophagy and their common methods of detection.	23
Table 2.1.	Metabolites identified by TARQUIN algorithm. The chemical shifts assigned to each of the metabolites and J-coupling properties are used to identify signals of a spectrum.	57
Table 3.1	Preliminary work was carried out to identify the percentage of dead cells after exposure to various concentrations of cisplatin and at different time intervals. Half of the cells were dead after 72 hrs exposure to 50 $\mu$ M cisplatin and majority of the cells were viable at shorter time intervals. Therefore, this concentration of cisplatin was used in the experiments described in chapters 3 and 4. The percentages of dead cells are presented as mean percentage $\pm$ SD (n=3, * $p$ <0.05; ** $p$ <0.001).	81
Table 3.2.	Cell cycle phase distribution. Cells were stained with PI and analysed by flow cytometry. In order to identify cell cycle phase distribution the data were analysed with multicycle software. The percentages of cells in each stage of the cell cycle are presented as mean percentage $\pm$ SD (* $p$ <0.05; ** $p$ <0.001).	88
Table 3.3.	Relative concentration of $^1\text{H}$ HR-MAS NMR detectable metabolites in untreated and cisplatin exposed cells for different times (12, 24, 48, or 72 hrs). The results are presented as mean $\pm$ SD. Three or more samples at each condition were analysed.	92
Table 3.4.	Significant $^1\text{H}$ HR-MAS NMR alterations detected in relative concentrations of the metabolites in response to cisplatin exposure. ( $\uparrow$ ) represents an increase in metabolite levels and ( $\downarrow$ ) represents a decrease in the metabolite levels compared to control cells (* $p$ <0.05, ** $p$ <0.001).	93
Table 4.1.	Relative quantities of $^1\text{H}$ HR-MAS NMR visible lipids in untreated and cisplatin exposed cells for different times (12, 24, 48 or 72 hrs). Three samples at each condition were analysed. The	123

results are presented as mean $\pm$ SD (\* $p$ <0.05, \*\* $p$ <0.001, compared to untreated samples).

Table 5.1.	Relative quantities of $^1\text{H}$ HR-MAS NMR visible lipids in control, and starved cells. Three samples at each condition were analysed. The results are presented as mean $\pm$ SD (* $p$ <0.05, ** $p$ <0.001, compared to untreated samples).	154
Table 5.2.	Relative concentration of $^1\text{H}$ HR-MAS NMR detectable metabolites in control and starved cells. The results are presented as mean $\pm$ SD. Three samples at each condition were analysed.	157
Table 5.3.	$^1\text{H}$ HR-MAS NMR alterations detected in the relative concentration of the metabolites during cell starvation. ( $\uparrow$ ) represents an increase in metabolite levels and ( $\downarrow$ ) represents a decrease in the metabolite levels compared to control cells (* $p$ <0.05, ** $p$ <0.001).	159

## Abbreviations

Ace	Acetate
Ala	Alanine
Annexin V- FITC	Annexin V-fluorescein-isothiocyanate
Arg	Arginine
Asn	Asparagine
Asp	Aspartate
ATM	Ataxia telangiectasia mutated
ATR	ATM and Rad 3 related
CCM	Choline containing metabolites
CDK	Cyclin dependent kinase
Cho	Choline
Cisplatin	Cis-dichlorodiammineplatinum II
CNS	Central nervous system
Cr	Creatine
CT	Computed tomography
Cys	Cysteine
D <sub>2</sub> O	Dideuterium monoxide

D-PBS	Dulbecco's phosphate buffered saline
DAG	Diacylglycerol
DAPI	4', 6-diamino-2-phenylindole
DMEM	Dulbecco's modified Eagles medium
DMG	Dimethylglycine
DMSO	Dimethyl sulfoxide
EDTA	Ethylenediaminetetraacetic acid
ER	Endoplasmic reticulum
FCS	Foetal calf serum
FT-IR	Fourier-transform infrared
G-3-P	Glucose-3-phosphate
GAPDH	Glyceraldehyde-3-phosphate dehydrogenase
GBM	Glioblastoma multiforme
GC-MS	Gas chromatography-Mass spectrometry
GCV gene therapy	Ganciclovir thymidine kinase gene therapy
GPC	Glycerophosphocholine
Gln	Glutamine
Glth	Glutathione

Glu	Glutamate
Gly	Glycine
Gua	Guanidinoacetate
H&E	Haematoxylin and eosin
h-tau	Hypo-aurine
His	Histidine
HR-MAS	High resolution magic angle spinning
Ile	Isoleucine
ISM	Industrial methylated spirit
Lac	Lactate
LC-MS	Liquid chromatography-Mass spectrometry
Leu	Leucine
LDH	Lactate dehydrogenase
Lys	Lysine
M- Ins	Myo-inositol
MDC	Monodansylcadaverine
Met	Methionine
MRI	Magnetic resonance imaging

MRS	Magnetic resonance spectroscopy
MS	Mass spectrometry
NEAA	Non-essential amino acid
Nile red	Nile blue oxazone (9-diethylamino-5H-benzo[ $\alpha$ ]phenoxazine- 5-one)
NMR	Nuclear magnetic resonance
PARP	Poly (ADP-ribose) polymerase
PC	Phosphocholine
PCA	Principal component analysis
PDH	Pyruvate dehydrogenase
PEth	Phosphatidylethanol amine
Phe	Phenylalanine
PI	Propidium iodide
PL	Phospholipid
PLA2	Phospholipase A2
PLC	Phospholipase C
PLD	Phospholipase D
PME	Phosphomonoester

Pro	Proline
PS	Phosphatidylserine
PtCho	Phosphatidylcholine
PUFA	Poly unsaturated fatty acid
RIF-1	Radiation induced fibrosarcoma
S-Ins	Scyllo-inositol
Ser	Serine
TARQUIN	Totally automatic robust quantitation in NMR
Tau	Taurine
TCA cycle	Tricarboxylic acid cycle
tCho	Total Choline
TEM	Transmission electron microscopy
TFP	Trans-fibre optic photography
TG	Triglyceride
Thr	Threonine
TLC	Thin layer chromatography
TMSP	Trimethylsilyl proprionate d4
Trp	Tryptophan

TSP	Trimethylsilyl-2,2,3,3-tetradeuteropropionic acid
Val	Valine
VLDL	Very low density lipoprotein
WHO	World health organisation

# **CHAPTER ONE**

## **INTRODUCTION**

## ***1.1. Introduction***

Early detection of tumour response to therapy influences tumour management and affects the outcome of the therapy. It allows for identification of unsuccessful strategies and application of alternative treatments. This would also prevent the patients from experiencing toxic side effects of unsuccessful chemotherapeutic drugs (1).

Examining the tumour size by conventional imaging techniques and histopathological examination of biopsy samples are the standard approaches to monitoring tumour treatment response. However, alterations in tumour size detected by conventional imaging techniques such as magnetic resonance imaging (MRI) usually occur weeks or months after the treatment is initiated. Histopathological examination is only reliable if the whole tumour can be removed and is unsatisfactory in particular for heterogeneous tumours that are difficult to resect completely such as glioma (2). This approach is invasive and is rarely used for tumours in regions which are not easily accessible such as the central nervous system (CNS). It also suffers from the disadvantage that it is difficult to repeat at different times during treatment.

A non-invasive and accurate technique for determining tumour response would greatly aid the management of many tumour types. Magnetic resonance spectroscopy (MRS) is a promising technique that can be used for early detection of tumour response to treatment by providing information on the metabolite profile of the tumours and their alterations in response to therapy.

MRS is one of several methods used to determine metabolite profiles. Metabolomics is the study of the complete set of metabolites of biological systems such as cells, tissues, or organisms which alter in response to physiological, developmental, or pathological status

(3, 4). As most of the metabolites are conserved, the results can be compared across species, making metabolomics a particularly useful approach amongst ‘-omic’ techniques (3).

In tumour studies, metabolomics has been used to understand better the pathogenic mechanisms by monitoring tumour growth, progression, regression and occurrence of events such as apoptosis (3). It has also been employed to monitor tumour treatment regimes and to identify new targets for anti-cancer drugs.

Various metabolomic analysis methods are available *in vitro*: nuclear magnetic resonance (NMR) spectroscopy (MRS in clinical settings), gas chromatography- and liquid chromatography- mass spectrometry (GC-MS and LC-MS), thin-layer chromatography (TLC), metabolite arrays, and Fourier-transform infrared (FT-IR) spectroscopy. These instruments are fully automated and after purchase, analysing samples is relatively cheap (3).

MS and NMR spectroscopy are the most common techniques used. MS is more sensitive than NMR (3). However, MS sample preparation is time consuming and some metabolites are poorly ionised. NMR is a non-invasive, reproducible and quantitative technique with the advantage that it can be used *in vivo*. Increased reliability and automation together with decreased acquisition times have increased the applicability of this method in the clinical setting and in particular as a complement to MRI.

Most of the tumour metabolomic research has involved MRS based studies. Some researchers have focused on identifying MRS metabolite alterations in response to tumour treatment and assigning them as biomarkers of effective tumour therapy (3). Clinical

management of certain tumour groups such as glioma may particularly benefit from MRS studies.

Glioma is the most common form of primary brain tumour (5). With a heterogeneous and highly invasive nature, the results of standard methods of diagnosing and treatment monitoring are often poor (2, 6). As the results influence the chosen treatment and the outcome of the therapy, MRS may improve the success of glioma treatment by identifying early markers of effective treatment. However, despite the increasing use of MRS in the clinical setting, there is still relatively little understanding of the metabolite changes detected and *in vitro* studies are required to improve this understanding. Rat glioma BT4C cells are a useful *in vitro* model to investigate the potential of MRS in detecting early markers of glioma response to treatment.

The majority of anti-cancer drugs induce apoptosis and some induce cytostasis in tumour cells (7, 8). However, as tumour cells develop resistance to apoptosis, application of necrosis-inducing treatments has been considered (9). Majority of studies have focused on MRS lipid and metabolite alterations in response to apoptosis (section 1.7) and although, <sup>1</sup>H MRS offers the potential to detect simultaneously a wide range of metabolites, in most previous studies small numbers of metabolites have been identified and examined.

MRS investigations of metabolite alterations in response to cytostasis prior to apoptosis may provide early markers of cell death and examining the metabolite profile of cells during necrosis may result in identification of specific markers of necrosis and/or may provide further information on the general markers of cell death. In addition studying the altered metabolite profiles may lead to better understanding of the effected pathways.

## ***1.2. Aim of This Thesis***

To identify general biomarkers of cell stress and specific markers of cytostasis and cell death in rat glioma BT4C cells by  $^1\text{H}$  high resolution (HR) magic angle spinning (MAS) NMR spectroscopy.

## ***1.3. Basic Principles of Magnetic Resonance Spectroscopy***

MRS is a non-invasive technique (2, 10) which can be used *in vivo* and *in vitro*. Therefore, the findings from cellular and animal models are potentially transferable to clinical settings (7) making it attractive to both biologists and clinicians. MRS is closely related to magnetic resonance imaging but MR spectroscopy provides information on low molecular weight metabolites (11, 12), mobile fatty acids (11), and polypeptides (13) rather than anatomical structure. MRS is a term used for *in vivo* studies and originates from the use of this technique in a clinical setting and the term NMR spectroscopy is used when MRS is applied *in vitro*.

MRS is based on the principle that a number of atomic nuclei have intrinsic magnetic properties when placed in magnetic fields and are able to align with the applied field. The magnetic property of some isotopes causes the nuclei to act as a small magnetic bar. In a magnetic field the magnets align (known as spinup) or oppose (Known as spindown) to the external field. Spinup is slightly favoured over spindown state. Nuclear spins can move between the two states by using radiation at the right frequency. The applied radiofrequency causes the nuclei to flip in to the other magnetic state (figure 1.1). After the radiofrequency, the system returns to equilibrium. The difference between the populations

of the two magnetic energy states is detected as radiowaves during the return of the nuclei to the start point (3). The radio waves resonate at specific frequencies determined by the atomic nuclei and their electronic environment (figure 1.1).

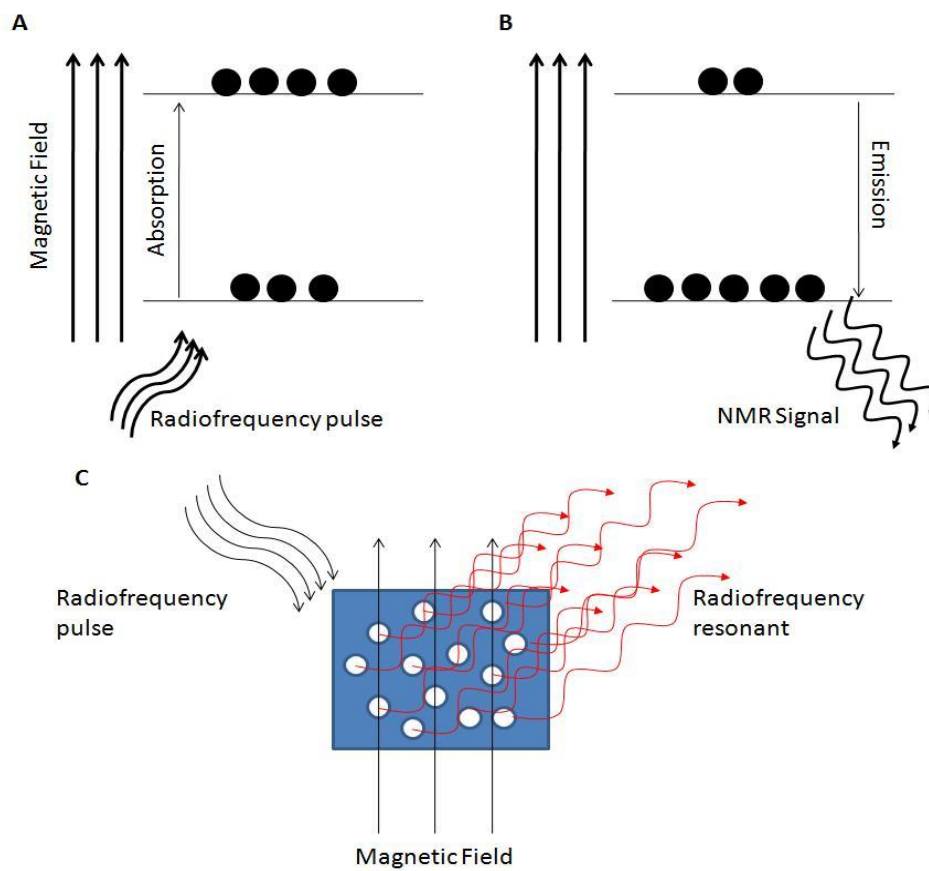


**Figure 1.1.** Schematic image of the magnetic resonance spectroscopy (MRS) effect. (A and B). A specific radiofrequency causes the nuclei to move to the other magnetic state. In absence of radiofrequency, the nuclei return to equilibrium. The resonant waves are registered and presented as peaks. (C). Radiofrequencies are applied during MRS and the waves resonate according to the nuclei and the surrounding environment.

The frequencies at which the radiation resonates, are detected and registered (10). The measured signals are then presented as peaks on a normalised frequency scale. The position of the peaks depends on the resonant frequencies of the related metabolite (14). The result is a spectral pattern of the chemical compounds. Each metabolite and component produces signals at different frequencies and frequencies are very much sensitive to the position of the atomic nuclei in the molecule and the surrounding environment of the nuclei (2, 10). The metabolite profile of the sample can be determined from these MR spectral patterns. The areas under the peaks are determined by the concentration of the metabolites and if the concentration of a reference metabolite is known (14) the relative concentration of the other metabolites can be calculated (2). Therefore MRS is a quantitative method as well as a qualitative technique (15).

Any nucleus with non zero spin can be studied by MRS, however only hydrogen ( $^1\text{H}$ ), phosphorous ( $^{31}\text{P}$ ) and carbon ( $^{13}\text{C}$ ) are commonly studied (15). Signals arising from  $^1\text{H}$  or  $^{31}\text{P}$  atoms of endogenous metabolites and  $^{19}\text{F}$  signals of anticancer drugs are the focus of clinical MRS of cancer. In addition  $^{13}\text{C}$  and  $^2\text{H}$  are used to investigate exogenously administered substances (2). Protons have a relatively large magnetic moment. Therefore,  $^1\text{H}$  MRS is a sensitive method, allowing small volumes to be examined (16). As protons are present in nearly all compounds (2), a large number of intracellular compounds such as small metabolites, phospholipids and polypeptides (17) are detectable; therefore  $^1\text{H}$  MRS contains wealth of information (2) and has been the most used and interesting MRS technique (10) for metabolite studies in biological systems *in vivo* and *in vitro* (17).

MRS can be fully automated and has a high degree of reproducibility in analysis of biofluid. The current detection limit using  $^1\text{H}$  NMR for tissue extracts and or biofluids is of

the order of 100  $\mu\text{M}$ . It is relatively easy to determine metabolites from simple one-dimensional spectra (3).

Although a monolayer culture does not represent characteristics of a three dimensional tumour, cell lines are useful models for studying NMR markers of therapy response. They are commercially available and by using the same culture conditions similar samples are achieved and assays can be repeated. Using tissue samples and animal models require ethical approval. The samples are limited and tumours are usually contaminated with normal cells. In addition studies are influenced by surrounding tissues and the micro-environment. Furthermore NMR spectroscopy on cell samples can be carried out at high fields (18), yielding a greater number of metabolites (19).

In this work  $^1\text{H}$  HR-MAS NMR is used. Due to restricted motion and high magnetic susceptibility, NMR spectroscopy analysis of tissue or cells at high magnetic field results in broad and overlapping signals. In  $^1\text{H}$  HR-MAS NMR a radiofrequency pulse at a specific angle of  $54.7^\circ$  is applied. Use of this angle reduces the effects of dipolar coupling, chemical shift anisotropy, and magnetic susceptibility differences. Therefore, spectroscopy of inhomogeneous samples such as cells or tissues results in high resolution data.

HR-MAS is an alternative technique to extraction methods. During extraction methods lipids and/or metabolites are removed from cells or tissues. Due to extraction of proteins during these procedures, the alteration of the metabolites and lipids are less likely. The samples are stable and low temperatures are not needed. In contrast to extraction studies, HR-MAS requires minimal preparations (3) on a small amount of samples. This technique allows investigation of cells and tissues that are better representative of *in vivo* models. Via HR-MAS high resolution data from inhomogeneous samples can be achieved and as this

technique is non-destructive, the cells or tissue sections can be further used for other assays such as viability tests. This technique has been used previously for detecting tumour response to treatment (20, 21).

#### ***1.4. Magnetic Resonance Spectroscopy of Tumours***

MRS is used to determine metabolite profiles of tumours which may be interpreted in the context of metabolic pathways in cells, tissues, or organisms. The detected changes reflect alterations occurring in tumours such as cell membrane proliferation or degradation, and changes in energy metabolism (14) and provides information on processes occurring during growth and death (22). The biochemical information obtained facilitates the better understanding of physiological and biochemical characteristics of tumours (2).

Metabolite profiling of tumours can facilitate tumour grading (2, 23), classification (24, 25) and malignancy determination (26). By identifying type and grade of tumours, MRS may contribute to non-invasive diagnosis. Comparison and quantification of metabolite profiles of healthy and diseased tissue (2) provides information on the contribution of metabolites to the development of healthy or pathological status (17). A large number of studies have been carried out to determine the characteristics of brain tumours by comparing normal and brain tumour tissues (16, 27, 28). Since 1980 metabolic profiles of brain tumours have been studied by MRS (29). The attraction of MRS for brain tumour investigation is that the brain has little motion and contains small amounts of mobile lipids (2), eliminating the problem of lipid interference with MRS ability to detect other

metabolites (28). MRI is also a standard investigation for patients with brain tumours allowing simple incorporation of MRS in clinical protocols.

Clinical management and therapy planning is founded on correct diagnosis based on tumour type and grade of malignancy. The current gold standard for identifying cancer type and the degree of malignancy is biopsy and histopathological examination of the samples (30). As the degree of malignancy can vary in the same lesion, histopathology of a small biopsy sample may not represent characteristics of the whole tumour mass (31). Therefore to reliably determine the degree of malignancy, gross resection or multiple biopsies are required (32). With 1.7% mortality rate associated with biopsy procedures (30), a non-invasive technique such as MRS is a promising tool for guiding biopsy and making a non-invasive diagnosis in regions that are difficult to biopsy within the CNS (33).

### ***1.5. Role of MRS in Monitoring Treatment Response***

Although non-invasive diagnosis is an important goal, a potentially more important role for MRS is in treatment monitoring and this is the focus of our attention. The traditional and current methods of detecting tumour therapy response are based on detecting a decrease in tumour size radiographically, by MRI, computed tomography (CT) or ultrasound. After a few months of therapy, changes in tumour volume are detectable with effective treatment. As it is not possible to collect information radiographically on the tumour response to therapy at early stages of treatment, patients might undergo a course of toxic therapy for weeks or months before it is realised that the treatment is not successful. Furthermore,

early detection of tumour response to therapy is a powerful determinant of long term treatment outcome for aggressive tumours (34). Therefore, there is a need for early predictors of tumour response to therapy.  $^1\text{H}$  MRS offers an alternative to tumour size for evaluating tumour response and identifying early predictors of successful treatment. MRS, by detecting and measuring tumour metabolites at early stages and during the course of treatment, has the potential to evaluate tumour response.

MRS can be used to compliment MRI in clinical settings. MRI is useful for determining anatomical localisation of intracranial tumours and to determine the extent of tumour mass for surgery and radiotherapy planning (31) and MRS by providing additional information on tumour metabolism can supplement the morphological data obtained from MRI. The aim is to use MRS and MRI in clinical settings and in some circumstances as a replacement for currently applied invasive diagnosis and monitoring methods. The combined application of imaging and spectroscopy in evaluating brain tumours has reached a stage that enables their use in a clinical environment in diagnosis, therapy planning and treatment follow-up (35, 36) but a more detailed understanding of metabolite profiles and their changes with treatment is required to inform these clinical studies.

### ***1.6. Treatment induced MRS alterations***

As discussed, detecting early biomarkers of tumour response to treatment is beneficial in predicting long term tumour outcome (34) and provides the opportunity to detect unsuccessful treatment early on. Assessment of tumours before and during treatment provides the opportunity to determine the pathophysiological changes occurring in response to treatment and the detected alterations in tumour metabolism by MRS may be

useful as predictors of treatment response early on and prior to detection of decrease in tumour size (7).

A number of studies have investigated alterations in lipids and low molecular weight metabolites in different tumours in response to various treatment methods. In the following sections a number of MRS studies identifying lipid and low molecular weight metabolite alterations in response to treatment are described.

### ***1.6.1. MRS Lipid Alterations***

In the past 10-15 years the phenomenon of NMR-visible lipids in cancer tissues has been the centre of interest (8). Mobile fatty acyl chains of triglycerides (TGs), free fatty acids and cholesteryl esters (22) give rise to well resolved signals in  $^1\text{H}$  NMR spectra of malignant cells (37, 38). There has been some controversy over the location of the fatty acyl chains. Using labelled radioisotopes and/or isolated membranes some studies suggest that NMR visible lipids arise from fatty acyl chains located in the membrane associated microdomains (39, 40).

Others provided increasing evidence that the cytoplasmic lipid droplets are the source of the detected lipids. The evidence was provided based on molecular diffusion experiments (41, 42), line width measurements of the lipid signals under different temperatures and spinning rates (21), light and/or fluorescent microscopy examination of samples stained with dyes such as Nile red (43-46), Oil red O (46-48) and/or electron microscopy studies of ultrathin sections or subcellular fractions (42, 44, 47, 49, 50).

Using radioisotope labelling and isolated membrane ghosts Mountford *et al.* associated the increases in lipid resonances detected in  $^1\text{H}$  NMR spectra of transformed cultured lymphocytes with lipid bilayers (40) which were in or attached to the cell membrane (37). They suggested the detected changes in human lymphoblastoid cell lines are indicative of type of transformation and stage of differentiation (51) and the detected increase in lipids is due to an increase in cell membrane fluidity caused by cell stimulation or transformation (40).

May *et al.* assigned the lipid resonances to the neutral lipids in the plasma membrane; with TGs as the main element (52). They were then shown to have similarities with very low density human lipoproteins, rich in TGs (Chylomicra and very low density lipoproteins (VLDL)) by Williams *et al.* (53).

Blankenberg and colleagues detected an increase in the methylene ( $\text{CH}_2$ ) resonance at 1.3 ppm in apoptotic Jurkat T-cell lymphoblast cultures induced by doxorubicin, glucocorticoids or serum deprivation. In addition, a similar increase in the methylene signal of apoptotic Daudi (B-cell) Burkitt's lymphoma cell cultures and JY T-cell ALL lines treated with doxorubicin was detected by this group (54). It was suggested that lipid resonances are rarely visible in viable, intact lymphocytes due to immobility of acyl chains in the lipid plasma membrane (54). Therefore, a decrease in microviscosity of the cell membrane along with other factors such as loss of cytoskeletal architecture were suggested to result in increase mobility and NMR visibility of lipid membrane during induction of apoptosis via various stimuli and within different cell lines (54). Down regulation of aminophospholipid translocase and increased activity of phospholipid scramblase during apoptosis were also suggested as the reasons behind increase in the cell membrane fluidity (55). The ratio of  $\text{CH}_2/\text{CH}_3$  was proposed as a means of estimating the proportion of

apoptosis in cultures (55). This group did not detect any changes in the lipid pattern of Jurket T-cells undergoing necrosis caused by freezing (54).

In 1994, Kuesel *et al.* also associated an increase in the lipid signal at 1.3 ppm in human grade IV astrocytoma tissues with necrosis. The origin of these lipids was not determined (56). In an *in vivo* study by Remy and his colleagues on an experimental model of rat intracerebral glioma, increases in NMR visible lipids were associated with necrosis and the origin of these lipids were identified as storage compartments of fatty acids, mainly TGs in the form of extracellular lipid droplets (42).

Early on in 1993 the work carried out by Callies *et al.* on a myeloma cell line, suggested that cytoplasmic lipid droplets contribute to the appearance of lipid resonances detected in  $^1\text{H}$  NMR spectra (49). The lipid alterations detected in *in vivo*  $^1\text{H}$  MRS patterns of necrotic C6 rat brain glioma were found to be associated with the lipid droplets within the cells (46). The same results were found by Barba *et al.*, in stimulated C6 rat glioma cells or in cells at saturation density and in a quiescent phase. They proposed that lipid increases can be used to determine the proliferation status of the cells (43).

An increase in  $^1\text{H}$  NMR lipid resonances was detected during apoptosis induced by cationic lipophilic phosphonium salts in human breast cell line HBL-100. The source of lipids was associated with an increase in lipid droplets (47). Di Vito *et al.* identified an increase in lipid patterns in both apoptotic and non-apoptotic, activated T-lymphoblastoid cells. Proposing lipid droplets as the source of the detected lipid increase, they also suggested a possible similarity between the mechanisms behind the rise in lipid intensity in both conditions (44). Feretti *et al.*, by studying NIH-3T3 fibroblast cells and their H-ras transformants (3T3<sup>ras</sup>) using electron microscopy, suggested contributions from both

cytosolic lipid droplets and membrane vesicles to the detected lipid increase in NIH- 3T3 fibroblasts (45).

Previous *ex vivo* and *in vivo* studies by Hakumaki *et al.* and Griffin *et al.* on rat BT4C glioma showed increases in MRS detectable lipids including polyunsaturated fatty acid lipids (PUFA) after apoptosis induction by Ganciclovir-Thymidine Kinase (GCV) gene therapy. They identified lipid droplets as the source of mobile lipids (21, 50).

During treatment different populations of apoptotic, necrotic, cell cycle arrested and even viable cells are detected. Although studies have associated the cytoplasmic lipid droplet alterations with the induction of apoptosis, necrosis or cell growth arrest, there has been little attempt to quantitatively determine alterations in the lipid droplets in each of the different cell populations.

### ***1.6.2. Low Molecular Weight Metabolite Alterations***

As is demonstrated in the following sections large numbers of studies have been carried out to identify alterations in non-lipid metabolites and to assess their potential as early or surrogate markers of treatment response.

#### ***1.6.2.1. Choline Containing Metabolites***

Much of the interest in  $^1\text{H}$  MRS has focused on choline containing metabolites (CCMs).

Recent *in vivo* (57, 58) and *in vitro* (59) studies on human breast tumours and *in vivo* studies of murine radiation-induced fibrosarcoma (RIF-1) showed a decrease in CCMs in

response to treatment. Suggesting the potential of CCMs as biomarkers of treatment efficacy in breast (58) and RIF-1 tumours (60).

However, *in vivo* studies by Lehtimäki *et al.* on rat glioma models have shown a decrease in CCMs only in advanced stages of cell death when tumour cell density has reduced (61). Further *in vivo* and *in vitro* studies on rat glioma models by Valonen *et al.* and Griffin *et al.* failed to show any changes in CCMs in response to gene therapy induced apoptosis (20, 62).

One explanation for this discrepancy may lie in the relative alterations of the individual CCMs since the  $^1\text{H}$  chemical shift dispersion of these metabolites is so small that they cannot be discriminated using *in vivo*  $^1\text{H}$  MRS. Evidence for this explanation comes from patterns of individual metabolites contributing to CCM signal identified in *in vitro* glioma studies. Valonen *et al.* showed increases in glycerophosphocholine (GPC) and phosphocholine (PC) levels at early stages of therapy induced apoptosis (62). In contrast, Hakumäki *et al.* identified a temporary decrease in PC and GPC levels at later stages of treatment (50). A decrease in the level of PC (20) and an increase in GPC (61) were also identified by other researchers. A decrease in tissue PC levels is frequently detected in reaction to chemotherapeutic agents (8) and has been suggested to serve as an early marker of effective tumour therapy *in vivo* (63). This further emphasises the potential of individual CCMs as markers of treatment and the importance of monitoring each of them separately. PC and GPC can be detected individually using  $^{31}\text{P}$  MRS *in vivo* and this technique also allows the detection of other phosphorylated metabolites such as CDP-choline (64, 65). However  $^{31}\text{P}$  MRS signals arising from these metabolites *in vivo* are weak and the method is not yet widely available clinically.

### ***1.6.2.2. Glycolytic Metabolites***

Alterations in glycolytic metabolites have been examined previously. *In vivo* and *in vitro*  $^{31}\text{P}$  MRS analysis of Friend erythroleukemia cells (FLC) and murine fibrosarcoma cells treated with tumour necrosis factor (TNF) revealed an increase in glycerol-3-phosphate levels (66). *In vitro*  $^{31}\text{P}$  NMR studies (cells and extracts) of Chinese hamster ovary cells and promyelocytic leukemia cells (HL-60) treated with various drugs also revealed increases in glycolysis intermediates. Activation of poly (ADP-ribose) polymerase (PARP) enzyme due to damage DNA was suggested as a possible reason for the detected alterations (65). Activity of PARP was also proposed by Ronen *et al.* as the underlying mechanism of the detected  $^{31}\text{P}$  NMR increase in glycolytic intermediates of doxorubicin treated colorectal tumour cells and mechlorethomin treated leukemia cells (L1210) (extract studies). They associated the identified alterations with apoptosis and suggested the potential of glycolytic intermediates as possible markers of cell death *in vivo* (67).

Alterations in lactate, a final product of glycolysis, have been examined previously. The *in vivo*  $^1\text{H}$  MRS levels of lactate in murine RIF-1 tumours remained constant after induction of necrosis by vascular disrupting agents (60).  $^1\text{H}$  NMR studies by Chung *et al.* on extracts of human colon tumours after induction of necrosis by histone deacetylase inhibitors showed a decrease in glucose levels (68).

However,  $^1\text{H}$  NMR lactate levels increased in IFN- $\gamma$ / TNF- $\alpha$  induced apoptosis in human colon carcinoma cells (69) and in TNF treated Friend erythroleukemia and murine fibrosarcoma (HeN4) cell extracts (66). In addition a decrease in lactate levels was identified in *in vivo* and *in vitro*  $^1\text{H}$  MRS examination of murin RIF-1 treated with 5-fluorouracil. The detected alterations were correlated with increased apoptotic regions in

the tumour after treatment (70). The same lactate alteration was detected in *in vivo* and *in vitro*  $^1\text{H}$  MRS examination of these cells treated with apoptosis inducing cyclophosphamide (71). Decreased glucose uptake and glycolytic rate have been suggested as the reasons for the identified alterations (70, 72) and lactate has been recommended to have potential as a non-invasive marker of tumour treatment response (69-71).

### ***1.6.2.3. Other Low Molecular Weight Metabolites***

$^1\text{H}$  MRS can measure a number of other small molecular weight metabolites. Metabolite alterations of rat glioma in response to apoptosis induced by ganciclovir treatment have previously been investigated (61, 62). Lehtimaki *et al.* detected a decrease in myo-inositol, taurine, glycine, and creatine *in vivo*. However, they detected increased myo-inositol levels and constant taurine levels using *in vitro*  $^1\text{H}$  NMR (61). Taurine levels investigated by Valonen *et al.* remained constant at early stages of apoptosis and reduced with loss of cell density at later stages. In addition, *in vitro* changes were not detected in the myo-inositol levels of glioma (62). More recently, a preliminary study of children with low grade brain tumours found myo-inositol to be useful in monitoring treatment (73).

A reduction in taurine levels has been associated with necrosis induced by vascular disrupting agent in *in vitro*  $^1\text{H}$  NMR studies of murine RIF-1 tumours (60). Also elevated levels of taurine have been noted to be associated with levels of apoptosis in untreated glioma biopsies (74).

Alterations in other low molecular weight metabolites were also detected in previous studies. A decrease in glutamine and glutamate levels and an increase in a number of

amino acids such as valine, leucine, and iso-leucine were detected in human colon carcinoma cells treated with histone deacetylase inhibitors (68).

The various profiles detected further emphasises that MRS metabolite profiles of different tumours may not be similar in response to treatment and although some metabolite changes may be common and be used as general markers, others may alter depending on the tumour type, the method of treatment and the nature of induced cell death.

### ***1.7. MRS alterations associated with Cell Death***

A number of studies detected elevated levels of NMR lipids in drug induced cell death models (44, 47, 48, 50, 54). As the main pathway of cell death initiated by the majority of anti-cancer agents (7, 8) and radiation therapy is apoptosis (75, 76), increasing numbers of studies have investigated lipid alterations in tumours after apoptosis induction and an increase in mobile lipids has been associated with this type of cell death (44, 48, 50, 54, 77).

Others have associated the detected changes in lipids to necrosis in tumours (42, 46, 47, 56) and some detected an increase in mobile lipids early on during treatment and prior to initiation of apoptosis (48, 50, 78, 79). The potential of lipid accumulation as a marker of cell cycle arrest and early indicator of tumour response has been demonstrated previously (50).

The potential of metabolites as markers of therapy induced cell death were also investigated in previous studies. Reduced levels CCMs in RIF-1 tumours treated with a vascular disrupting agent has been associated with necrosis and cell death (60). Although changes in CCMs have been associated with widespread cell death there have been several studies which have linked the metabolite changes with earlier events in tumour related treatment response.

Apoptosis induced by various drugs was associated with changes in PC and phosphoethanolamine (PEth) in hamster ovary and human promyelocytic leukemia cell lines (64). There have also been a small number of studies associating changes in CCMs with cell cycle arrest. Decreased levels of PC were detected in treated BT4C glioma cells (50, 79) and correlated to the number of cells arrested in G2/M phase of the cell cycle (50). Reduced levels of PC were also detected in TNF- $\alpha$  treated breast cancer cells arrested in G0/G1+S phase of the cell cycle, prior to apoptosis initiation (80). An increase in total choline (tCho) and GPC levels were also identified in growth arrested human prostate carcinoma (48). However, the relationship of these metabolite changes to cell death and cell cycle arrest has not been well established and some studies have associated them with loss of cell density (61, 62).

Glycolytic intermediates have also been suggested as potential indicators of cell death (64, 67). Elevated levels of fructose-1,6-bisphosphate along with CDP-choline has been suggested as a potential apoptotic marker (64). Lactate levels independently (70, 71) or in association with NTP levels (69) have been proposed as markers of effective treatment. Based on the association of taurine level with apoptosis in gliomas, Opstad *et al.* suggested that taurine measurements could be useful for *in vivo* monitoring of apoptosis in glioma (74).

## ***1.8. Features of Cell Death***

Based on circumstances of occurrence and morphological or biochemical characteristics (81), cell death can be classified into three main types: apoptosis, necrosis, and autophagy (table 1.1). In organisms homeostasis is sustained by a balance between cell proliferation, differentiation and cell death mainly by apoptosis. Impaired apoptotic pathways may lead to cancer development amongst many other diseases (64). Although apoptosis plays an important role in tumourgenesis, other types of cell death also implicate tumour development.

<i>Type of cell death</i>	<i>Nucleus changes</i>	<i>Cell membrane alterations</i>	<i>Cytoplasm changes</i>	<i>Biochemical features</i>	<i>Common detection methods</i>
<b>Apoptosis</b>	Chromatin condensation; nuclear fragmentation; DNA laddering	Blebbing	Fragmentation and formation of apoptotic bodies	Caspase-dependent	Electron microscopy; TUNEL staining; annexin staining; caspase-activity assays; DNA fragmentation assay; detection of changes in mitochondrial membrane potential
<b>Necrosis</b>	Clumping and random degradation of nuclear DNA	Swelling; rupture	Increased vascuolation; organelle degradation; mitochondrial swelling	-	Electron microscopy; nuclear staining; detection of inflammation and damage in surrounding tissues
<b>Autophagy</b>	Partial chromatin condensation; no DNA laddering	Blebbing	Increased number of autophagic vesicles	Caspase-independent; increased lysosomal activity	Electron microscopy; protein- degradation assays; assays for marker-protein translocation to autophagic membranes; Monodansylcadaverine (MDC) staining

**Table 1.1.** Morphological and biological features of apoptosis, necrosis, and autophagy and their common methods of detection (82).

An acute inflammation occurring during tumour cell necrosis may stimulate inflammatory response against malignant cells. However, it has been suggested a sustained inflammatory response (chronic) can promote tumourgenesis. Further studies are required to identify the role of necrosis in tumour development. Although the contribution of autophagy to tumour

development is not well understood, it may prevent transformation of normal cells to malignant cells by degrading proteins that promote tumourgenesis or by reducing cell stress. After a certain threshold, autophagy may promote tumourgenesis by protecting malignant cells against stressful conditions (83).

Chemotherapeutic or hormonal tumour treatment results in apoptosis induction (84). However, anti-cancer therapies also induce non-apoptotic cell death and as tumour cells develop resistance to apoptosis, treatment methods inducing other methods of cell death are being investigated.

In this work NMR markers of treatment efficacy is investigated and associated with cell stress and cell death using various morphological and molecular methods. Therefore, the following sections describe various cell death pathways and explain the different methods of detection used.

In addition, as some drugs such as cisplatin induce growth arrest prior to apoptosis, the different phases of cell cycle and the importance of the cell cycle check points are also discussed. Cell cycle checkpoints ensure proliferation of intact chromatin and detect damages to the double strand DNA. This results in cell cycle arrest and initiation of the repair systems. However, unsuccessful repair of the damaged DNA may trigger cell death.

### ***1.8.1. Necrosis***

Necrosis was previously considered as an unregulated process (85). However, recent evidence suggests that this method of cell death is regulated and consists of serial steps (86, 87). Research is ongoing to improve the understanding of the genetic and biochemical

pathways involved in necrosis (86). It is initiated in response to cell injury, stress stimuli, and activation of ion channels (85, 86). Combined with apoptosis, it has a major role in tissue renewal, embryogenesis and immune response. For example, in small intestine, apoptosis and necrosis are involved in renewal of enterocytes (87). In situations where apoptosis is blocked, necrosis is stimulated (85).

Necrosis occurs in a number of neighbouring cells and leads to distortion and degradation of organelles, followed by cell swelling and rupture (85, 88). Due to cell rupture and release of intracellular components, an inflammatory response is activated. Inflammation activates immune response, resulting in repair or elimination of damaged or infected tissue (85).

During the initial stages of necrosis chromatin is compact. This stage is known as pyknosis. This progresses to clumping of nuclear chromatin on the membrane of the nucleus. Mitochondria may become flocculent and sometimes granular matrix is apparent. This is followed by swelling of the mitochondrial matrix and rupture of the nucleus, organelles, and plasma membrane. The chromatin masses may initially be dispersed and be observed as small discrete masses (karyorrhexis) but they will disappear. Cell rupture leads to inflammation in adjacent viable tissues and the debris are engulfed by phagocytic cells (81) (figure 1.2.).

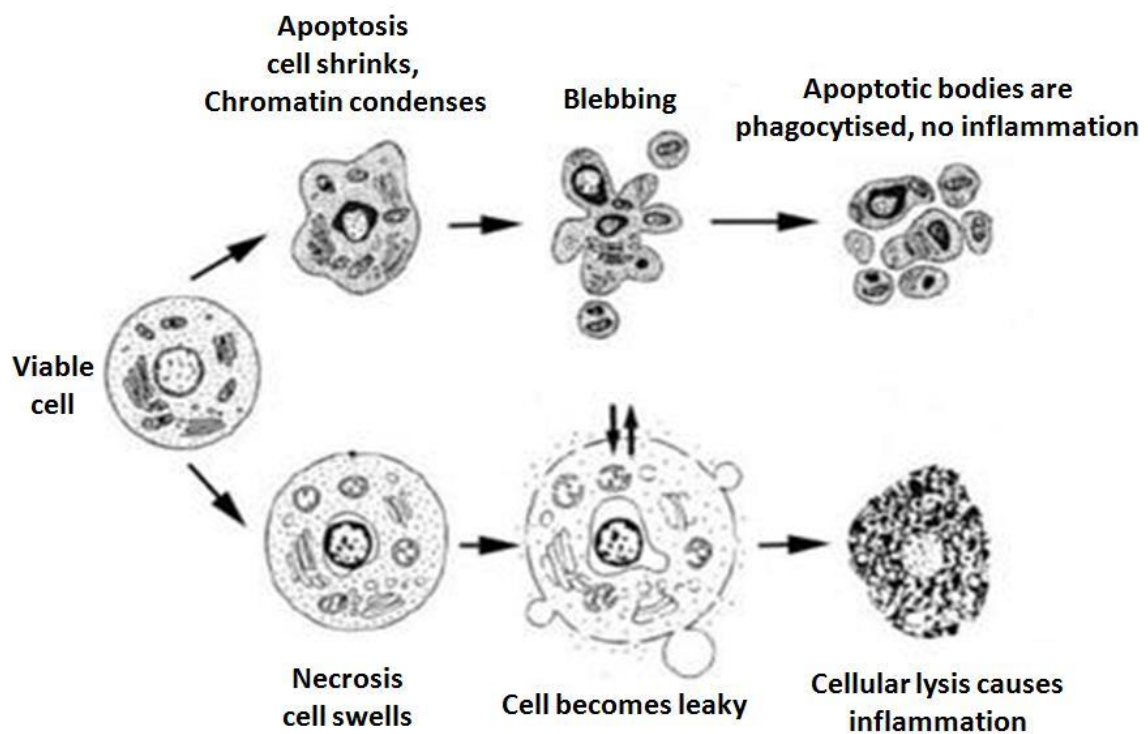


**Figure 1.2.** Schematic image of the events occurring in cells during apoptosis and necrosis cell death (89). During apoptosis, chromatin condenses and the cell shrinks and membrane blebbing occurs. During the final stages, the cell breaks up into a cluster of apoptotic bodies. During necrosis, the cell swells and blebbing and vacuolisation occurs. The cell membrane becomes permeable and at the final stages, cell shrinkage and lysis occur

### ***1.8.2. Apoptosis***

Based on morphological characteristics, apoptosis was originally known as shrinkage necrosis (90). High occurrence and importance of apoptosis in healthy and diseased organisms, and further morphological studies led to better understanding of this phenomenon and therefore it was described and re-named as apoptosis (Greek, meaning

apo “off”; ptosis, “falling”) by Kerr *et al.* in 1972 (88). Apoptosis plays an important role in developing and mature organisms. Morphogenesis during development and homeostasis in mature stages are mainly due to apoptosis. In addition apoptosis eradicates cells containing cellular and genetic damage and eliminates pathogen infected cells (85).

Apoptosis is a complex and genetically controlled method of cell death. Vast numbers of factors may stimulate apoptosis. Environmental stimuli and cell damage initiate a train of signals effecting regulatory proteins including the BCL-2 family, inhibitors of apoptosis proteins, and components of death receptor signalling systems. Cell death is controlled by these proteins and is carried out by a set of cysteine proteases known as caspases (85).

Apoptosis occurs in single, scattered cells. The chromatin becomes dense and transforms to large granular masses that border with the nuclear membrane. The nucleus becomes convoluted and large. The nuclear granules become coarse and abnormally scattered. Alongside nuclear alterations, cytoplasm is affected. The cytoplasm becomes condensed and translucent cytoplasmic vacuoles develop. Usually blunt protuberances are observed on the cell surface. The integrity of many cellular organelles remains intact. Due to condensation of the cytoplasm, the organelles become crowded. By this stage, the nucleus is broken up into condensed chromatin fragments; some are surrounded by a double membrane (81).

During the final stages of apoptosis, the protuberances on the cell membrane are detached from the cell membrane and form membrane-bound apoptotic bodies. The apoptotic bodies of different composition and size enter the intercellular tissue spaces and are mainly phagocytised by tissue cells or monocellular phagocytic system. Some may enter the adjacent lumen. Due to engulfment of apoptotic bodies, inflammation is not detected

during this process. The apoptotic bodies within the phagosome are digested by primary and secondary lysosomes and undergo a similar process as cell necrosis (81).

In culture, apoptotic cells are not phagocytosed. These cells are detached from the adjacent cells and float in the medium. The plasma membrane is eventually permeabilised and secondary necrosis occurs (87) (figure 1.2.). Various assays have been developed to detect apoptosis at different stages of progression and a number of these assays applied in this work are described in section 1.9.

### ***1.8.3. Autophagy***

Autophagy is a highly complex process (91) during which, the cell digests itself (85) and the cytoplasmic components are degraded in lysosomes (91).

Although there are three types of autophagy- macroautophagy, microautophagy, and chaperon mediated autophagy- the term autophagy usually describes macroautophagy (91). Macroautophagy is divided into induced macroautophagy during which, amino acids are produced in response to starvation and the constitutive turnover of the cytosolic component occurs during basal macroautophagy (92).

Autophagy has many physiological and pathological roles (figure 1.3). By engulfing damaged or unwanted proteins and organelles it has influence on intracellular clearance (86, 91). During embryogenesis and morphogenesis, autophagy has been detected. For example intersegmental muscles are eliminated by this process (86). In mature organisms, autophagy along with apoptosis and necrosis influences homeostasis (85). In addition, autophagy plays an important role in cell death (86), elimination of microorganisms,

antigen presentation, and tumour suppression (92). There are four stages to completion of autophagy (86) (figure 1.3).

**(1) Autophagy induction and cargo packaging.** Various environmental (high temperature, low oxygen) and intracellular factors (damaged organelles) may induce autophagy (93). However, the main and typical inducer of autophagy is lack of nutrients and starvation (86, 91). Autophagy is induced in an attempt to provide nutrients by digesting macromolecules. A unique, flat, and Golgi cistern like membrane called phagophore or isolation membrane, sequesters cytoplasmic components such as organelles (91).

**(2) Formation and completion.** Cytoplasmic components are engulfed completely by a double membrane organelle formed from autophore and known as an autophagosome. The selection of cytoplasmic constituents is random, although autophagosomes have the ability to recognise some proteins and organelles (91).

**(3) Ducking and fusion.** The formed autophagosome binds to lysosomes and the inner membrane of the autophagosome, then the cytoplasmic material is digested by lysosomal hydrolases.

**(4) Breakdown.** The monomeric units formed from macromolecule degradation are transferred back to the cytoplasm to be reused. It has been suggested that energy is produced during autophagy with the amino acids reused in tricarboxylic acid (TCA) cycle. However, this stage has not yet been fully established (91).

Although apoptosis leads to cell death and autophagy contributes to cell survival (93), a number of genes and functions involved in apoptosis and autophagy overlap. Hence these two procedures coordinate and they can modify and regulate the activity of each other (86,

93). Autophagy may promote or inhibit tumourgenesis. Inactivation of autophagy genes may increase tumourgenesis. During cancer development these genes may be deactivated by tumourgenesis promoting genes. Autophagy by promoting cell death and regulating cell growth may prevent cancer. Therefore, there is potential to develop drugs to manipulate autophagy pathways. However, further research is required to determine when or how to activate or deactivate autophagy in an attempt to have the best effect on tumours (93).

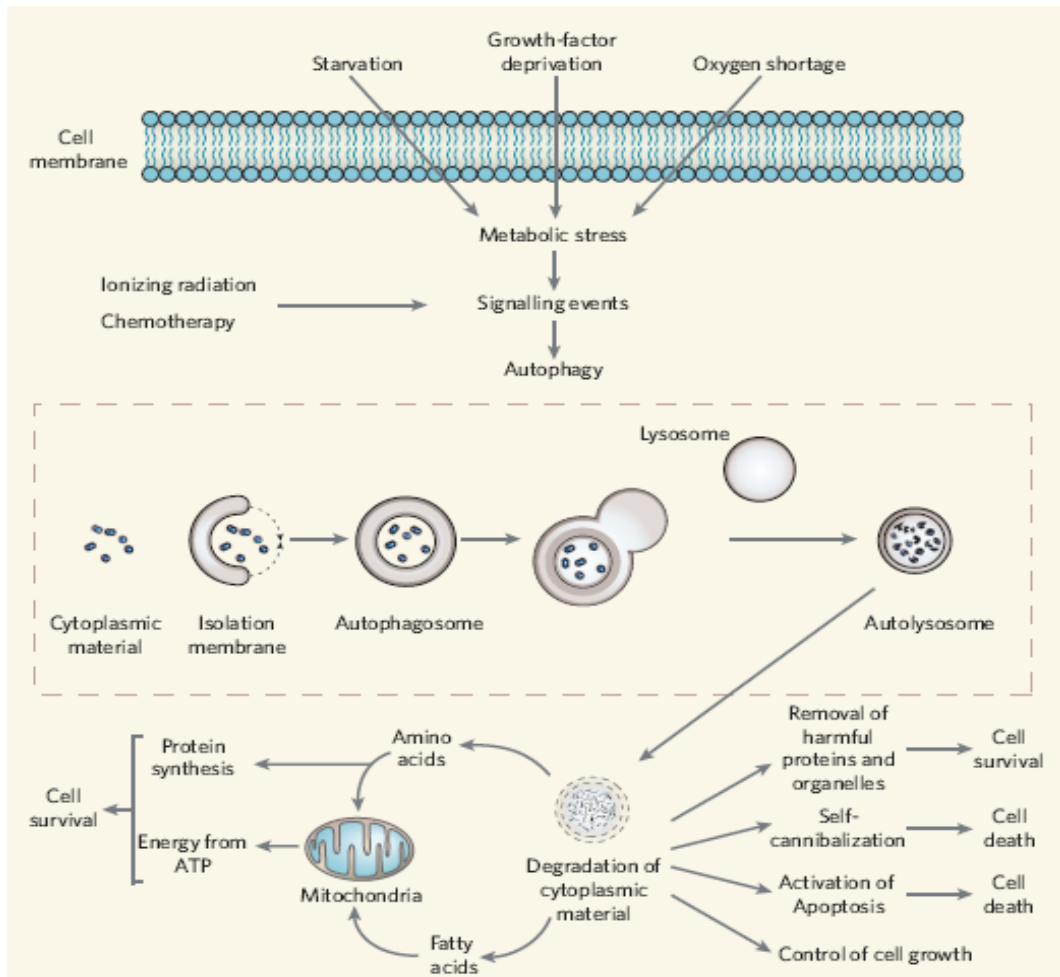


**Figure 1.3.** Autophagy pathway and its many functions. Autophagy is stimulated by metabolic stress or cancer therapies. Autophagosome sequesters cytoplasmic material and fuses with lysosome, forming an autolysosome. Degradation of cytoplasmic material generates free fatty acids and amino acids, which can result in energy production, protein synthesis, or removal of harmful proteins. Autophagy can cause cell death by self-cannibalism and/or apoptosis (93).

#### ***1.8.4. Cell Cycle and Cell Cycle Control***

The cell cycle is highly regulated, comprising of a series of steps leading to division of the parental cell to two daughter cells with identical chromosomes. Cell proliferation is very important in normal development and it is controlled by timing of DNA replication and mitosis. Loss of cell cycle control may result in cancer development.

The cell cycle is divided into four phases (figure 1.4). During the first phase known as G1, the cell synthesises RNA and proteins. DNA synthesis and chromosome replication occurs in the S phase and mitosis takes place after G2 phase in M stage of the cell cycle. Most differentiated cells in multi-cellular organisms leave the cell cycle and enter a stage known as G0. These cells may survive in this stage from a few days to the life time of the organism.

Regulation of the cell cycle occurs by heterodimeric protein kinases. These proteins are formed from a regulatory subunit known as cyclin and a catalytic subunit called cyclin-dependent kinase (CDK). There are three major cyclin-CDK complexes regulating progression through phases of the cell cycle; G1, G2, and mitotic cyclin-CDK complexes (figure 1.4).

The regulatory effects of these complexes are carried out by phosphorylation of the targeted proteins. For example one of the substrates of G1 cyclin-CDK complex is Rb protein. This protein is a product of Rb tumour suppressor gene. Activation of this protein results in cell halt at restriction point (late G1) and cell cycle arrest. Attachment of the Rb to transcription factor E2F, results in binding of deacetylase complex. Deacetylation of histone results in transcriptionally inactive chromatin. In contrast, phosphorylation of Rb protein liberates E2F and transcription of genes required for entry to S phase is activated.

In most cancers Rb protein is deactivated due to mutation or abnormalities in phosphorylation.

There are various check points at different stages of the cell cycle to ensure the chromosome is intact and cell phase is completed before the next phase is begun. For example, one of the check points identifies DNA damage caused by chemical agents and irradiation, which results in cell cycle arrest until the damage is repaired. Arrest in G1 and S phase prevents copying of damaged bases to the new cells and arrest in G2 phase provides the opportunity to fix the DNA double strand breaks. p53 is a tumour suppressor protein causing G1 and G2 arrest in cells containing damaged DNA. p53 is a transcription factor with a short half life, which is degraded by proteasomes after binding to Mdm2. Phosphorylation by protein kinases such as ATM (ataxia telangiectasia mutated) and ATR (ATM and Rad 3 related) prevents p53 degradation. Accumulation of p53 and increase in transcription activity of this protein leads to encoding of genes such as p21<sup>CIP</sup>. This gene inhibits the activity of cyclin-CDK complexes. Consequently cells are arrested in G1 and G2 until DNA is repaired. In situations when DNA damage is extreme, p53 activates genes inducing apoptosis (94).

Increased knowledge of cell cycle and cell cycle control may improve our understanding of the mechanisms of the anti-tumour drugs effecting the cell cycle and may provide useful information for designing new drugs.

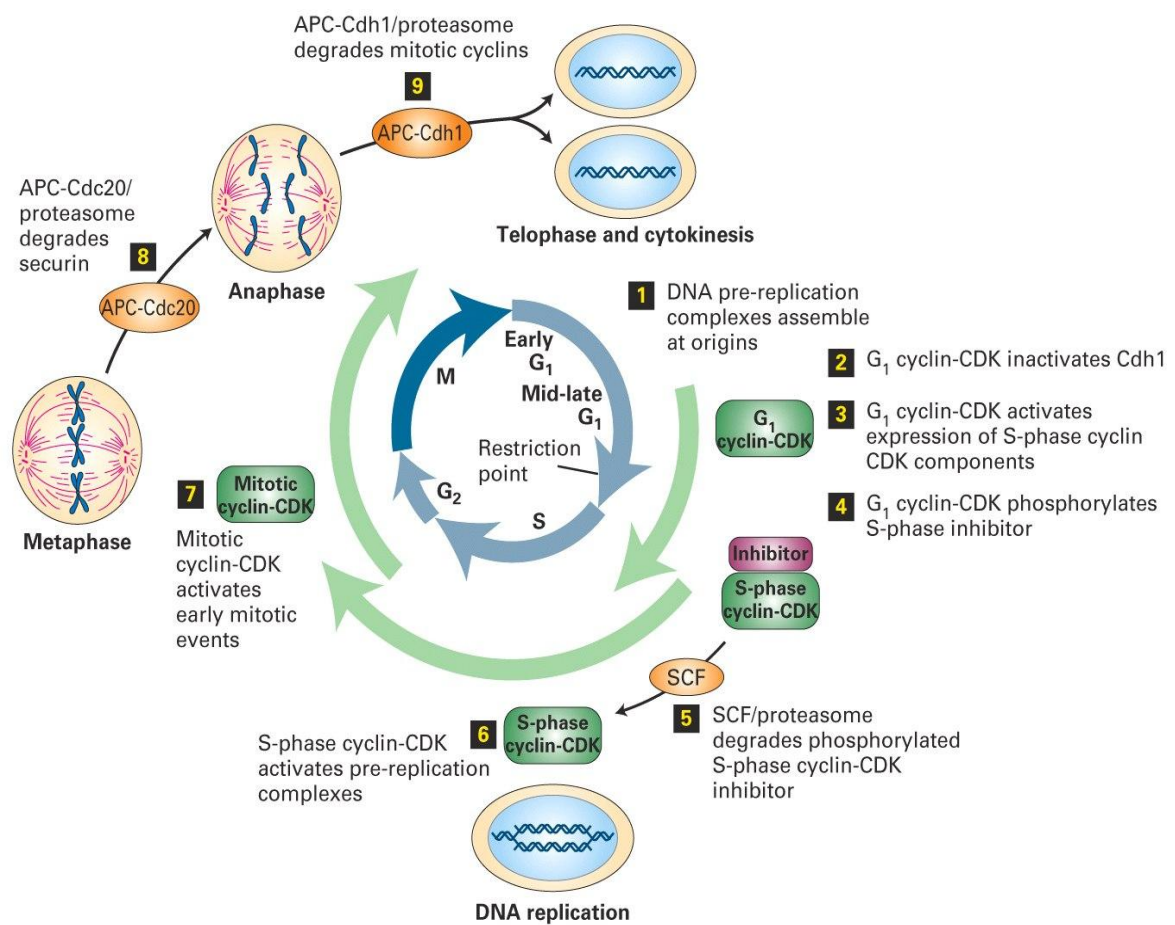


**Figure 1.4.** Cell cycle process and cell check points. The cell cycle is controlled by G<sub>1</sub>, S-phase, and mitotic cyclin-dependent kinase complexes (Green). Ubiquitin ligase complexes SCF and APC polyubiquitinate S phase inhibitors, securing and mitotic cyclins for degradation by proteasomes. Proteolysis of these substrates activates the relevant cyclin-CDK complexes, leading to cell cycle progression (94).

## ***1.9. Cell Death Assessment***

As previously described, different pathways of cell death have certain morphological and biochemical features that can be the basis of their identification and distinction. Morphological characteristics can be visualised by light or electron microscopy and other features that are not readily visible by microscopy can be investigated by various available assays. In this section a brief description of techniques used during the following chapters in order to identify cell death has been described.

### ***1.9.1. Light and Electron Microscopy***

Cell shrinkage, membrane blebbing, chromatin condensation, DNA fragmentation and formation of apoptotic bodies; all representing morphological features of apoptosis can be identified by microscopy. Features representing necrosis such as cell swelling, membrane rupture, dispersed and fragmented chromatin are also visible by microscopic techniques. In addition, cell ultra-structural features can be visualised by electron microscopy and alterations to the cell organelles such as nuclei and mitochondria due to cell death can be identified.

### ***1.9.2. Light Microscopy Analysis of Haematoxylin and Eosin stained Cells***

Although the haematoxylin and eosin (H&E) staining technique is not a specific method for cell death detection, it is a common histopathology method that provides information on morphological features of the cell, specifically the nucleus. The cell nucleus and

cytoplasm are reasonably distinguished by haematoxylin and eosin dyes, respectively and the morphological features of the cells are studied by light microscopy. During this method of staining, the cell nucleus is stained blue and the cytoplasm becomes red-purple.

### ***1.9.3. 4', 6-diamino-2-phenylindole Staining***

4',6-diamino-2-phenylindole (DAPI) is a blue fluorescent dye and useful for nuclear counter-stain for multicolour fluorescent techniques. DAPI preferentially attaches to the double strand DNA specially the AT clusters of the minor groove (95). DAPI can be excited with a xenon or mercury-arc lamp or with a UV laser. The maximum excitation of this dye is 358 nm and the emission maximum is 461 nm. As this dye can transfer through the intact membrane of viable cells, it can be useful for examining the morphological features of the cell nucleus and to identify viable, apoptotic and necrotic cells based on their nuclear characteristics.

### ***1.9.4. Trypan Blue Exclusion***

The viability of cells can be examined by exclusion of trypan blue. Apoptotic cells retain their membrane integrity to the final stages. Therefore viable cells and apoptotic cells exclude trypan blue whereas cells at late stages of apoptosis and necrotic cells have impaired cell membranes and are not able to exclude the dye and are stained (96).

### ***1.9.5. Detection of Nucleosomal DNA Fragments on Agarose Gel***

#### ***Electrophoresis***

Activation of endogenous endonuclease in apoptotic cells results in cleavage of DNA in linker regions between the nucleosome cores (81). A ladder pattern of approximately 180-200 bp integer multiples are detected on gel electrophoresis of the extracted DNA from apoptotic cells (figure 1.5). The detected ladder pattern is a hallmark of apoptosis in most cell types (96).

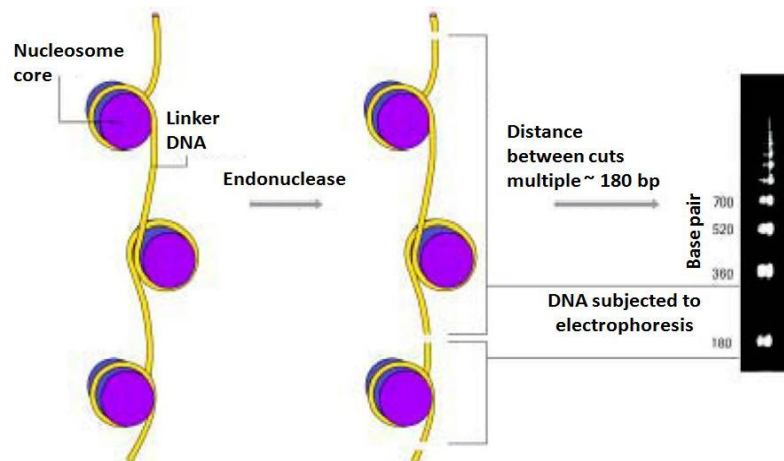


**Figure 1.5.** The biochemistry of DNA fragmentation during apoptosis and the appearance of 180-200 bp DNA fragments as ladder pattern on gel electrophoresis (97).

### ***1.9.6. Flow cytometry Analysis of Annexin V-FITC Labelled and Propidium Iodide Stained Cells***

Viable cells maintain their membrane phospholipid asymmetry by  $Mg^{2+}$ /ATP-dependent translocases, known as flippases (98). The choline containing phospholipids such as phosphatidylcholine (PtCho) and sphingomyelin are based mainly in the outer layer of the plasma membrane and aminophospholipids, PEth and phosphatidylserine (PS) are located at the inner layer (figure 1.6) (99, 100).

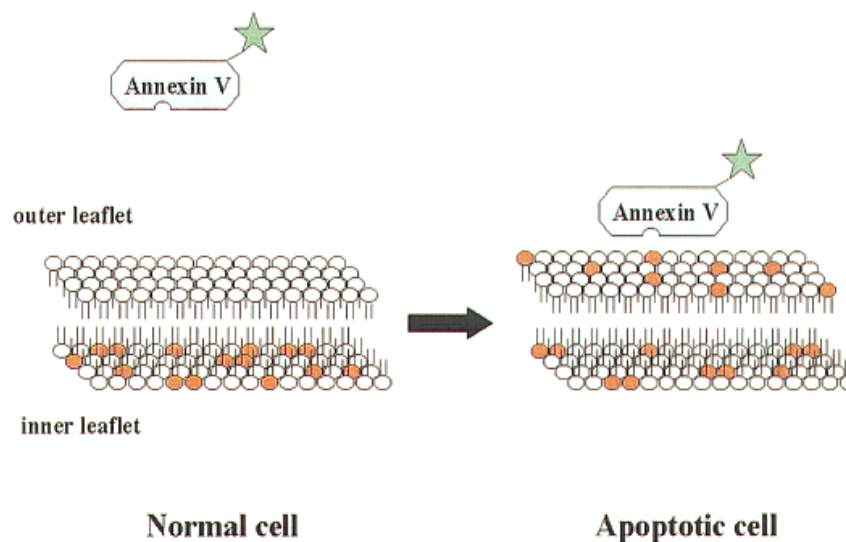


**Figure 1.6.** Schematic representation of loss of cell membrane asymmetry during early stages of apoptosis. PS molecules are located in the inner layer of the cell membrane (orange circles). During apoptosis they are translocated to the outer membrane. FITC labelled annexin V has high affinity to the exposed PS (100).

During apoptosis PS is translocated to the outer layer of the cell membrane. PS exposure occurs at early stages of apoptosis induction and remains on the surface until the late stages. PS exposure is a marker for detection of dying cells by macrophages *in vivo* (100). The affinity of annexin V, bound to fluorescein-isothiocyanate (FITC), to a negatively charged phospholipid such as PS (101, 102) is used for detection of apoptotic cells. As it is not able to penetrate the membrane and bind to viable cells, viable and apoptotic cells are distinguished from each other (figure 1.6). Although PS is translocated on the cell surface of apoptotic cells, the membrane integrity is intact. However, the membrane of necrotic cells is impaired and permeable hence, these cells can be recognised by uptake of DNA binding dyes such as propidium iodide (PI) (96). Simultaneous addition of DNA stains assists in differentiating necrotic and apoptotic cells (100).

### ***1.10. The Use of Cisplatin to Induce Cell Cycle Arrest and Cell***

#### ***Death***

Cisplatin (cis-dichlorodiammineplatinum) is a platinum drug developed clinically in the 1970s (103) and it is used for treatment of a number of tumours including glioblastoma (104). Cisplatin induces apoptosis or cytostasis followed by apoptosis depending on the dosage used. In a study by Qin *et al.* on human hepatoma cell lines, low doses of cisplatin resulted in apoptosis in Hep3B cells (with deleted p53) and caused transient arrest in G1 followed by progression and block of cell growth in the S phase of the cell cycle in HepG2 cells. A number of HepG2 cells then progressed to apoptosis. At high doses of cisplatin, apoptosis was detected in both Hep3B and HepG2 cells (105). This property makes

cisplatin a useful agent in the study of cell cycle arrest and cell death and it is a clinically relevant choice for a member of brain tumours.

Effects of cisplatin on morphology and cycling of rat glioma cells (C6) was investigated by Mares *et al.* Enlargement of cells was detected in exposed cultures and restructuring of the processes within the cells due to cisplatin resulted in reduced proliferation rate and progression to cell death at later stages of treatment (106).

Cisplatin enters the cells through transmembrane channels. The mechanisms of action of these channels are not well understood. After entry, cisplatin becomes strongly hydrated and chloride concentration decreases in order to form species with a positive charge. This results in interaction of cisplatin with nucleophils (107). Therefore, nucleophil sites such as DNA, RNA, proteins, membrane phospholipids, cytoskeletal microfilaments and thiol-containing molecules interact with cisplatin. Only 1% of the cisplatin within the cells interact with DNA and although other sites interacting with cisplatin contribute to cytotoxicity, the interactions between DNA and cisplatin have been identified as the main target leading to death in exposed cells. If the detected DNA damage is not repairable apoptosis is induced. A number of different adducts including inter- and intra-strand cross-links and DNA-protein cross-links are formed in the DNA (103) (figure 1.7). The most common adduct is an intra-strand cross-link between adjacent guanines (108). Unrepaired DNA adducts may lead to cell arrest and progression to apoptosis (103, 104).

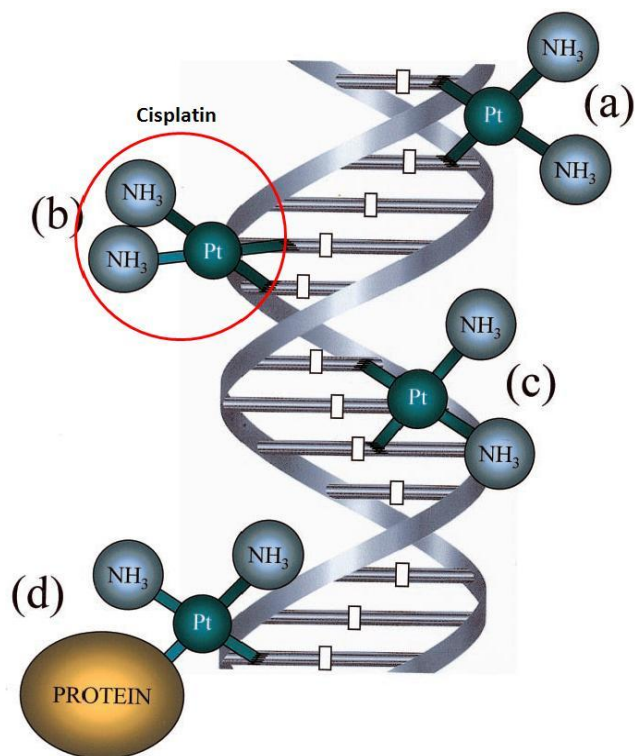


**Figure 1.7.** Cisplatin interaction with DNA. (a) inter-strand cross-link. (b) 1,2-intra-strand cross-link. (c) 1,3-intra-strand cross-link. (d) protein-DNA cross-link (103).

### ***1.11. Objectives of the Thesis***

The main objective of this work is to identify general markers of cell stress and specific markers of cytostasis and cell death in rat BT4C glioma cell line by studying alterations of a number of metabolites and lipids in response to cell stress using  $^1\text{H}$  HR-MAS NMR spectroscopy. In addition morphological and molecular assays are used to identify the type of cell death contributing to the detected alterations.

In the **chapters 3 and 4**, BT4C cells are exposed to a common anti-tumour drug cisplatin for various time intervals. A number of assays are carried out to determine the viability status of the cisplatin exposed cells and  $^1\text{H}$  HR-MAS NMR is performed on cells using a Varian 600MHz nanoprobe to identify alterations induced by cisplatin in these cells. The main focus of **chapter 3** is to identify  $^1\text{H}$  HR-MAS NMR metabolite alterations in the cisplatin exposed cells and **chapter 4** focuses on identifying alterations in the  $^1\text{H}$  HR-MAS NMR visible lipid signals and recognising the origin of the detected lipid resonances.

In **chapter 5**, starvation is used to induce necrosis in BT4C cells, allowing a comparison in the pattern of lipids and metabolites caused by two different types of stress stimuli. In this Chapter cells are maintained in a substrate free medium for various time intervals. The type of cell death is identified with various assays and the alterations in lipid and metabolite profiles of these cells are investigated by  $^1\text{H}$  HR-MAS NMR.

## **CHAPTER 2**

### **MATERIALS AND METHODS**

## ***2.1. Rat Glioma Cells***

All solutions and equipment used for cell culture were obtained sterile. Work was carried out under sterile conditions in a cyttox II laminar flow cabinet (Gelman Sciences Ltd., Northampton, UK). The work surface and equipments used were sterilised with 70% ISM (industrial methylated spirit) where required.

### ***2.1.1. Cell Culture***

Rat glioma cell line, BT4C, was cultured in 75 cm<sup>2</sup> flasks with filter-vented caps (IWAKI, Appleton Woods Ltd, Birmingham, UK) and maintained in 20 ml Dulbecco's modified Eagles medium (DMEM F:12), without L-glutamine (GIBCO, Invitrogen Co, Paisley, UK) supplemented with 10% (v/v) foetal calf serum (PAA Laboratories, Somerset, UK), 1% 200 mM L-glutamine (100x) (GIBCO), and 1.8% MEM non essential amino acid solution (100x) (Sigma-Aldrich, Dorset, UK). The cells were incubated at 37°C in a humidified atmosphere (5% CO<sub>2</sub>, 95% air). Cells were seeded at approximately 2 x 10<sup>6</sup> cells/Flask and were passaged on day 2 of culture.

### ***2.1.2. Detachment of Confluent Cells***

Once the cells were 70-80% confluent, the medium was removed using sterile plastic pipettes. The cells were then washed with phosphate buffered saline (Dulbecco's A PBS, Oxoid, Hampshire, UK). PBS was removed and 1 ml accutase in PBS with 0.5 mM EDTA (TCS Cellworks, Buckingham, UK) was added to the flask. The flask containing the cells

was placed in the 37°C humidified chamber for 1-2 minutes until the cells had started to lift off from the flask surface. 9 ml of supplemented DMEM F:12 (without L-glutamine) (1 in 10 dilution) was added to the cells to stop the action of accutase and to wash the surface of the flask. The cells were then gently pipetted up and down few times to separate them from each other. 1 ml of the cell suspension was removed to a new 75 cm<sup>2</sup> flask and DMEM medium was added to make the volume to 20 ml. The cells and fresh medium were gently mixed and the flask was placed in the humidified chamber (37°C, 5% CO<sub>2</sub>).

### ***2.1.3. Cell Counting***

After the cells were detached from the flask, one drop (~20 µl) of the cell suspension in PBS/medium was added to the chamber of a Neubauer haemocytometer (Ruling 1/400 mm<sup>2</sup>, cell depth 0.1 mm±1%; Hawksley, Sussex, UK) by a sterile plastic transfer pipette. The cells were then counted under a Nikon TMS microscope (Nikon Ltd, Kingston upon Thames, UK) with the 40 x magnification lens (Figure 2.1).

### ***2.1.4. Cell Cryopreservation***

The detached cells with accutase were frozen down for future use. The cells were resuspended in supplemented DMEM F:12 (without L-glutamine) medium containing 10% (v/v) cryoprotectant (sterile DMSO, Dimethyl sulfoxide, Sigma-Aldrich). The number of cells was counted in the cell suspension using the method described previously (section 2.1.3.). Approximately 1 ml of the cell mixture was aliquoted into 2 ml cryovials (Nunc, Roskilde, Denmark). The cryovials were placed in a freezing container (Fisher Scientific

Nalgene, Loughborough, UK) and were kept in -70°C freezer for 24 hours and were then placed in liquid nitrogen.

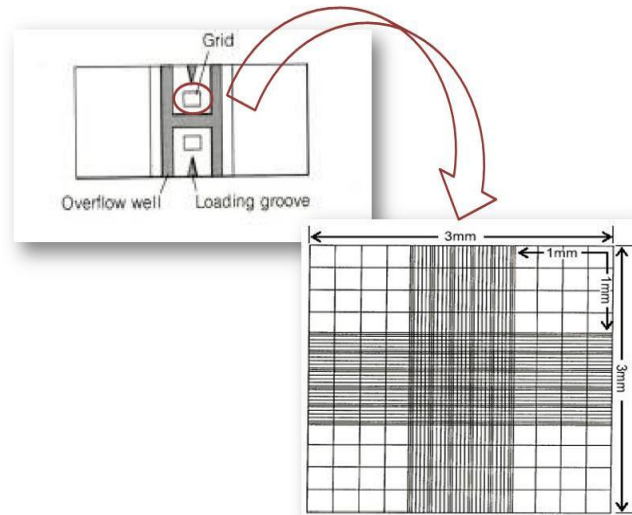


**Figure 2.1.** A schematic image of a Neubauer haemocytometer slide and the grids used to count the cells.

### ***2.1.5 .Cell Culture from Frozen Samples***

Cryovials containing cells were removed from liquid nitrogen and placed in a waterbath at 37°C for 1-2 minutes to thaw. The cryovials were wiped with IMS prior to opening. The content of each vial was then transferred to 75cm<sup>2</sup> flask. 10 ml supplemented DMEM F:12

(without L-glutamine) was added slowly to the flasks. This was done to provide the time and the opportunity for the cells to become adapted to the new temperature. The cell suspension was mixed and the volume was made up to 20 ml using the supplemented medium. The flasks were then placed in 37°C humidified chamber (5% CO<sub>2</sub>).

### ***2.1.6. Cytospin Preparation and Cyto centrifuge***

Shandon cytospin (Shandon, Thermo Scientific, Loughborough, UK) (figure 2.2) was used to separate and place a monolayer of cells on slides while preserving their integrity. The slides were assembled with filter cards (Shandon, Thermo Scientific) and cytofunnel disposable sample chambers (Shandon, Thermo Scientific) and they were then placed in cytoclips (Shandon, Thermo Scientific) (figure 2.3). 100 µl of cell suspension containing  $1 \times 10^6$  cells was placed in each cytofunnel. The samples were then spun at 500 rpm for 5 minutes in room temperature.



**Figure 2.2.** A Shandon cytopspin (Shandon, Thermo Scientific).

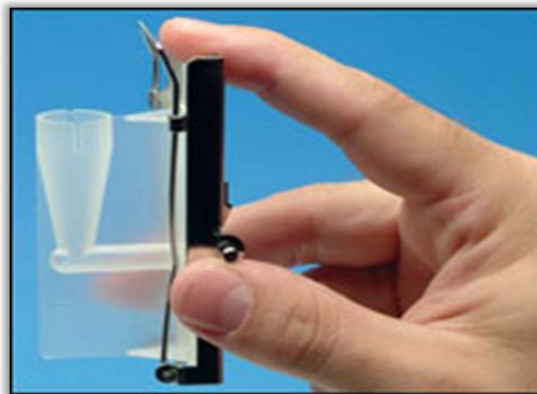


**Figure 2.3.** Image of assembled filter card, cytofunnel, and cytoclip.

## ***2.2. Cell Stress Stimuli***

### ***2.2.1. Cisplatin***

Cisplatin was used to induce cell cycle arrest in BT4C cells. 100 mg of this drug was purchased from Sigma-Aldrich (P4394) in powder form.

#### ***2.2.1.1 .Preparing Cisplatin for Cell Treatment***

To prepare a stock solution of cisplatin with the concentration of 200 mM, 100 mg of this drug was dissolved in 1.66 ml sterile DMSO. 100 µl aliquots of the prepared cisplatin stock solution were placed in sterile microcentrifuge/ependorf tubes and stored in -70°C freezer.

The cells were exposed to 50 µM cisplatin for various times. On the day of treatment, the required amount of cisplatin stock solution was removed from the freezer and thawed at room temperature. Cisplatin was further diluted to a concentration of 50 µM in fresh, supplemented DMEM F: 12 (without L-glutamine).

#### ***2.2.1.2. Adding Cisplatin to the Cells***

Cultured cells were incubated overnight. Medium was removed and the cells were washed with PBS. Fresh DMEM F:12 (without L-glutamine) containing 50 µM cisplatin was added to the cells. The flasks containing cultured cells were further incubated for 12, 24, 48, or 72 hours in humidified chamber (5% CO<sub>2</sub>) at 37°C.

### ***2.2.2. Culture in Phosphate Buffered Saline***

To cause necrosis in BT4C cells, starvation was induced by culturing cells in PBS (1x) (without CaCl<sub>2</sub> and MgCl<sub>2</sub>) (GIBCO, Invitrogen Co). BT4C cells were cultured in DMEM F:12 medium overnight. The medium was then removed and 20 ml PBS (without CaCl<sub>2</sub> and MgCl<sub>2</sub>) was added to the flasks. The cells were further incubated in humidified chamber (37°C, 5% CO<sub>2</sub>) for 4, 6, 12, 18, or 24 hours.

### ***2.3. Harvesting Cells for Morphological and Molecular Assays***

After exposing the cells to PBS or cisplatin for a specific duration; the medium containing cisplatin or the PBS was removed from the flask and transferred to 50 ml sterile centrifuge tube. The cells were washed with PBS and the used PBS was transferred to the 50 ml tube. 1 ml accutase was added to the flask and after covering the cells with accutase the flask was placed in the humidified chamber (37°C, 5% CO<sub>2</sub>) for 1-2 minutes until the cells were lifted off from the flask surface. Using the medium in the tube, the cells were transferred to the 50 ml centrifuge tube. The cell suspension containing attached and floating cells was then centrifuged at 250 rpm (Centrifuge 5804, Eppendorf, Cambridge, UK) for 6 minutes at room temperature. The supernatant was then removed and the cells were resuspended in 10 ml PBS and pipetted up and down few times. The cell suspension was centrifuged again at room temperature for 6 minutes at 250 rpm. After centrifuging, PBS was removed and the cell pellet was resuspended again in fresh PBS. In total the cells were washed three times with PBS. The cells were then ready to be used in various morphological and molecular assays as discussed in section 2.5.

## ***2.4. <sup>1</sup>H HR-MAS NMR Spectroscopy***

### ***2.4.1. Harvesting Cells for <sup>1</sup>H HR-MAS NMR Spectroscopy***

After each time point the medium or PBS was removed from the flask and transferred to a sterile 50 ml centrifuge tube. The cells were then washed with ice-cold PBS (without CaCl<sub>2</sub> and MgCl<sub>2</sub>) and scraped from the flask surface. The detached cells were added to the tube and centrifuged for 6 minutes at 250 rpm. The supernatant was removed and the cell pellet containing floating and previously attached cells was washed 3 times with 10 ml ice-cold PBS (without CaCl<sub>2</sub> and MgCl<sub>2</sub>). The number of cells in 10 ml ice-cold PBS (without CaCl<sub>2</sub> and MgCl<sub>2</sub>) was counted according to the method described in section 2.1.3. To prevent biochemical degradation, approximately 50x10<sup>6</sup> cells (from two 75 cm<sup>2</sup> flasks) were snap frozen and kept in liquid nitrogen. Cells were kept on ice during preparation.

### ***2.4.2. <sup>1</sup>H HR-MAS NMR Spectroscopy Sample Preparation***

Just before performing <sup>1</sup>H HR-MAS NMR spectroscopy, the prepared cells in cryovials were removed from liquid nitrogen and thawed in room temperature. 32 µl of harvested cells and 8 µl (20% of the total volume placed in the nanoprobe) dideuterium monoxide (D<sub>2</sub>O; Sigma-Aldrich) were placed in a 4-mm gHX nanoprobe (Varian NMR Inc, Oxford, UK). After thawing, the cells were placed on ice and were kept on ice until the samples were inserted in the pre-cooled NMR probe. The approximate time from thawing to experimentation was 5 minutes.

### 2.4.3. Performing $^1\text{H}$ HR-MAS NMR Spectroscopy

A vertical bore Varian 600 MHz (14.1T) spectrometer (figure 2.4) with a three channel Inova console running VNMRj software, was used to record magic angle spinning spectra of prepared samples (The Henry Wellcome Building, The University of Birmingham). The samples were spun at 2500 Hz at a probe temperature of 0.1°C corresponding to a rotor temperature of 6.7°C (methanol calibration).

A pulse and acquire sequence with a repetition time of 3.3s was applied to collect 256 scans. The repetition time of 3.3s was used based on the previous work carried out by Peet *et al.* (167). They examined the use of prolonged repetition time in  $^1\text{H}$  MRS of a human neuroblastoma cell line. Peet *et al.* increased the repetition time to 8.3s and discovered an average increase of less than 10% in the metabolite concentration. This study indicated prolonging the repetition time has little effect on the metabolite concentration and increases the experimental time. Therefore, a repetition time of 3.3s was used here; resulting in 14 minutes acquisition time for each sample.

The receiver band width was 7200 Hz with 16k complex points in the free induction decay. The rotor was spun at a speed of 2500 Hz. Tuning and matching was carried out on each sample and a presaturation pulse (1 sec) at water frequency was applied to suppress the water signal before applying a 90° read pulse.



**Figure 2.4.** A Varian 600 MHz spectrometer at the Henry Wellcome Building, The University of Birmingham.

#### ***2.4.4. Assigning and Quantitating $^1\text{H}$ HR-MAS NMR Signals***

The spectra were phased and referenced to the creatine signal at 3.03 ppm and the peaks were assigned and quantified. Metabolites were quantified using an automated algorithm, TARQUIN (109) and  $^1\text{H}$  HR-MAS NMR visible lipids were quantified using a modified version of this algorithm. The TARQUIN algorithm measures the metabolite and lipid quantities by fitting a series of simulated individual metabolite and lipid signals to the experimentally acquired data (figure 2.5 and table 2.1). The relative quantity of  $^1\text{H}$  HR-MAS NMR visible lipids was determined in relation to the macromolecule signals at 0.94,

1.68, and 3.00 ppm. The assignment of the resonances at 0.94, 1.68, and 3.00 ppm to macromolecules rather than mobile lipids follows assignments by Opstad *et al.* (110) and is substantiated by their broad nature, strong correlation with each other and invariance during cisplatin treatment and PBS exposure when compared with other spectral features.

The relative concentrations of metabolites were measured in relation to the sum of the metabolites in each sample. For *in vivo* studies, absolute quantification is difficult to attain and metabolites are usually quoted as a ratio relative to other metabolites or tissue water. In this work metabolite alterations during cell death were investigated. Deregulation of osmolyte homeostasis followed by increase in cell volume or cell shrinkage are features associated with necrosis and apoptosis, respectively. Therefore, water may alter between investigations. Where serial  $^1\text{H}$  MRS is undertaken to investigate response to treatment, relative metabolite concentrations are likely to be the most consistent measurements. Hence this approach was used in this *in vitro* work to measure the relative concentration of the metabolites.

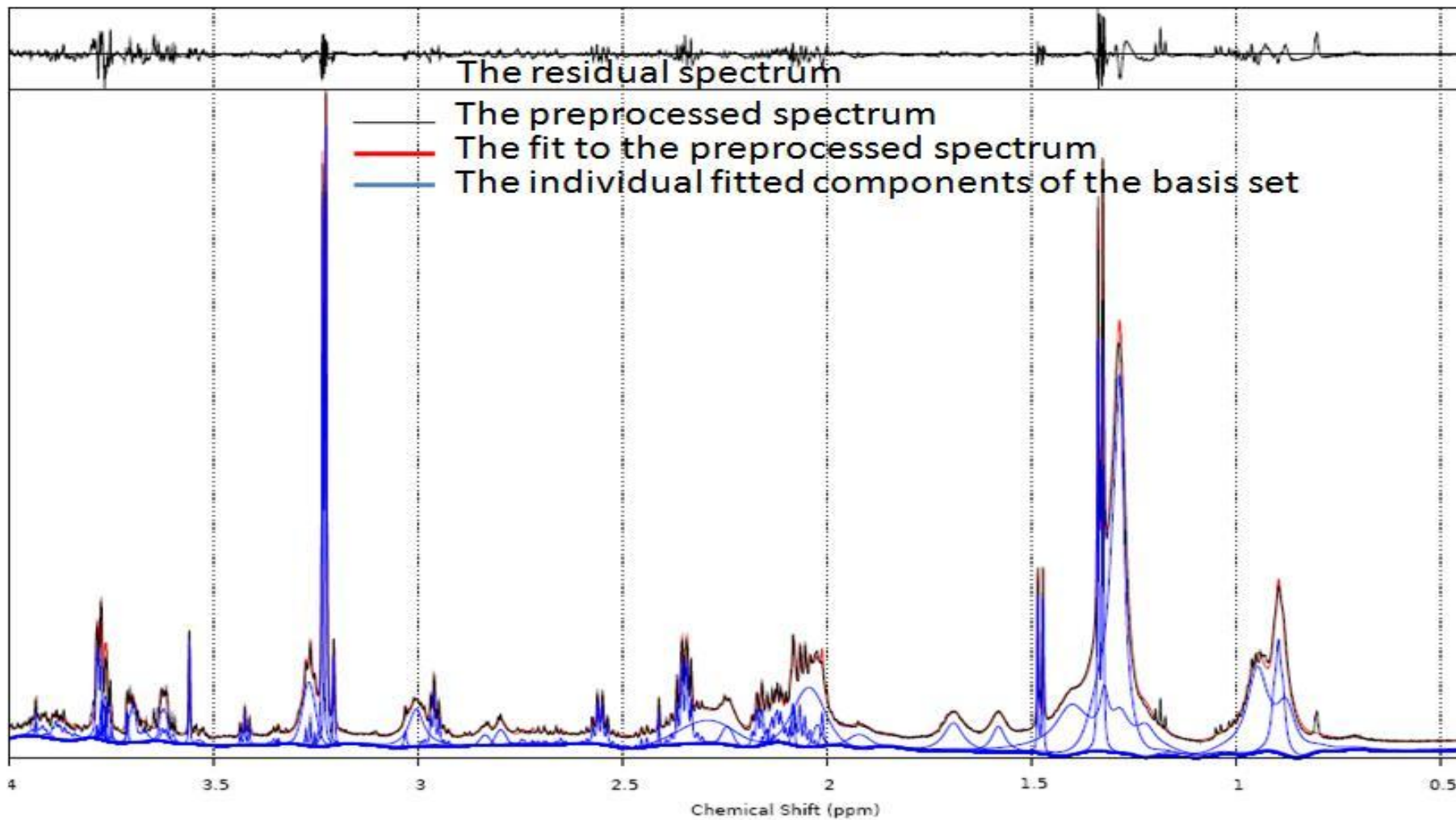


**Figure 2.5.**A typical spectrum of BT4C cells. The TARQUIN algorithm was used to identify and quantitate metabolite and lipids in the spectrum. The residual spectrum is shown at the top section of the image.

(Preprocessed spectrum  Fit to the preprocessed spectrum 

The individual fitted components of the basis set )

metabolite	Moiety	Chemical Shift (ppm)	metabolite	Moiety	Chemical Shift (ppm)
<b>Acetate</b>		1.90	<b>Glutamine</b>		3.75
<b>Alanine</b>		3.77			2.12
		1.46			2.1
<b>Aspartate</b>		3.89			2.43
		2.80			2.45
<b>Choline</b>		3.18			6.81
		4.05			7.52
		3.50	<b>GPC</b>	Glycerol	3.6
<b>Creatine</b>		3.02			3.67
		3.91			3.9
		6.64			3.87
<b>Glutathione</b>	Glycine	3.76			3.94
		7.15		Choline	4.31
	Cystein	4.50			3.65
		2.92			3.21
		2.97	<b>Glycine</b>		3.54
		8.17	<b>Lactate</b>		4.09
	Glutamate	3.76			1.31
		2.15	<b>Myo- inositol</b>		3.52
		2.14			4.05
		2.51			3.52
		2.56			3.61
<b>Glutamate</b>		3.74			3.26
		2.03			3.61
		2.12	<b>PC</b>		4.28
		2.33			3.64
		2.35			3.2
<b>Taurine</b>		3.42	<b>PEth</b>		3.97
		3.24			3.21
<b>Guanidinoacetate</b>		3.70	<b>Scyllo-Inositol</b>		3.34
			<b>Succinate</b>		2.39

**Table 2.1.** Metabolites identified by TARQUIN algorithm. The chemical shifts assigned to each of the metabolites and J-coupling properties are used to identify signals of a spectrum.

## ***2.5. Assessing Cell Viability and Cell Death***

### ***2.5.1. Trypan Blue Staining***

The cells were harvested as described in section 2.3. The cell pellet was resuspended in 10 ml PBS. A volume of cell suspension in PBS was mixed with an equal volume of 0.4% solution of trypan blue (Sigma-Aldrich). The suspension was pipetted a few times and was left at room temperature for 5 minutes. Using a sterile transfer pipette one drop (~20  $\mu$ l) of the cell mixture in trypan blue was placed on a Neubauer haemocytometer and the number of dead and viable cells in 3 independent samples was counted as described in section 2.1.3. Microscopic observation of trypan blue stained samples distinguishes viable cells as bright, unstained cells and the dead cells as dark and blue stained cells (figure 2.6).



**Figure 2.6.** Trypan blue staining of BT4C cells. Dead cells appear darker and viable cells are identified as brighter, unstained cells. Only a few of the dead cells are labelled in this image.

## ***2.5.2. Haematoxylin and Eosin Staining***

### ***2.5.2.1. Preparing Cells for H&E Staining***

The cells were harvested as described in section 2.3 and resuspended in 10 ml PBS. The number of cells was then counted according to the method described in detail in section 2.1.3 and the volume of the cell suspension was adjusted so the number of cells was approximately  $1 \times 10^7$  per ml. 100  $\mu$ l of the cell suspension was then placed on slides using a cytocentrifuge (described in section 2.1.6). The slides were then immediately fixed in 70% ice-cold methanol (Sigma-Aldrich) and air dried.

### ***2.5.2.2. H&E staining of the prepared slides***

The slides were placed in haematoxylin for 5 minutes and then in acid ethanol few times for few seconds. After the slides were washed with water they were placed in eosin for 30 seconds. The samples were dehydrated in series dilutions of alcohol (95 and 100%) and were placed in 100% alcohol and xylene (50:50). Finally using a mounting solution coverslips were mounted on the prepared slides.

With H&E dyes, viable, apoptotic and necrotic cells are distinguished based on their morphological features. Apoptotic cells contain condensed and fragmented chromatin and necrotic cells have diffused nuclei and at later stages disrupted cell membranes. The viable cells are distinguished from dead cells by their homogenous chromatin (figure 2.7). The percentages of viable, apoptotic, and necrotic cells were calculated in 500 random cells in each prepared sample.

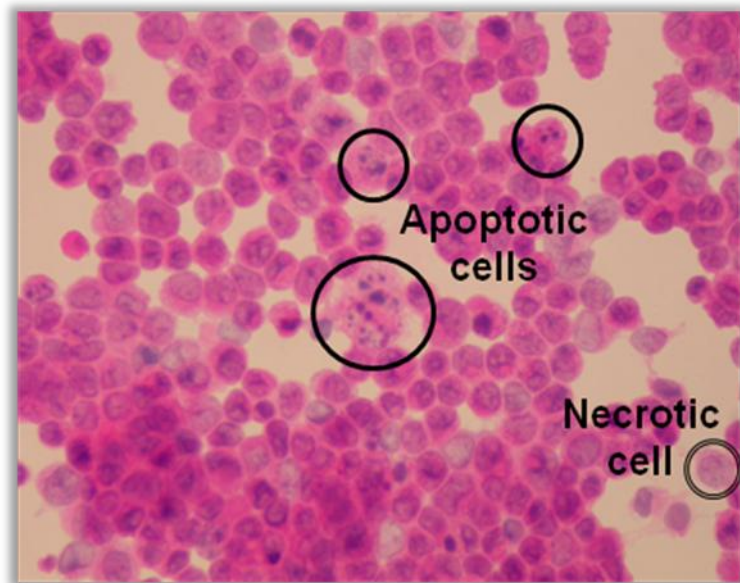


**Figure 2.7.** Haematoxylin and eosin staining of BT4C cells. Morphological characteristics of the cell nuclei help in identifying necrotic and apoptotic cells. Apoptotic cells contain fragmented nuclei and necrotic cells have dispersed nucleus.

### ***2.5.3. Transmission Electron Microscopy***

#### ***2.5.3.1. Sample Preparation for Transmission Electron Microscopy***

The cells were harvested and washed according to the procedures discussed in section 2.3. After removal of PBS, the cell pellet was fixed in 2.5% glutaraldehyde (TAAB Laboratories Equipment Ltd, Aldermaston, UK) solution in PBS, overnight. The samples

were post-fixed in 1% osmium tetroxide (OsO<sub>4</sub>; Oxxem, Reading, UK) for 1 hour at room temperature. They were then dehydrated in alcohol gradients.

#### ***2.5.3.2. Cutting the Samples and observing with Transmission Electron Microscopy***

The samples were embedded in epoxy resin (TAAB Laboratories Equipment Ltd) by routine procedures. Ultrathin sections of approximately 90 nm were prepared and placed on copper grids. The sections were then stained in saturated uranyl acetate (TAAB Laboratories Equipment Ltd) and lead citrate (TAAB Laboratories Equipment Ltd) solution in 0.1 mol low carbonate NaOH (VWR International, Lutterworth, UK). The samples were observed by Zeiss-EM 109 transmission electron microscope (Zeiss Ltd, Welwyn Garden City, UK) and images were captured using a TFP (trans-fibre optic photography) camera system (Zeiss Ltd).

#### ***2.5.4. Flow Cytometry Analysis of Annexin V-FITC labelled and Propidium Iodide stained Cells***

ApoDETECT annexin V-FITC kit was purchased from Zymed laboratories (Invitrogen Immunodetection) and the supplied protocol was used to label and stain the samples.

The cells were harvested as described in section 2.3. They were resuspended in the 1 x binding buffer (part of the kit, 10 mM hepes/NaOH, pH 7.4, 140 mM NaCl, 2.5 mM CaCl<sub>2</sub>). The cell density was adjusted to 2x10<sup>6</sup> cells/ml. After adding 10 µl FITC conjugated Annexin V to 190 µl of the cell suspension in binding buffer, the samples were

mixed gently and incubated in the dark for 10 minutes at room temperature. 200 µl 1 x binding buffer was added to the cells and the suspension was centrifuged at 3000 rpm for 1 minute. Supernatant was removed and the cells were resuspended in 190 µl 1 x binding buffer. 10 µl of 20 µg/ml PI (part of the kit) was added and the cells were transferred to FACS tube and flow cytometry was immediately performed. The samples were evaluated on a Coulter EPICS XL analyser (Beckman Coulter Ltd, High Wycombe, UK) and the data were analysed using FlowJo (version 7.5, Tree Star Inc, Oregon, USA) (111).

### ***2.5.5. Detecting DNA Fragmentation***

In apoptotic cells, endogenous endonuclease cleaves DNA in between nucleosomes and in the linker regions. The fragments of 180-200 bp are visualised as a typical ladder pattern on gel electrophoresis and are convincingly good end markers of apoptosis in cells (81, 89, 96, 102).

#### ***2.5.5.1. Preparing Buffers***

A litre of 10 x TBE buffer was made from 108 g tris base, 55 g boric acid, and 40 ml 0.5 M EDTA (pH 8). A 0.5 x dilution of this buffer was made with deionised water and was used for DNA electrophoresis. The compounds were purchased from Sigma-Aldrich.

### ***2.5.5.2. Preparing the Sample and Running the Agarose Gel***

Cells were harvested as described in section 2.3. 20 million cells were resuspended in 10 ml PBS. The samples were centrifuged at 2300 rpm for 3 minutes. The supernatant was removed and the cell pellet was vortexed vigorously in the remaining supernatant. While the samples were vortexed, 3 ml cell lysis solution (Puregene, Genra Systems, Crawley, UK) was added to the cell suspension. 15 µl RNase A (Puregene, Genra Systems) solution was added and the samples were mixed by inverting the tube 25 times. The cells were then incubated at 37°C for 30 minutes. The samples were then removed and placed on ice for 5 minutes. After adding 1 ml protein precipitation solution (Puregene, Genra Systems), the samples were vortexed vigorously for 20 seconds. Cell suspension was centrifuged at 4600 rpm for 10 minutes. The supernatant containing DNA was removed from the protein pellet, and 3 ml 100% isopropanol (Sigma-Aldrich) was added to the supernatant. The samples were mixed and DNA became visible by inverting the tube gently 3-5 times. Clump DNA was removed to an eppendorf tube and centrifuged at 130 x 100 rpm for 3 minutes. After removal of the supernatant, 1 ml 70% ethanol (Sigma-Aldrich) was added to the DNA. The tube was inverted 3-5 times to wash the DNA pellet. Ethanol was then removed by centrifuging the samples for 1 minute at 130 x 100 rpm. The sample was air dried for 20 minutes and then 50 µl DNA hydration solution (Puregene, Genra systems, UK) was added. To rehydrate the DNA, the tubes were placed in 50°C hot block for 10 minutes and were kept at room temperature over night. DNA was diluted with deionised water and stained with bromophenol blue (3',3'',5',5''-tetrabromo phenolsulfonphthalein) prior to loading on the gel. 1kb DNA ladder (Invitrogen Co) was used as positive control and deionised water was used as negative control.

1% agarose gel (Sigma-Aldrich) was made in 0.5 x TBE solutions containing (2x10<sup>5</sup>:1) ethidium bromide (10 mg/ml). The gel was placed on a plastic tray in an electrophoresis tank and submerged just beneath 0.5 x TBE. The samples were placed on the gel and were run for 90 minutes at 120 V. The DNA fragments were observed by ultraviolet light.

## ***2.6. Assessing Cell Cycle Phase Distribution***

To identify cell cycle distribution in untreated and cisplatin exposed cells, samples were stained with PI and analysed by flow cytometry. The position of the cells in the cell cycle can be determined by measuring the amount of DNA present in the samples. The amount of DNA in cells at G2 or M stage is twice the concentration of DNA detected in cells at G0 or G1 phase and the detected amount of DNA in cells at S phase is variable. In this method, PI is attached to double strand DNA and the amount of the stained DNA is measured by flow cytometry.

### ***2.6.1. Preparing Buffers and Solutions***

DNase solution was made by dissolving DNase (Deoxyribonuclease I from bovine pancreas; Sigma-Aldrich) in SMT buffer (20 mM trizma base (2-Amino-2-hydroxymethyl)-1,3-propanediol), 250 mM sucrose, 5 mM MgCl<sub>2</sub>, pH=7.4; Sigma-Aldrich) at a concentration of 500 µg/ml. The prepared DNase solution was aliquoted and stored at -20°C. On the day of testing the solution was thawed at room temperature. RNase solution was made from ribonuclease A (from bovine pancreas; Sigma-Aldrich) and PBS

(without CaCl<sub>2</sub> and MgCl<sub>2</sub>) at a concentration of 50 µg/ml. The aliquots were stored in -20°C freezer and thawed at room temperature on the day of the experiment. To make DNA staining solution with a concentration of 1 mg/ml, PI (Sigma-Aldrich) was dissolved in PBS (without CaCl<sub>2</sub> and MgCl<sub>2</sub>). The solution was then filtered using a 0.22 µm syringe tip filter. This was carried out to remove solid and undissolved stain. The prepared staining solution was kept in the dark and at 4°C.

### ***2.6.2. Preparing Untreated Samples for Flow Cytometry Analysis***

Untreated samples were harvested as described in section 2.3. The number of cells was counted and approximately 1x10<sup>6</sup> cells were fixed. While the cells were vortexed vigorously, 10 ml 70% cold ethanol (Sigma-Aldrich) was added. The first 1-2 ml was added drop by drop. The cells were kept as cold as possible during this procedure. As soon as the fixative was added to the cells, samples were placed in -20°C freezer for at least half an hour. The cells were then centrifuged at 1750 rpm for 5 minutes. The fixative was removed and the cells were washed with 10 ml PBS. After centrifuging at 1750 rpm for 5 minutes supernatant was removed and the cells were resuspended in 1 ml RNase solution (Final concentration used 50 µg/ml). The suspension was then transferred to a FACS tube and incubated for 20 minutes at 37°C. The samples were removed and 50 µl PI solution was added. The samples were gently mixed and incubated for a further 10 minutes at room temperature.

### ***2.6.3. Preparing Cisplatin Exposed Cells for Flow Cytometry Analysis***

Cisplatin treated cells were harvested according to the procedures described in section 2.3. Cells were counted and  $1 \times 10^6$  cells were removed to an eppendorf tube. Cells were resuspended in 1 ml DNase solution with final concentration of 500  $\mu\text{g/ml}$  and were incubated at 37°C for 15 minutes. The tubes containing cells and the DNase solution were then placed in an ice bath. The cells were kept on ice for 10 minutes to inactivate DNase. The cells were then centrifuged at 1000 rpm for 5 minutes and the DNase solution was removed. Cells were vortexed vigorously in the remaining DNase. To fix the cells, 10 ml ice cold 70% ethanol was added while vortexing. The first 1-2 ml of the fixative was added drop by drop. By placing the samples on ice in between vortexing, the cells were kept as cold as possible. After adding the fixative, the tubes containing the cells were placed in -20°C freezer for at least 30 minutes. After 30 minutes, the cells were centrifuged at 1750 rpm for 5 minutes and the supernatant was removed. The cells were then washed with 10 ml PBS and resuspended in 1 ml RNase solution giving a final concentration of 50  $\mu\text{g/ml}$ . Samples were transferred to FACS tubes and placed in 37°C chamber for 20 minutes. 50  $\mu\text{l}$  PI was added after 20 minutes and the cells were mixed gently. The samples were analysed by flow cytometer after 10 minutes incubation in room temperature.

### ***2.6.4. Flow cytometry analysis***

Cell cycle distribution was evaluated on a Coulter EPICS XL analyser (Beckman Coulter Ltd). The samples were run and the analysis was stopped automatically after 20,000 events. Both histogram and listmode files were saved and the cell cycle distribution was

determined as percentages after selecting the single cell cycle option of the multicycle software version 3 (Phoenix Flow Systems, San Diego, USA) (figure 2.8).

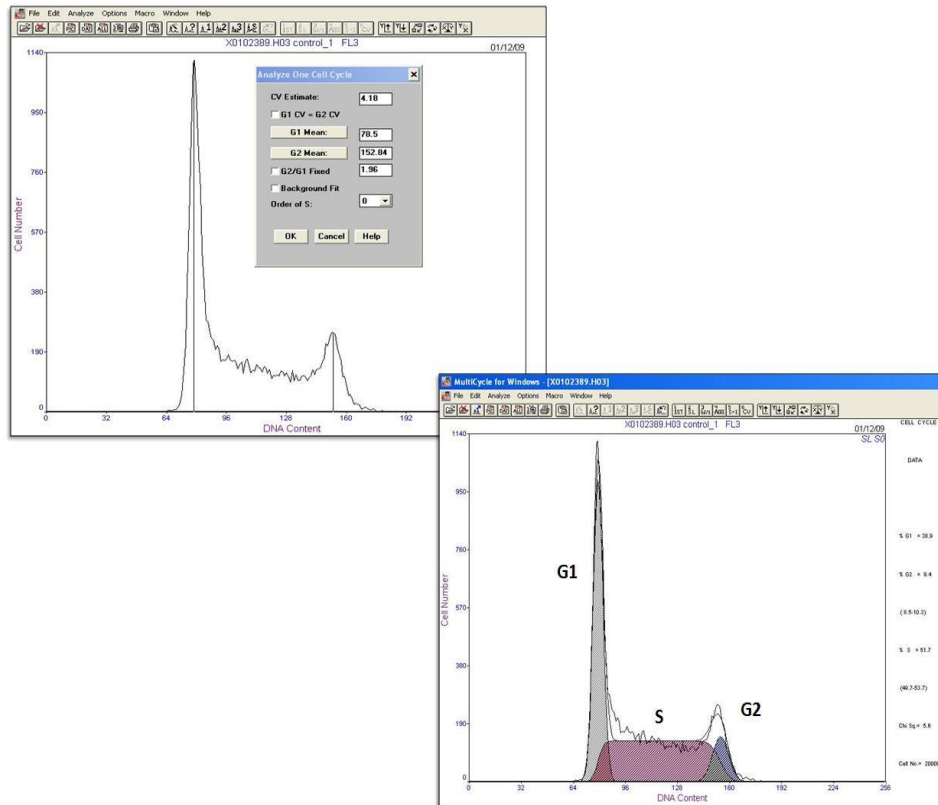


**Figure 2.8.** Cell cycle analysis platform of multicycle software version 3. A control sample is used to define the G1 and G2 ranges. The defined regions are used to fit the treated samples and the optimal fits are presented as fraction of cells in each phase of the cell cycle.

## ***2.7. Nile Red and DAPI Co-Staining***

Nile red or Nile blue oxazone (9-diethylamino-5H-benzo[ $\alpha$ ]phenoxazine-5-one) is an excellent dye for staining lipids (112, 113). Therefore, it was used in this work to detect the presence of cytoplasmic lipid droplets. The yellow-golden lipid droplets in cell cytoplasm were detected at wave lengths of 450-490 nm with fluorescent microscopy. At these wave lengths, neutral lipids such as TGs, cholesterol, and cholesterol esters are detectable (113); indicating the nature of the identified lipid droplets. The faint background in Nile red images represents hydrophobic proteins and amphipathic lipids such as phospholipids in the cell membrane (113). These structures fluoresce red in the wave lengths of 540-580 nm using a Texas red excitation filter.

In order to determine the viability status of the cells containing cytoplasmic lipid droplets and to identify the type of cell death (apoptosis/necrosis) in these cells, DAPI dye in combination with Nile red was used. The advantage of Nile red and DAPI co-staining is that it allows the status of the cells containing lipid droplets to be determined. Viable cells are distinguished by their homogenous nuclei and necrotic cells have inhomogeneous and dispersed chromatin. Cells with condensed and fragmented nuclei were identified as apoptotic cells.

### ***2.7.1. Preparing Nile Red and DAPI Stock Solutions***

A stock solution of 10 mg/ml Nile red (Sigma-Aldrich) in acetone was made. After removal of undissolved stain with filter papers, the staining solution was kept in the dark at 4°C. On the day of staining, Nile red was further diluted to a concentration of 1  $\mu$ g/ml in

PBS. 1 mg/ml DAPI (Sigma-Aldrich) in PBS was made as stock solution and was passed through a filter paper. The prepared solution was stored at 4°C in the dark. A dilution of 0.2 µg/ml was made in PBS on the day prior to staining.

### ***2.7.2. Nile Red and DAPI Staining Procedures***

Nile red staining was carried out based on the procedures described by Greenspan *et al.* (113).

Cells were harvested according to the methods described in detail in section 2.3. The cells were washed with PBS and counted. Approximately  $10^7$  cells were resuspended in 1 ml Nile red with a concentration of 1 µg/ml. The mixture was placed in the dark for 5 minutes. The samples were then centrifuged at 3000 rpm for 1 minute. Nile red was removed and 1 ml PBS was added to the cells. After mixing gently, the cells were placed in the dark for 1 minute. The samples were then centrifuged at 3000 rpm for 1 minute. The supernatant was removed and the cell pellet was resuspended in 0.2 µg/ml DAPI. Samples were incubated in dark for 30 minutes. The stained cells were then placed on the slides using a cytocentrifuge, according to the procedures described in section 2.1.6.

### ***2.7.3. Fluorescence Microscopy and Image Capture***

The slides were visualised using a Nikon E600 microscope coupled to a SPOT RT KE colour 3 shot CCD camera (Diagnostic Instruments Inc, Michigan, USA) for image capture. Nile red stained lipid droplets were observed with a FITC (B-2A) filter set, using an excitation wave length of 450-490 nm. A DAPI UV (UV-2A) filter with excitation

wavelength of 340-380 nm was used to detect DAPI stained nuclei of untreated and treated cells. Images were captured at 40 x magnification monochromatically and in grey scale. Nile red and DAPI signal were pseudo-coloured red and blue respectively before combining.

#### ***2.7.4. Image Processing***

ImageJ 1.38X software (National Institute of Health, Maryland, USA) was used to process the images in gray scale and prior to merging. Using this software, the images were calibrated and their brightness and contrast were adjusted.

The threshold levels of the cell and lipid droplet area were identified from the gray scale Nile red images and were assigned based on their detection on the threshold scale. The average threshold of cells in three gray scale Nile red images were used to identify and measure the cell and lipid droplet area. Measurements were performed on individual cells and results were reported as percentage of cell area covered by lipid droplets. Lipid area was measured in 500 random cells in each prepared sample (figure 2.9). To measure lipid droplet diameter similar procedures were used. The measurements were carried out using ImageJ software and on gray scale images. The diameter of each lipid droplet in the 500 randomly selected cells was measured by drawing a line across the lipid droplet and the results were reported in micrometer ( $\mu\text{m}$ ) (figure 2.10).

The viability status of the cells containing lipid droplets was determined based on the morphological characteristics of DAPI stained nucleus of each cell. The viable cells contain homogenous nuclei and the necrotic cells have inhomogeneous nuclei with

dispersed chromatin. Apoptotic cells are detected as cells with condensed and fragmented nuclei. The numbers of apoptotic, necrotic, and viable cells were counted in 500 cells of each prepared sample and the results were reported as percentages. A second observer independently validated the results.

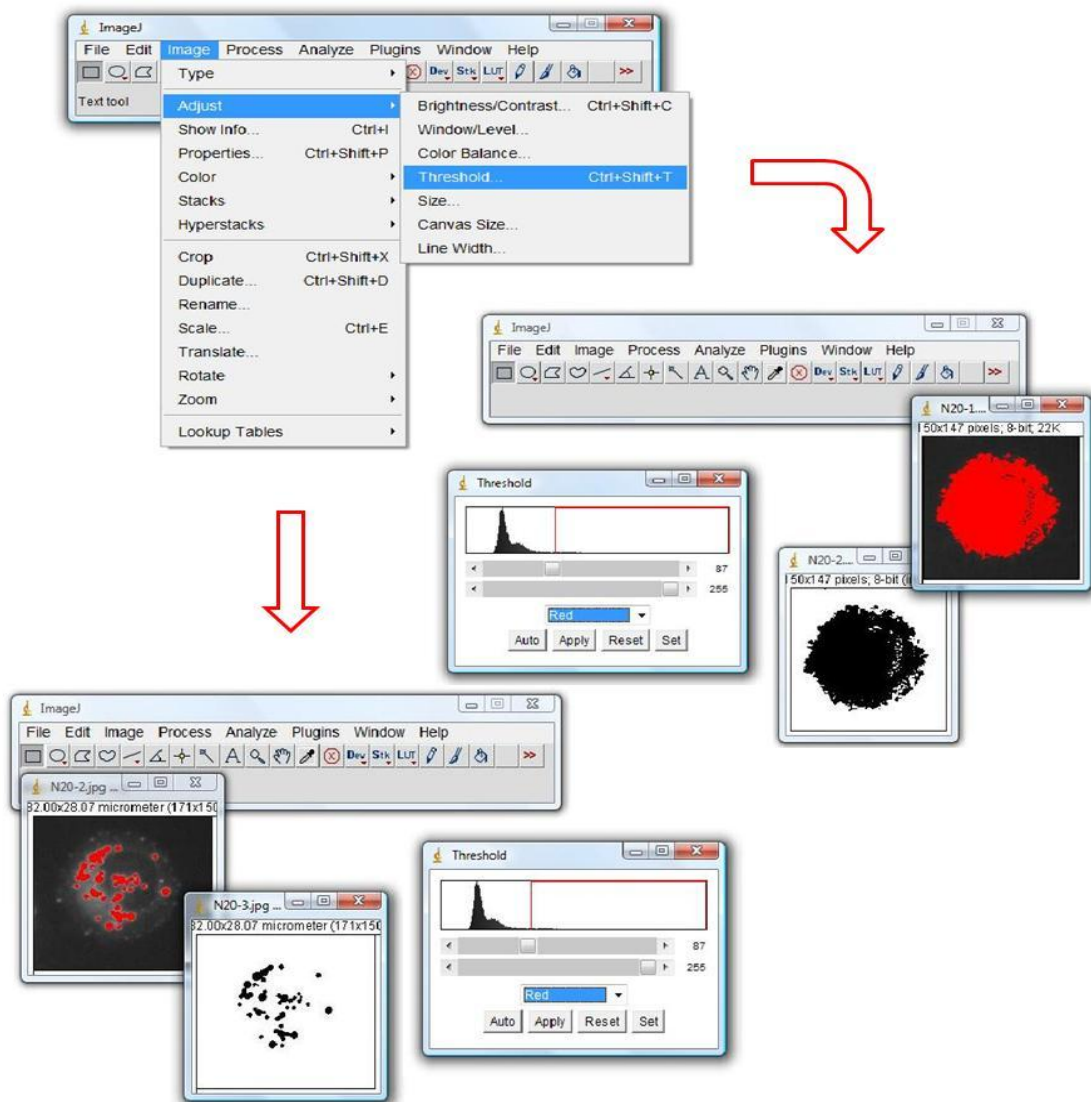


**Figure 2.9.** ImageJ 1.38X platform for threshold detection. The threshold of the lipid droplet and the whole cell were selected based on where they were identified. The selected areas were then measured and the percentage of the cell area covered by lipid droplets was calculated.

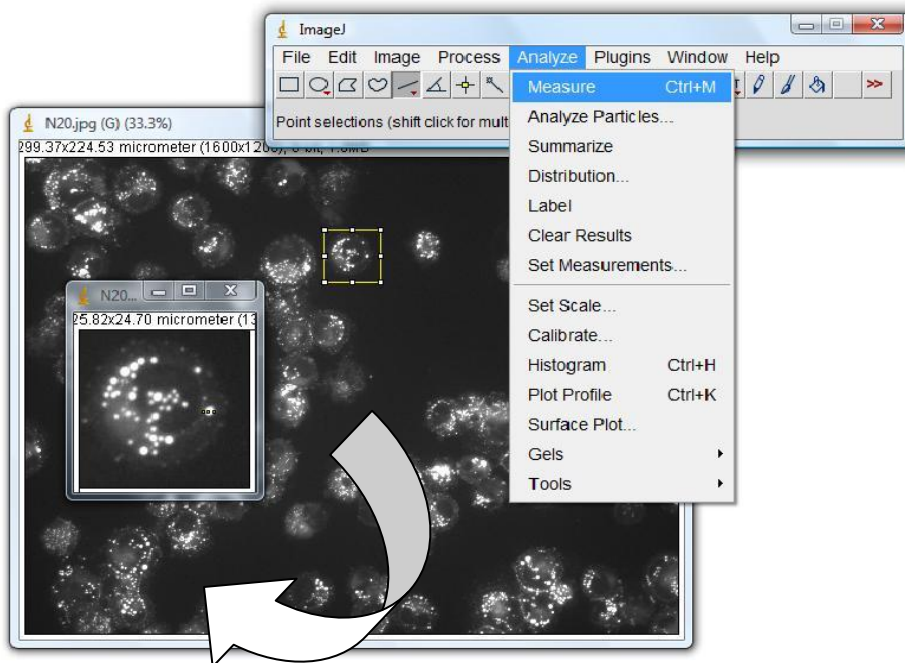


**Figure 2.10.** ImageJ 1.38X platform for image measurements. The diameter of a lipid droplet is measured by drawing a line across the droplet and measuring the length of the line.

## ***2.8. Statistical Tests***

The data in this work were analysed using SPSS version for windows (Version 16, SPSS Inc, Chicago, USA). One-way ANOVA test was performed on the data after testing the normal distribution of the data and the homogeneity of the variance. The significant level was set at 5% and the significant differences presented are between control samples and each time point tested.

## ***2.9. Principal Component Analysis***

Principal component analysis (PCA) is a statistical technique used for analysing and finding patterns in large data sets such as metabolite data collected from MRS. PCA transforms a number of possibly correlated variables to a smaller number of uncorrelated variables known as principal components in order to identify their similarities and differences. Principal component findings can be presented as scores and loading plots. Scores plots project the data in the new coordinate system which is based on the PC values and the loading plots define the size of the contribution of each original data to the PCs. The first principal component accounts for a maximal amount of variability in data as possible and the next principal components represent as much as the remaining variability as possible. Therefore, an overview of the data can be achieved by the score plots of the two most important PCs.

PCA was performed on  $^1\text{H}$  HR-MAS NMR metabolites of cisplatin treated cells of various time points and on the metabolite data set of starved cells of different durations. In addition, PCA was performed on combined metabolite data of cisplatin treated and starved

cells. The PCA scores were shown using scores and loading plots. By performing PCA on the <sup>1</sup>H<sup>R</sup>-MAS NMR metabolite data sets it is easier to determine which metabolites contribute more to the variance between groups and which metabolites distinguish and separate the groups from each other. PCA of the cisplatin exposed/starved cells and the control cells identifies the metabolites that are most different between the control and drug treated/starved cells. In addition, PCA of the combined data identifies metabolites that distinguish the two conditions from each other. The average metabolite quantities of each time point in starved and cisplatin treated cells were calculated and PCA was performed using the MATLAB statistics Toolbox implementation of PCA (Mathworks Inc, Cambridge, UK) (114).

## **CHAPTER 3**

# **<sup>1</sup>H HR-MAS NMR METABOLITE ALTERATIONS OF CISPLATIN INDUCED GROWTH ARREST IN RAT BT4C GLIOMA CELLS**

### ***3.1. Introduction***

Physiological, developmental, and pathological changes alter metabolites in biological system such as cells, tissues and organisms (3, 4). Therefore, analysis of metabolite profiles has the potential to be used in monitoring treatment. MRS with its ability to be used as part of clinical imaging (3, 115), is one of the few techniques applied to monitor metabolite profiles directly in patients (8) and to determine metabolite alterations during treatment with the aim of identifying early biomarkers of successful therapy to monitor tumour treatment response *in vivo* (3, 20). Poor spectral resolution of *in vivo* MRS makes *ex vivo* NMR of tissue (62) and *in vitro* studies of cells and tissue (62, 116) invaluable aid to the *in vivo* studies. Studies on cell lines have the particular advantage of allowing the effects of drugs on a pure population of tumour cells to be studied, giving valuable information on the metabolite changes and molecular pathways involved.

<sup>1</sup>H HR-MAS NMR is used in this chapter and in the following chapter to investigate rat glioma BT4C cells treated with cisplatin. The BT4C glioma cell line has a rapid growth rate and consistent structure and features. It also has the advantage of being used as a xenograft model for *in vivo* MRS studies of cell death (20, 21, 41, 50, 61, 62, 117). *In vitro* NMR of intact cells allows quantitation of several metabolites that may not be detectable *in vivo* and the identified metabolite profile may provide improved insight into the altered biochemical pathways during treatment (118). In the following chapters *in vitro* <sup>1</sup>H HR-MAS NMR has been used to identify markers of cell stress and cell death.

Cisplatin is a chemotherapeutic drug that has shown efficacy against primary CNS malignancies (119) such as glioma (104). This drug inhibits the cell cycle and results in apoptotic cell death. Therefore, cisplatin is an excellent model of cell cycle arrest prior to

apoptosis allowing the potential of metabolite profiles to act as early indicators of treatment response. In this chapter,  $^1\text{H}$  HR-MAS NMR metabolite alterations in response to cisplatin exposure are identified and in the following chapter  $^1\text{H}$  HR-MAS NMR visible lipid changes in growth arrested cells are investigated.

### **3.2. Methods**

BT4C cells were treated with 50  $\mu\text{M}$  cisplatin for 12, 24, 48, or 72 hours. Cell viability was examined by trypan blue and H&E dyes. The type of cell death induced by cisplatin was investigated via flow cytometry of annexin V-FITC labelled and PI stained cells and the detection of DNA fragments on gel electrophoresis. The effects of cisplatin on cell cycle distribution were identified by flow cytometry examination of PI stained cells.

To identify the metabolite and lipid profile of cisplatin exposed BT4C cells,  $^1\text{H}$  HR-MAS NMR spectroscopy was performed. The detected levels of metabolites and lipids were quantitated relative to sum of metabolites and macromolecules, respectively. PCA was carried out on the HR-MAS metabolite data to identify alterations occurring in cisplatin exposed cells. Changes in metabolite profile of cisplatin exposed cells are discussed in this chapter. In chapter 4 alterations in lipid profile of these cells have been studied. Three independently prepared samples were examined at each time point for each of the tests carried out (figure 3.1).

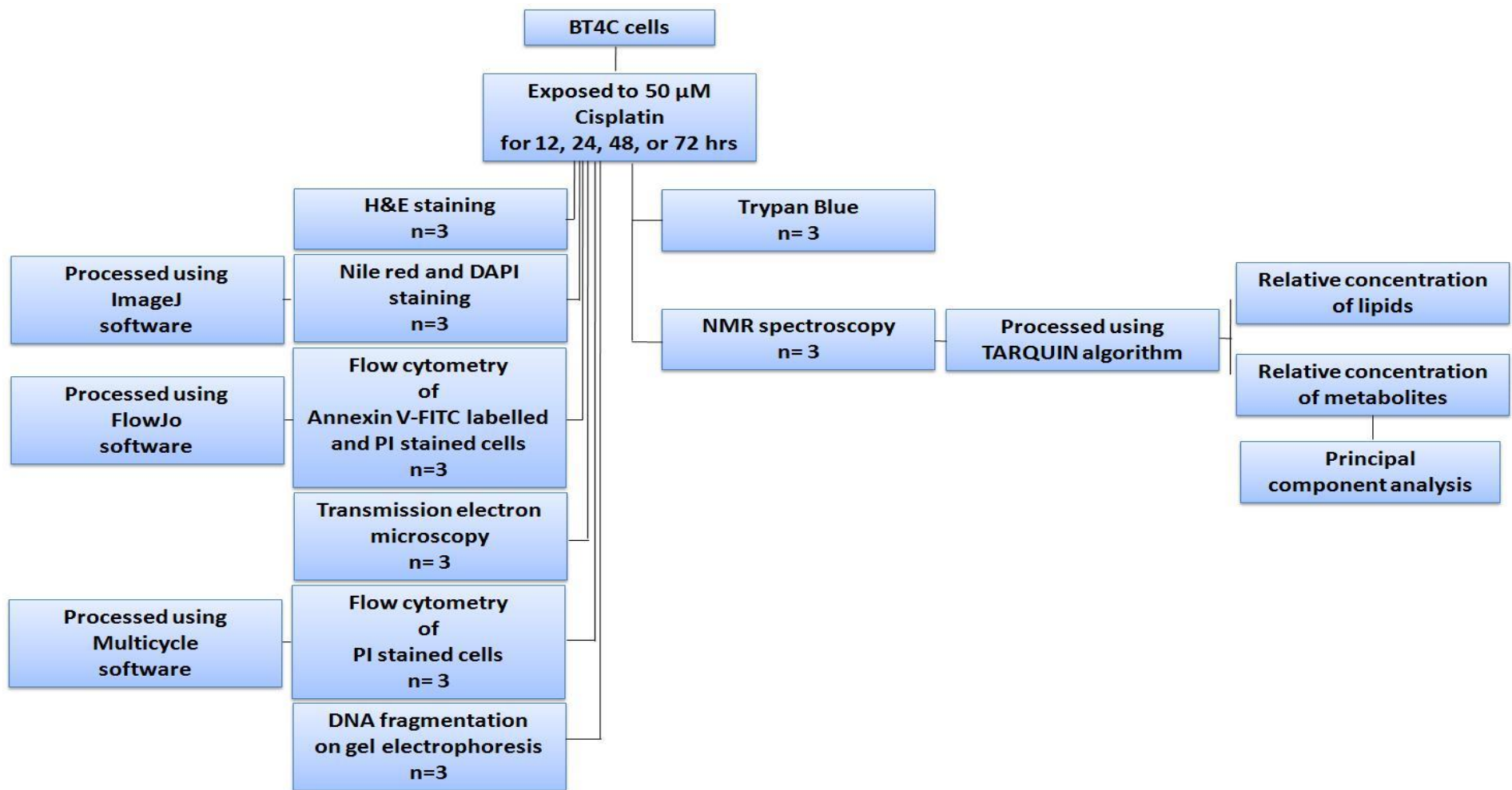


**Figure 3.1.** Flow chart of the methods used in chapter 3 and 4.

### 3.3. Results

#### 3.3.1. Preliminary work

As part of the preliminary work for this study, trypan blue dye was used to investigate BT4C cell death at various concentrations of cisplatin and at different time intervals. Approximately 50% cell death occurred after 72 hours exposure to 50  $\mu$ M cisplatin and the majority of cells were viable at shorter time intervals. With high percentages of viable cells at shorter time points of 12, 24, 48 hours and almost half of the cells being dead after 72 hour cisplatin exposure, for the experiments presented in this thesis, BT4C cells were exposed to 50  $\mu$ M cisplatin for time intervals of 12, 24, 48, or 72 hours (Table 3.1).

	12 hrs	24 hrs	48 hrs	72 hrs
25 $\mu$ M	7 $\pm$ 4.73	9 $\pm$ 1.53	7 $\pm$ 2.31	10 $\pm$ 2.65
50 $\mu$ M	16 $\pm$ 3.40*	17 $\pm$ 4.65*	22 $\pm$ 6.51*	51 $\pm$ 17.47**
75 $\mu$ M	24 $\pm$ 4.04*	50 $\pm$ 9.71**	58 $\pm$ 6.24**	60 $\pm$ 14.93**
100 $\mu$ M	61 $\pm$ 8.54*	68 $\pm$ 13.11**	80 $\pm$ 15.50**	81 $\pm$ 18.04**

**Table 3.1.** Preliminary work was carried out to identify the percentage of dead cells after exposure to various concentrations of cisplatin and at different time intervals. Half of the cells were dead after 72 hrs exposure to 50  $\mu$ M cisplatin and majority of the cells were viable at shorter time intervals. Therefore, this concentration of cisplatin was used in the experiments described in chapters 3 and 4 The percentages of dead cells are presented as mean percentage $\pm$ SD (n=3, \* $p$ <0.05; \*\* $p$ <0.001).

### ***3.3.2. Morphological Analysis of Cell Death: Trypan Blue and H&E Staining***

Trypan blue and H&E staining (figure 3.2) revealed that the majority of cells are morphologically viable up to 48 hours cisplatin exposure but after 72 hours, the percentage of dead cells increased significantly (figure 3.3).

The number of dead cells revealed by trypan blue dye increased from  $5.5 \pm 2.5\%$  in untreated cells to  $22 \pm 6.5\%$  ( $p < 0.05$ ) in 48 hours cisplatin exposed cells, showing that the majority of the cells are viable at this time point (results from 3 independent samples). H&E staining confirmed this finding detecting  $25 \pm 0.5\%$  dead cells ( $p < 0.001$ ) at 48 hours cisplatin exposure (results of 500 random cells from each 3 independent samples). However, at the longer cisplatin exposure time of 72 hours, increasing number of cells showed features of cell death.  $50.8 \pm 17.5\%$  and  $63.2 \pm 6.8\%$  dead cells were detected in these samples by trypan blue and H&E staining, respectively ( $p < 0.001$ ).

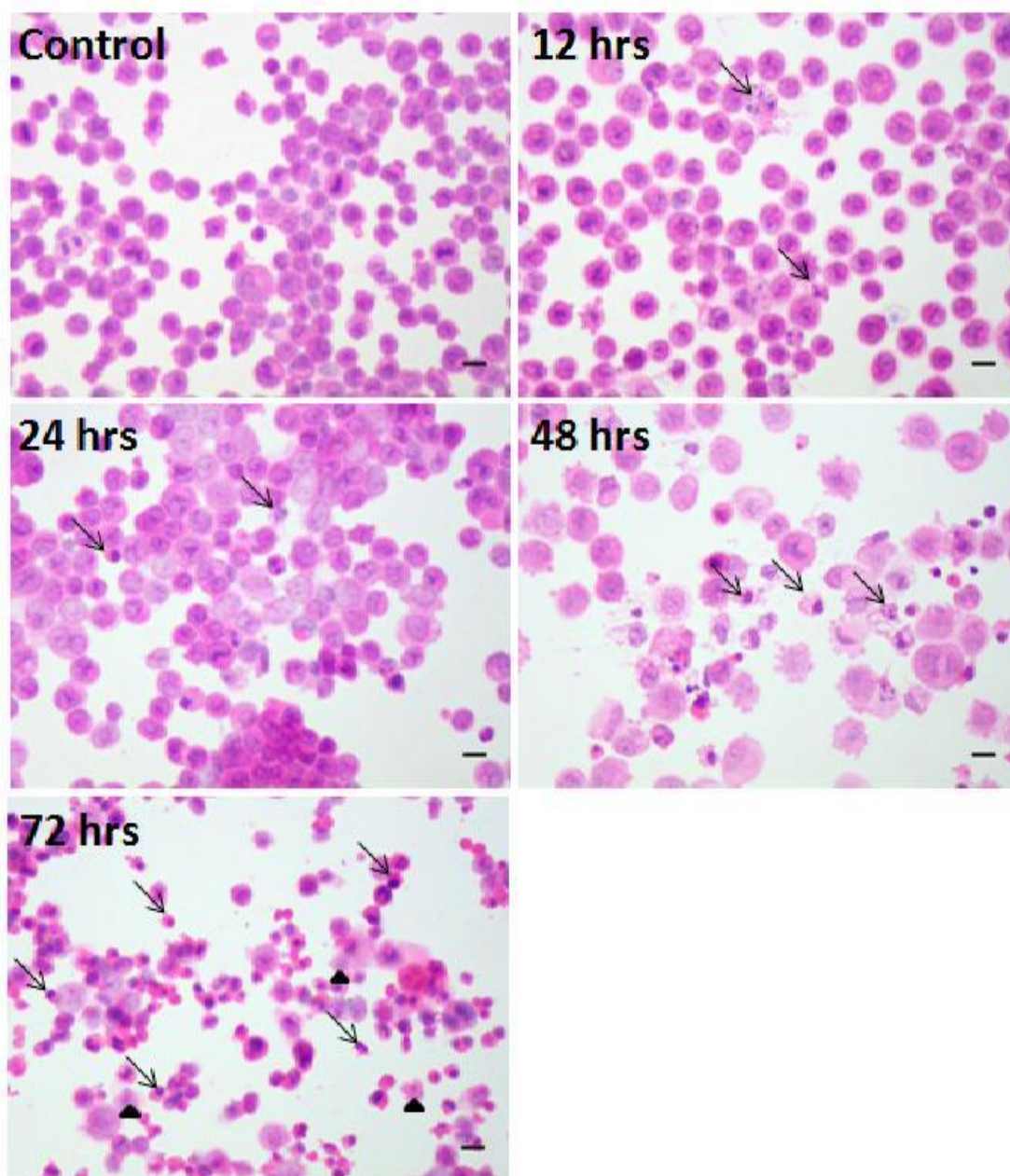


**Figure 3.2.** Images of control and cisplatin treated cells after various time intervals (12, 24, 48, 72 hrs), stained with H&E. The arrows are pointing to apoptotic cells and the arrow heads are showing the necrotic cells. The scale bars represent 20 micrometer.

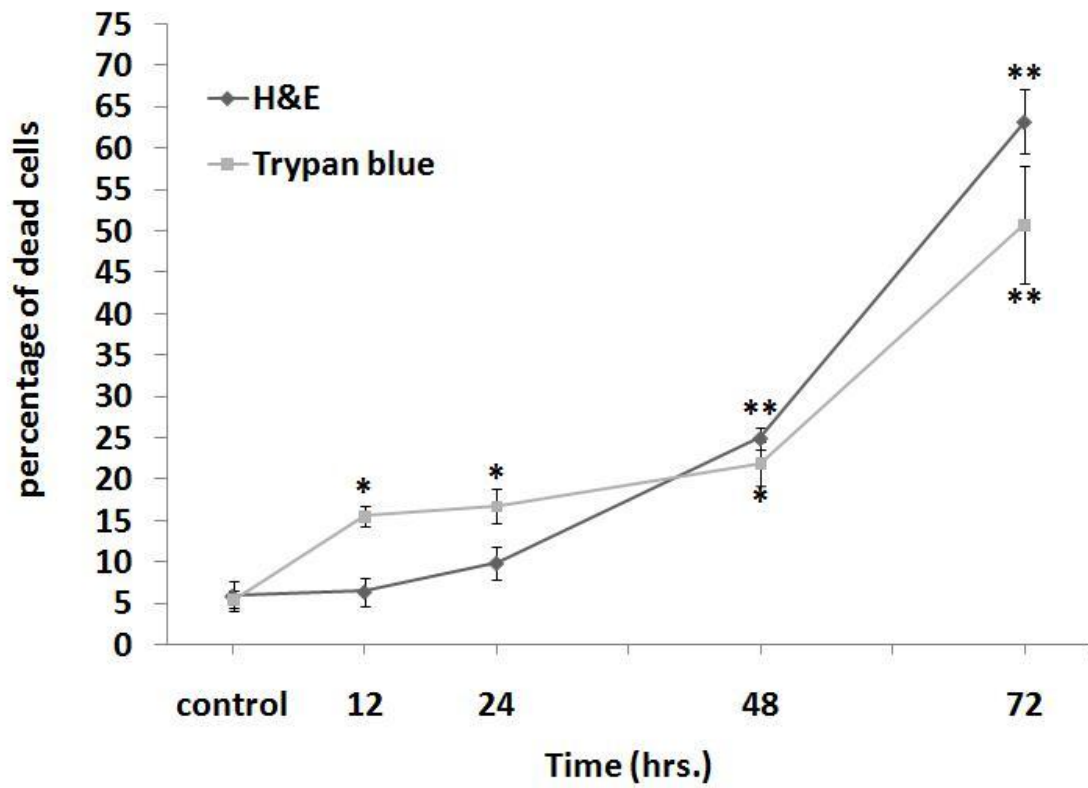


**Figure 3.3.** Percentages of dead cells revealed by H&E (◆) and trypan blue (■) staining in untreated and after 12, 24, 48, or 72 hrs cisplatin exposure in BT4C cells. The error bars are SEM and the significant differences are identified by comparing each time point with the control, untreated samples (n=3 for each time point, \* $p$ <0.05, \*\* $p$ <0.001).

### ***3.3.3. Molecular Analysis of Cell Death: Flow cytometry Analysis of Annexin V-FITC Labelled and PI Stained Cells and Detection of DNA Laddering***

Flow cytometry analysis of annexin V-FITC labelled and PI stained cells of cisplatin exposed samples revealed a trend in the number of identified apoptotic and necrotic cells (figure 3.4). With longer exposure to cisplatin, there was a tendency towards increasing numbers of apoptotic and necrotic cells. However, even up to 48 hours cisplatin exposure, the percentage of apoptotic and necrotic cells were  $15.0 \pm 15.4\%$  and  $9.3 \pm 5.7\%$ , respectively. The flow cytometry findings confirmed the low numbers of dead cells detected via microscopic analysis of stained samples.

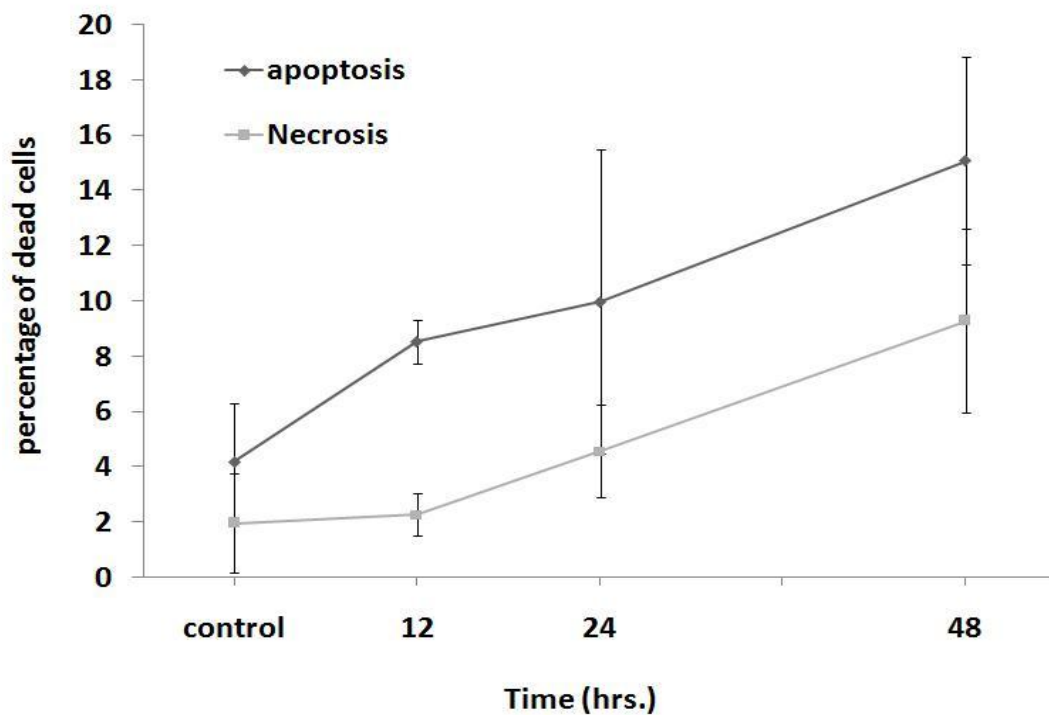


**Figure 3.4.** Percentages of apoptotic and necrotic cells revealed by annexin V-FITC flow cytometry. To confirm the high percentages of viable cells and low numbers of dead cells detected by trypan blue and H&E staining after 12, 24, or 48 hrs cisplatin exposure, cells were labelled and stained with annexin V-FITC and PI. The cells were then analysed with flow cytometer and the data were processed with FlowJo (n=3 for each time point).

In the DNA laddering experiments, the ladder pattern was not detected on the gel electrophoresis of cisplatin exposed BT4C cells until 72 hours of drug exposure when a weak DNA pattern became visible (figure 3.5).

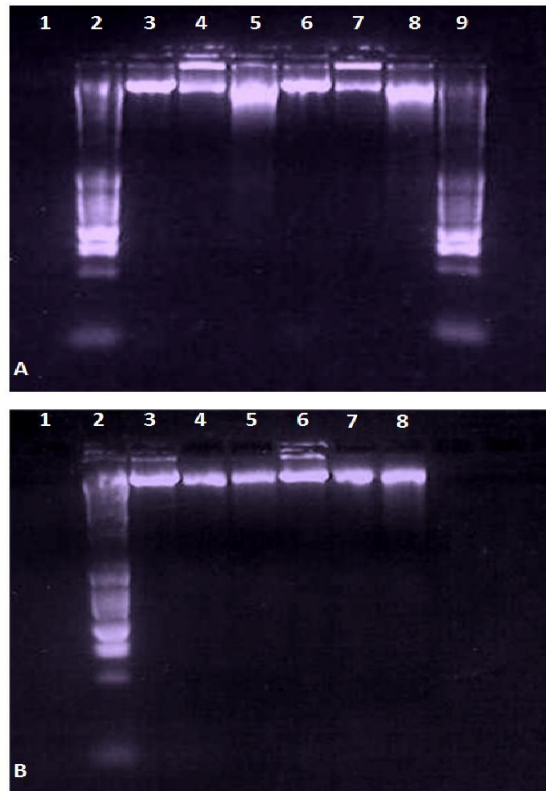


**Figure 3.5.** Detecting DNA fragmentation. DNA was harvested from untreated and cisplatin treated BT4C cells (12, 24, 48, or 72 hrs) according to the procedures described in the method section. The DNA harvested from the cells was run on gel electrophoresis to determine presence of the ladder pattern, a typical late stage marker of apoptosis (**A.** 1: negative control, 2,9: positive control, 3,6: untreated cells, 4,7: 48 hrs cisplatin exposed cells, 5,8: 72 hrs cisplatin exposed cells; **B.**1: negative control, 2: positive control, 3,6: untreated cells, 4,7: 24 hrs cisplatin exposed cells, 5,8: 48 hrs cisplatin exposed cells).

### 3.3.4. Cell Cycle Phase Distribution

To further investigate the status of cells at early stages of cisplatin treatment, the cell growth phase was identified by staining the cells with PI and examining them with flow cytometry as described in chapter 2 section 2.6. Cell cycle measurements clearly indicated accumulation of the cells in G1 Phase of the cell cycle and cell growth arrest in this phase in treated BT4C cells (Table 3.2).

	G1	S	G2/M
<b>control</b>	40.2±1.3	50.5±1.1	9.3±0.3
<b>12h</b>	40.4±1.8	48.3±1.7	11.3±1.1
<b>24h</b>	50.3±1.4**	42.0±1.0**	7.0±0.7*
<b>48h</b>	58.4±1.3 **	39.3±1.5**	2.3±2.8*
<b>72h</b>	44.2±16.4	54.5±17.2	1.3±1.1**

**Table 3.2.** Cell cycle phase distribution. Cells were stained with PI and analysed by flow cytometry. In order to identify cell cycle phase distribution the data were analysed with multicycle software. The percentages of cells in each stage of the cell cycle are presented as mean percentage±SD (n=3, \* $p < 0.05$ ; \*\* $p < 0.001$ ).

With longer exposure to 50  $\mu$ M cisplatin, the percentage of cells accumulating in the G1 stage of the cell cycle increased and after 24 and 48 hours exposure to the drug, the percentage of the cells in the G1 phase increased significantly from 40.2 $\pm$ 1.3% in untreated samples to 50.3 $\pm$ 1.4% and 58.4 $\pm$ 1.3%, respectively ( $p$ <0.001). The proportion of cells in the S phase of the cell cycle decreased with longer exposure to the drug, reaching 39.3 $\pm$ 1.5% after 48 hours of cisplatin exposure ( $p$ <0.001). However, the percentages of cells in G1 and S phase of the cell cycle did not alter after 72 hours of cisplatin exposure compared to the control samples. This may indicate that the cells progressed through the stages of cell cycle which resulted in cell death and an increase in the number of dead cells.

### **3.3.5. $^1\text{H}$ HR-MAS NMR Metabolite Alterations**

$^1\text{H}$  HR-MAS NMR identified several metabolites in cisplatin exposed cells (figures 3.6 and 3.7).

The relative concentration of each of the metabolites was calculated to the sum of all the metabolites. The data showed quantitative time dependent changes in the metabolite profile of BT4C cells in response to cisplatin exposure (table 3.3). Significant differences in the relative levels of metabolites are given in table 3.4.

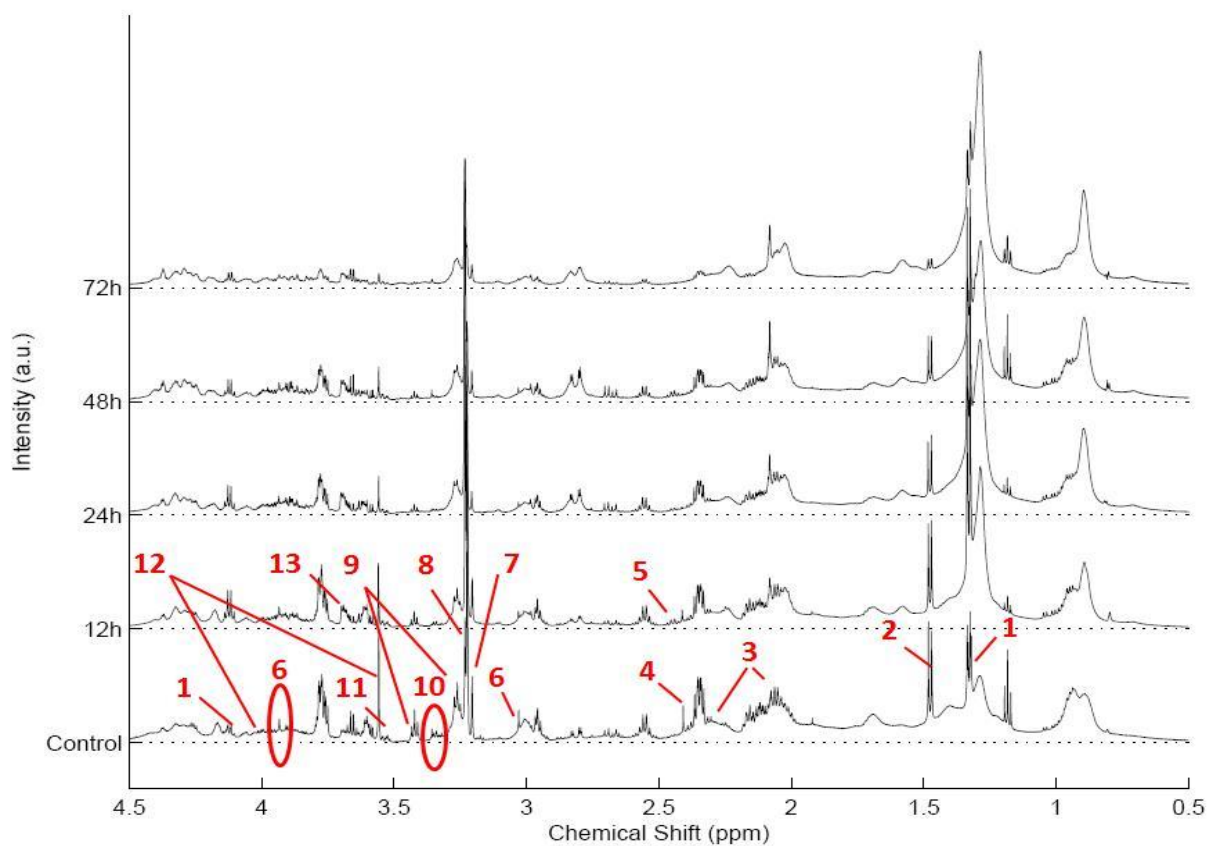


**Figure 3.6.** <sup>1</sup>H HR-MAS NMR spectra of BT4C cells following cisplatin exposure. (A) 0.5 to 4.5 ppm region. Metabolites labelled are as follows: **1**- lactate, **2**-alanine, **3**- glutamate, **4**- succinate, **5**- glutamine and aspartate, **6**- creatine, **7**- choline, **8**- GPC and PC, **9**- taurine, **10**- scyllo-inositol, **11**- glycine, **12**- myo-inositol, **13**- Guanidinoacetate.

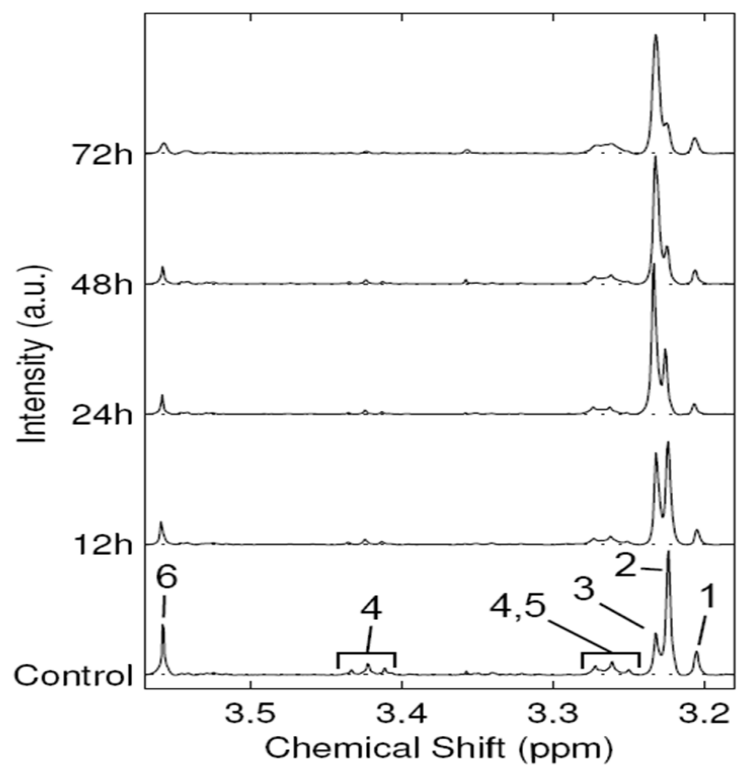


**Figure 3.7.** Choline containing region. Metabolites labelled on the control spectrum are as follows: **1-** choline, **2-** phosphocholine, **3-** glycerophosphocholine, **4-** taurine, **5-** phosphatidylcholine **6-** glycine).

Metabolites	Untreated cells	12h	24h	48h	72h
Acetate	8.08E-04 $\pm$ 7.04E-04	1.97E-04 $\pm$ 3.42E-04	0.00E+00 $\pm$ 0.00E+00	1.45E-03 $\pm$ 1.80E-03	0.00E+00 $\pm$ 0.00E+00
Alanine	9.90E-02 $\pm$ 4.30E-03	9.71E-02 $\pm$ 5.92E-03	7.61E-02 $\pm$ 7.32E-03	6.64E-02 $\pm$ 1.81E-03	4.45E-02 $\pm$ 1.08E-02
Aspartate	4.58E-02 $\pm$ 6.64E-03	2.33E-02 $\pm$ 4.83E-03	4.39E-02 $\pm$ 8.67E-03	4.40E-02 $\pm$ 1.11E-02	2.74E-02 $\pm$ 3.22E-03
Choline	1.28E-02 $\pm$ 3.09E-03	1.14E-02 $\pm$ 1.24E-03	9.07E-03 $\pm$ 2.72E-03	1.33E-02 $\pm$ 6.19E-03	1.57E-02 $\pm$ 3.81E-03
Creatine	1.34E-02 $\pm$ 3.87E-03	1.10E-02 $\pm$ 4.59E-04	9.50E-03 $\pm$ 2.75E-03	9.23E-03 $\pm$ 2.11E-03	1.24E-02 $\pm$ 1.64E-03
Glutathione	7.01E-02 $\pm$ 3.19E-02	8.07E-02 $\pm$ 6.03E-03	8.55E-02 $\pm$ 6.79E-03	8.28E-02 $\pm$ 3.72E-03	5.56E-02 $\pm$ 8.27E-03
Glutamate	2.59E-01 $\pm$ 2.91E-02	1.69E-01 $\pm$ 4.26E-02	1.69E-01 $\pm$ 2.64E-02	1.77E-01 $\pm$ 1.16E-02	1.35E-01 $\pm$ 6.98E-03
Glutamine	2.06E-02 $\pm$ 6.43E-03	2.22E-02 $\pm$ 4.64E-03	2.17E-02 $\pm$ 6.16E-03	5.43E-02 $\pm$ 2.71E-03	4.31E-02 $\pm$ 4.23E-02
GPC	3.87E-02 $\pm$ 2.11E-02	6.70E-02 $\pm$ 6.47E-03	1.02E-01 $\pm$ 3.34E-03	1.20E-01 $\pm$ 9.08E-03	1.06E-01 $\pm$ 2.45E-02
Glycine	1.09E-01 $\pm$ 2.15E-02	4.28E-02 $\pm$ 4.97E-03	3.56E-02 $\pm$ 3.41E-03	3.97E-02 $\pm$ 1.68E-03	3.43E-02 $\pm$ 3.20E-03
Lactate	1.06E-01 $\pm$ 3.00E-02	2.82E-01 $\pm$ 1.30E-02	2.85E-01 $\pm$ 4.10E-02	2.75E-01 $\pm$ 1.36E-02	3.73E-01 $\pm$ 4.74E-02
Myo-Inositol	7.79E-03 $\pm$ 1.13E-02	2.24E-03 $\pm$ 2.74E-03	0.00E+00 $\pm$ 0.00E+00	0.00E-00 $\pm$ 0.00E+00	2.64E-05 $\pm$ 4.57E-05
PC	8.38E-02 $\pm$ 7.63E-03	7.24E-02 $\pm$ 9.52E-04	4.57E-02 $\pm$ 1.34E-03	2.67E-02 $\pm$ 5.29E-03	2.62E-02 $\pm$ 2.92E-03
PEth	0.00E+00 $\pm$ 0.00E+00	3.07E-02 $\pm$ 5.00E-02	2.95E-02 $\pm$ 5.10E-02	0.00E+00 $\pm$ 0.00E+00	1.05E-02 $\pm$ 1.81E-02
Scyllo-Inositol	3.13E-03 $\pm$ 1.38E-03	2.66E-03 $\pm$ 5.44E-04	1.02E-03 $\pm$ 5.18E-04	3.62E-04 $\pm$ 1.01E-04	1.64E-04 $\pm$ 2.69E-04
Succinate	5.59E-03 $\pm$ 2.60E-03	5.15E-03 $\pm$ 6.86E-04	5.62E-04 $\pm$ 8.77E-04	0.00E+00 $\pm$ 0.00E+00	1.41E-03 $\pm$ 2.41E-03
Taurine	7.82E-02 $\pm$ 1.93E-02	2.93E-02 $\pm$ 4.49E-03	2.35E-02 $\pm$ 5.14E-03	2.24E-02 $\pm$ 2.86E-03	2.71E-02 $\pm$ 2.15E-02
Hypo-Taurine	2.40E-02 $\pm$ 5.54E-03	1.40E-02 $\pm$ 3.18E-03	1.14E-02 $\pm$ 5.77E-03	1.31E-02 $\pm$ 7.35E-03	2.30E-02 $\pm$ 2.13E-03
Guanidinoacetate	4.05E-03 $\pm$ 4.38E-03	1.86E-02 $\pm$ 9.85E-04	3.04E-02 $\pm$ 3.08E-03	2.63E-02 $\pm$ 5.71E-03	2.23E-02 $\pm$ 1.47E-02

**Table 3.3.** Relative concentrations of  $^1\text{H}$  HR-MAS NMR detectable metabolites in untreated and cisplatin exposed cells for different times (12, 24, 48, or 72 hrs). The results are presented as mean $\pm$ SD. Three samples at each condition were analysed.

Metabolites	Cisplatin exposed cells			
	12h	24h	48h	72h
PC		**↓	**↓	**↓
GPC		**↑	**↑	**↑
Lactate	**↑	**↑	**↑	**↑
Alanine		*↓	**↓	**↓
Succinate		*↓	*↓	
Glycine	**↓	**↓	**↓	**↓
Glutamate	*↓	*↓	*↓	**↓
Taurine	**↓	**↓	**↓	**↓
PC/GPC		*↓	*↓	*↓

**Table 3.4.** Significant <sup>1</sup>H HR-MAS NMR alterations detected in relative concentrations of the metabolites in response to cisplatin exposure. (↑) represents an increase in relative metabolite levels and (↓) represents a decrease in the relative metabolite levels compared to control cells (\**p*<0.05, \*\**p*<0.001).

The relative levels of PC, succinate, glutamate, glycine and taurine decreased with longer exposure to cisplatin. Changes occurred within 12 hours of treatment in taurine, glutamate and glycine. Increases were detected during treatment in lactate and GPC, with lactate relative levels being increased at 12 hours.

The scores plot for the PCA of the metabolite profiles is presented in Figure 3.8.A. The first and second principal components, account for 36% and 19% of the variance, respectively. Cisplatin exposure is associated with an increase in the first principal component and this change occurs early in the time course. From the loadings plot for principal component 1 (figure 3.8.B) cisplatin exposure is associated with changes in many metabolites, the most prominent changes being decreases in PC, glycine, succinate, taurine, alanine, glutamate, and scyllo-inositol with an increase in GPC and lactate.

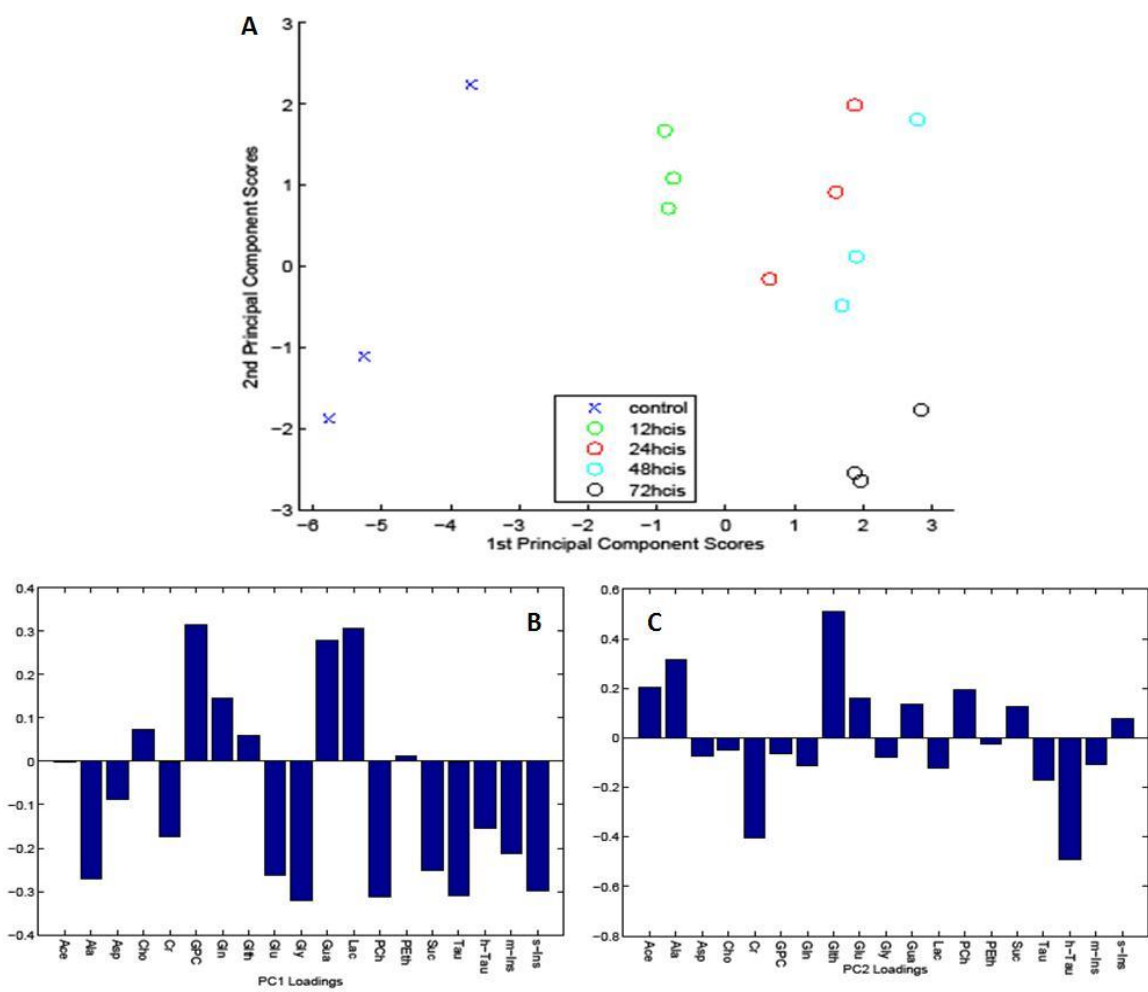


**Figure 3.8.** PCA of the quantities of 19 NMR fitted metabolites of cisplatin exposed cells.

(A) Scores plot. (B) Loadings for principal component 1. (C) Loadings for principal component 2.

### ***3.4. Discussion***

H&E and trypan blue staining of BT4C cells showed low numbers of apoptotic and necrotic cells up to 48 hours of cisplatin exposure and revealed an increase in the percentage of dead cells in samples exposed to cisplatin for 72 hours. H&E images showed that the majority of cells after 12, 24, and 48 hours of cisplatin exposure represent morphological characteristics of viable cells and cells representing morphological characteristics of apoptosis increased after 72 hours cisplatin exposure. Flow cytometry analysis of annexin V-FITC labelled and PI stained cells and the lack of ladder pattern on gel electrophoresis confirmed the staining and microscopic findings. Further investigation into the status of cisplatin exposed BT4C cells with PI and flow cytometry revealed growth arrest in these cells. Therefore, presuming that the contribution from the low numbers of apoptotic and necrotic cells is small, the  $^1\text{H}$  HR-MAS NMR metabolite alterations seen represent changes occurring in cell metabolism during cell cycle arrest and prior to apoptosis.

There is a possibility that the NMR spectra represent contribution from metabolites with vast alterations within apoptotic and necrotic cells. However, low numbers of apoptotic and necrotic cells were detected by morphological and molecular techniques and an association was detected between  $^1\text{H}$  HR-MAS metabolite alterations and increasing numbers of growth arrested cells detected by flow cytometry analysis of PI stained cells.

There is a possibility that large changes in few metabolites would influence the relative concentration of the detected metabolites. However, using the sum of all the metabolites in calculating the relative concentration of individual metabolites reduces this effect.

Furthermore, previous studies are in agreement with findings described here. Hakumaki *et al.* (50) examined the extracts of BT4C glioma cells by MRS. TSP (trimethylsilyl-2,2,3,3-tetradeuteropropionic acid) was used as an external reference and the metabolite levels were measured relative to TSP. Although different references were used in this study and the work presented in this chapter, similar metabolite alterations were detected. For example a decrease in PC relative levels and an increase in GPC relative concentrations were detected in both studies. This confirms that large metabolite changes and the application of sum of all the metabolites do not influence the metabolite profiles. In addition the metabolite changes detected by Hakumaki *et al.* (50) were associated with cell cycle arrest prior to apoptosis and previous studies have described low PC/GPC ratios as markers of cell cycle arrest (8,50,63). These metabolite changes were similar to the work described here and provide further evidence for the detected association between metabolite alterations of cisplatin exposed cells and growth arrest prior to apoptosis.

### ***3.4.1. Choline Containing Metabolite Alterations***

A decrease in relative levels of PC and an increase in GPC relative levels were detected in growth arrested BT4C cells in response to cisplatin exposure and this resulted in a reduced ratio of PC/GPC. Changes in the PC/GPC ratio, represent alterations in choline homeostasis (8) and PtCho turnover (1, 63). An increase in PC/GPC ratio has been associated with increased phospholipid turnover and PtCho synthesis (63) and a decrease in this ratio prior to apoptosis has been suggested as an indicator of growth arrest (50). A reduced PC level has been identified in response to chemotherapy in tumour tissue samples and has been proposed as an early biomarker of effective treatment *in vivo* (63).

PC and GPC are compounds of phospholipid metabolism. PC is used in phospholipid synthesis and it is produced during phospholipid degradation by phospholipase C (PLC) activity. Phospholipase A2 (PLA2) and lysophospholipase produce GPC from the final product of the Kennedy pathway, PtCho (Fig 3.9). During this process, fatty acids are formed which may be used in production of TG. The activity of phospholipases has been suggested as a possible reason underlying PC and GPC alterations (8, 78).

Decreased levels of PC were also detected in ganciclovir treated BT4C cells (50) and TNF- $\alpha$  treated breast cancer cells (80). The detected alteration in BT4C cells were associated with widespread growth arrest (50) and the PC levels of treated breast cancer cells were identified prior to apoptosis and in cells arrested in G0/G1+S phases of the cell cycle (80). The detected increase in GPC levels of prostate carcinoma cells was also associated with cell cycle arrest (48). However the association of CCMs with cell growth arrest has not been well established.

Individual CCMs are not discriminated by *in vivo*  $^1\text{H}$  MRS and the different changes in GPC and PC may explain the conflicting reports in the literature on tCho as a marker for tumour response to treatment. The sum of GPC, PC, and Cho signals did not alter significantly in cisplatin treated BT4C cells, consistent with the *in vivo* studies of treatment response in gliomas (20, 61, 62). This and the previously discussed results emphasise the role of *in vitro* studies in understanding the alterations of the individual metabolites contributing to the CCM signal and the possible altered biochemical pathways.

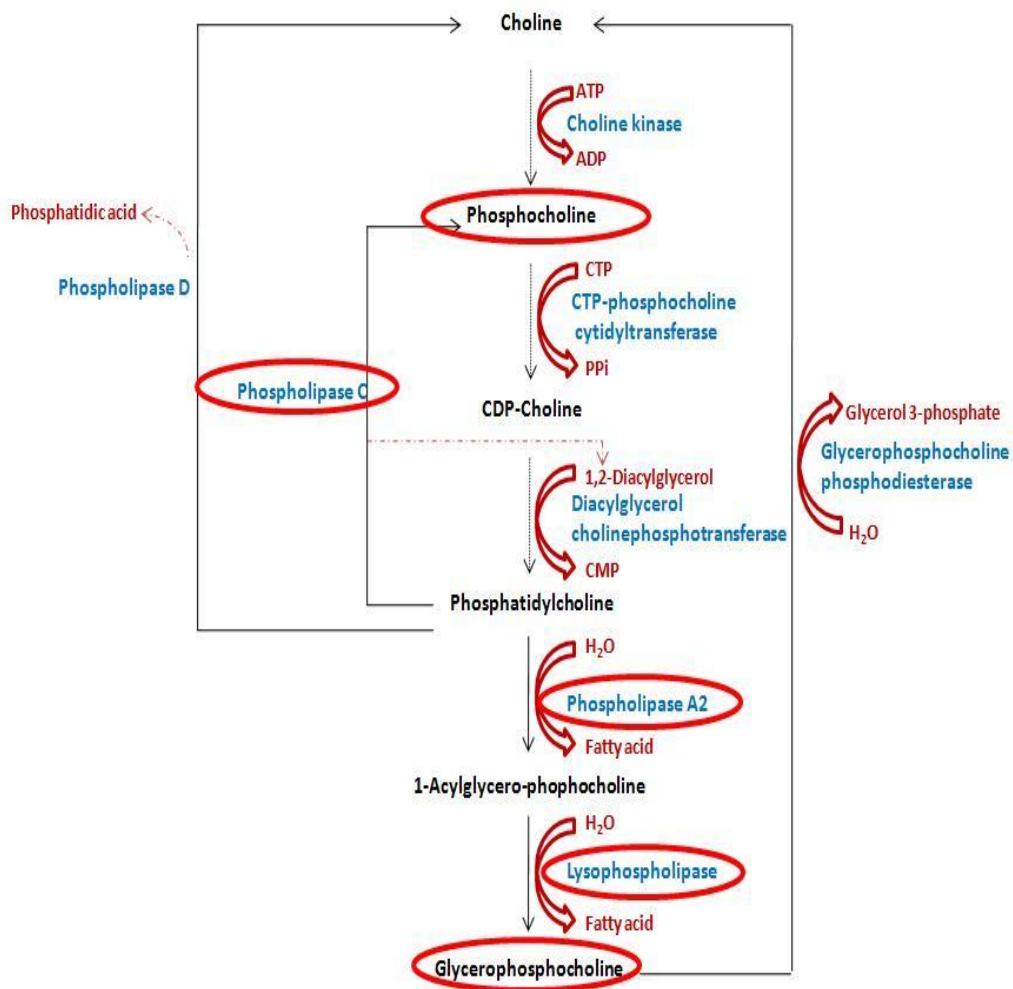


**Figure 3.9.** Phospholipid metabolism. The activities of phospholipase A2 and lysophospholipase result in production of GPC and fatty acids and phospholipase C activity results in degradation of phosphatidylcholine and production of phosphocholine.

### ***3.4.2. Energy Related Metabolite Alterations***

An increase in relative levels of lactate and decreases in alanine, succinate, glycine, and glutamate relative levels were detected in growth arrested BT4C cells in response to cisplatin exposure. Similar changes in lactate and alanine were identified in INF- $\gamma$ /TNF- $\alpha$  treated human colon adenocarcinoma (HT-29) cells. An increase in lactate and a decrease after an initial increase in alanine were reported in these cells prior to the appearance of apoptosis (69). The detected alterations are likely to represent changes to energy metabolism.

In non-malignant cells glucose is converted to pyruvate in the cell cytosol through the glycolysis pathway. The pyruvate produced is then transferred through the mitochondrial membrane and it is further metabolised during TCA cycle. The NADH and FADH<sub>2</sub> produced during this process are donated to the electron acceptors across the inner mitochondrial membrane and via oxidative phosphorylation, high levels of ATP are produced. In the absence of oxygen or electron acceptors pyruvate is converted to lactate by the enzyme lactate dehydrogenase. During this pathway less ATP is produced (120).

In tumours, glucose metabolism is altered and glucose is converted to lactate in the presence of oxygen. This is known as the Warburg effect (121). Although oxidative phosphorylation is more efficient in producing ATP, glycolysis can generate energy in a more rapid rate (122) and the processes involved can be beneficial to tumour cell survival and growth (123-125). Growing cells produce ATP mainly from glucose (126) and use lipids and amino acids for synthetic procedures whereas vegetative cells have a limited glucose uptake and are able to use a variety of metabolites to produce energy (9). As growth is inhibited in BT4C cells there is a possibility that the metabolites are not used in

synthetic pathways and are redirected to energy metabolism resulting in the detected alterations of lactate, the TCA cycle intermediates (eg. succinate), and amino acids (eg. glutamate, alanine and glycine) (figure 3.10).

In addition, by causing inter- and intra-strand cross-links, cisplatin causes damage to the DNA structure (103). It is well known that damaged DNA activates a DNA repair enzyme known as poly (ADP-ribose) polymerase (PARP). This enzyme consumes NAD and depletion of this compound inhibits the activity of a glycolysis enzyme known as glyceraldehyde-3-phosphate dehydrogenase (69). Therefore PARP activity inhibits glucose dependent ATP production (127) (figure 3.10). Inhibition of glycolysis and conversion of glucose to pyruvate may provide another explanation for redirecting metabolites to energy metabolism pathways and the detected increase in lactate and decrease in succinate, alanine, glycine, and glutamate in an attempt to remain viable.

Under optimal conditions in a test tube biochemical reactions will reach equilibrium. In cells, biochemical pathways are linked together. Product of one pathway may act as a reactant for another pathway or it may be secreted from the cell. In biological systems the linked pathways are in a steady state and the rate of production is similar to the rate of consumption. This prevents accumulation of intermediates and reduces their possible toxic side effects. The steady state is disrupted by changes in production or consumption of metabolites and their reaction rates. This influences the related pathways and causes alterations in their reaction rates and metabolite levels (94). There is a possibility that in cisplatin exposed cells glycolysis inhibition causes increases in the rate of other energy producing pathways and therefore resulting in high relative levels of lactate and low relative levels of amino acids in BT4C cells.

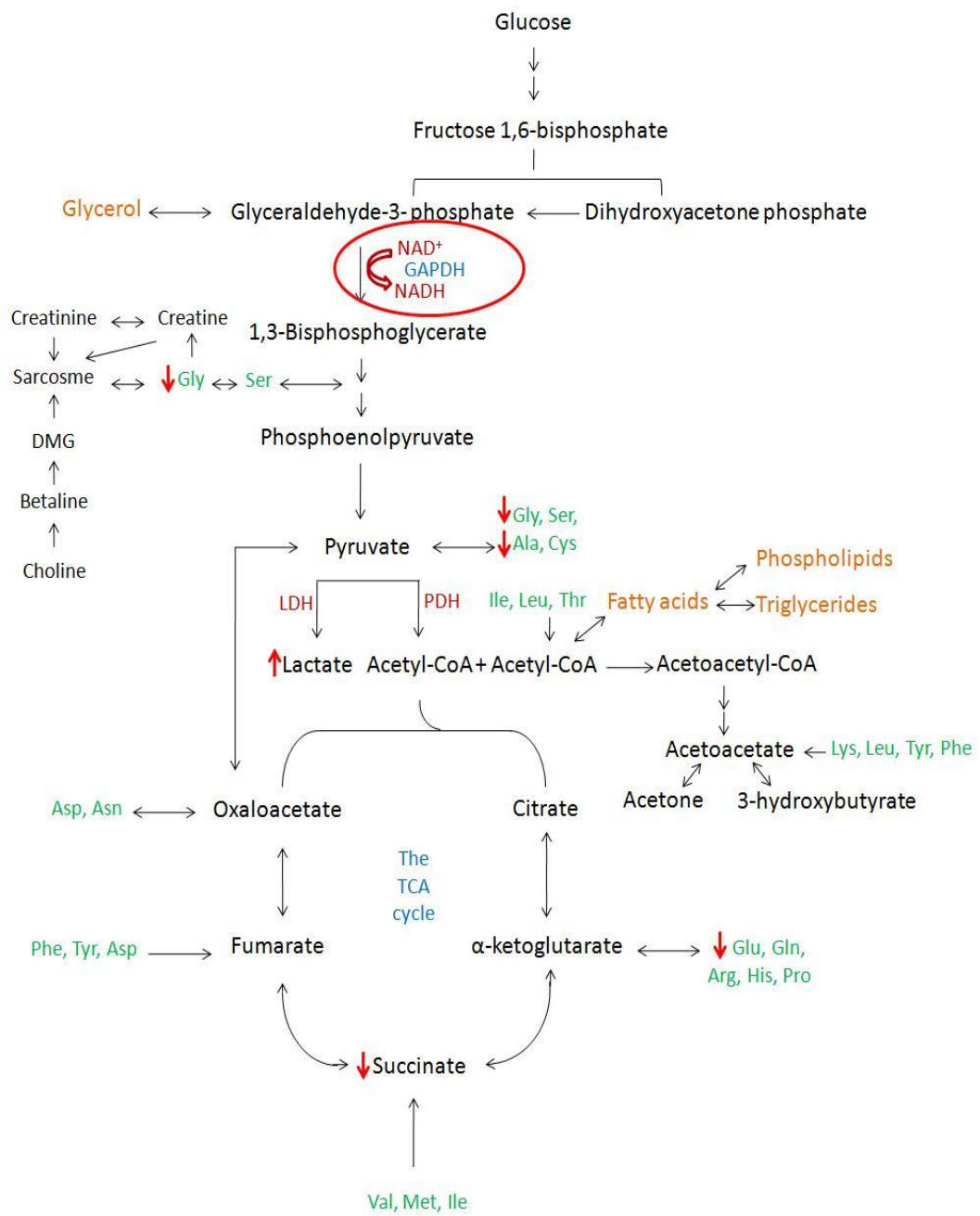


**Figure 3.10.** The metabolite pathways relevant to metabolite alterations in cisplatin exposed BT4C cells. Damaged DNA activates poly (ADP-ribose) polymerase, a DNA repair enzyme which results in consumption of NAD and inhibition of glyceraldehyde-3-phosphate dehydrogenase (GAPDH) activity (indicated by a red circle). Hence glucose dependent ATP production is inhibited. In this diagram the metabolites with red arrows altered significantly with longer exposure to cisplatin in BT4C cells (Ala. alanine, Arg. Arginine, Asn. asparagine, Asp. aspartate, Cys. cysteine, Glu. glutamate, Gln. glutamine, Gly. glycine, His. histidine, Ile. isoleucine, Leu. leucine, Lys. lysine, Met. methionine, Phe. phenylalanine, Pro. proline, Ser. serine, Thr. threonine, Trp. tryptophan, Tyr. tyrosine, Val. Valine).

Furthermore, several studies suggest that the levels of glycine, taurine, and glutamate are markers of malignancy (116, 128, 129). These metabolites are therefore key candidates as biomarkers of treatment response. Reports from *in vitro* studies in brain tumours have shown that glycine increases with WHO grade (130-133) and increases between diagnosis and relapse (134, 135). In recurrent astrocytoma, higher ratios of alanine, glycine over creatine were detected with increase in malignancy (135). *In vivo*, an increase in glycine levels of a rat glioma model was also observed (136). A recent study has also shown that glycine can be measured by *in vivo* MRS at a field strength of 1.5T clinically and that glycine concentrations increase with grade in childhood brain tumours (128). The potential of glycine in particular to act as a biomarker of both prognosis and treatment response is interesting for clinical application and further studies in this area are required.

### ***3.4.3. Taurine Alterations***

The highest levels of taurine are seen in primitive neuroectodermal tumours (137), which have very high levels of cell proliferation. A decrease in relative levels of taurine during cell cycle arrest would be consistent with this association between taurine and cell turnover. However, taurine concentration has been correlated with levels of apoptosis in astrocytomas and has been suggested as a clinical monitoring tool for apoptosis in gliomas (74). This would at first appear contrary to the presented findings where taurine levels decrease with drug treatment and in growth arrested cells.

Release of taurine and other osmolytes such as  $K^+$  and  $Cl^-$  from cells, lead to extrusion of water and cell shrinkage which is a distinctive hallmark of early stages of apoptosis (138, 139). Perhaps taurine accumulates in the surrounding tissue *in vivo* and in cell cultures is

discarded during wash steps. However, after cisplatin exposure few BT4C cells showed signs of apoptosis and cell shrinkage and the association of taurine with apoptosis was not strictly tested. A full understanding of taurine significance in apoptosis and the mechanisms behind its changes is yet to emerge.

### **3.5. Conclusion**

Metabolite alterations of cisplatin exposed rat BT4C glioma cells were investigated as potential biomarkers of cell cycle arrest prior to apoptosis.

A decrease in relative levels of PC and an increase in GPC relative levels were detected in BT4C cells following cell cycle arrest induced by cisplatin. PC decrease and GPC increase indicate growth arrest in BT4C cells and provide early markers of treatment response in these cells. Although PC and GPC relative levels altered, tCho relative level remained unchanged. This was similar to previous *in vivo* studies and further indicated the importance of discriminating individual metabolites contributing to the CCM signal.

With the cell cycle being inhibited in BT4C cells in response to cisplatin exposure, energy metabolism is altered in these cells. Increased relative levels of lactate and decreased relative levels of succinate, glutamate, alanine, taurine, and glycine were detected in growth arrested cells, prior to apoptosis. Since glutamate, glycine, and taurine are novel markers of malignancy, the detected decrease in the relative concentration of these metabolites may potentially be useful in identifying tumour treatment response.

Increased taurine levels have been associated with increased cell proliferation. Therefore reduced relative levels of taurine detected in cisplatin exposed BT4C cells provide further insight into the role of taurine in tumours and may have the potential to be used as a marker of growth arrest and treatment response.

The specificity of the detected metabolite alterations to cell cycle arrest is not known and further investigations are required to identify and compare metabolite relative levels of growth arrested cells with dead cells. Therefore in chapter 5 alterations of <sup>1</sup>H HR-MAS

NMR profile in response to starvation induced necrosis in BT4C cells are investigated. In chapter 5, relative metabolite alterations associated with cell growth arrest and necrosis are compared in order to identify general markers of cell stress and specific markers of cell necrosis and cell growth arrest prior to apoptosis.

In addition to metabolites lipid alterations detected by  $^1\text{H}$  MRS have attracted a vast interest as potential markers of treatment efficacy and the next chapter is dedicated to identifying  $^1\text{H}$  HR-MAS NMR alterations of mobile lipids in response to cisplatin induced growth arrest in BT4C cells. Further investigations are carried out to determine the association of the detected lipid alterations with cytoplasmic lipid droplet diameter and size to further investigate the origin of the  $^1\text{H}$  HR-MAS NMR signals.

## **CHAPTER 4**

**<sup>1</sup>H HR-MAS NMR LIPID ALTERATIONS  
OF CISPLATIN INDUCED GROWTH ARREST IN  
RAT BT4C GLIOMA CELLS  
AND  
THE SOURCE OF THE NMR VISIBLE LIPIDS**

## ***4.1. Introduction***

A number of signals in  $^1\text{H}$  NMR spectra of malignant cells are from elevated levels of isotropically tumbling mobile lipids (37, 38). These lipid signals arise from mobile fatty acyl chains of TGs, free fatty acids and cholesteryl esters (22) and an increase in their levels has been associated with cell death (21, 42, 46, 47, 50, 54, 56), transformed and differentiated cells (51), stimulated (43, 44), or quiescent (43, 78) cells.

This indicates the possibility of similar underlying mechanisms for the detected lipid accumulation during various circumstances. Therefore, an increase in lipids during cell death is of particular interest, as they have the potential to be used as biomarkers of treatment response. Lipid alterations during cell death have been associated in particular with apoptosis (48). Several studies have correlated increases in the methylene ( $\text{CH}_2$ ) moieties of the lipid peak at 1.3 ppm with apoptosis in various drug- treated cell models (44, 47, 48, 54). In addition, a number of studies have associated lipid accumulation with another method of cell death, necrosis (42, 46, 56). Lipid accumulation in human brain tumour biopsies, have been associated with the extent of necrosis (56) but the origin of the detected mobile lipids in *in vivo* MRS is not fully understood (43).

An increase in lipids has also been identified at early stages of cell death prior to apoptosis (44) and during growth arrest (43, 45, 49, 79, 140). If lipid accumulation can be detected early on before the occurrence of cell death, then  $^1\text{H}$  MRS lipids may have the potential to be used as early biomarkers of cell death and may provide useful information on cellular response to treatment.

The location of fatty acyl chains of NMR detectable lipid signals remains somewhat controversial as discussed in chapter 1. Initially membrane associated microdomains (40,

52) were identified as the source of lipids, however recent findings point to cytoplasmic lipid droplets as the origin of increasing lipid resonances (22, 42-44, 46-49).

It was shown in the previous chapter (chapter 3) that 50  $\mu\text{M}$  cisplatin exposure of glioma BT4C cells results in cell cycle inhibition. In this chapter, experiments are continued on these growth arrested cells and the potential of lipid alterations as early biomarkers of anti-cancer drug therapy is investigated. The Evidence is provided that lipid droplets in the cytoplasm of morphologically viable cells are the source of the accumulated NMR mobile lipid signals detected in these cells. The accumulation of lipid droplets in cells undergoing cell cycle arrest has not been demonstrated previously.

## ***4.2. Methods***

<sup>1</sup>H HR-MAS NMR was used to determine lipid accumulation in growth arrested rat glioma BT4C cells of 3 samples in response to different cisplatin exposure times. The <sup>1</sup>H HR-MAS NMR lipid data presented in this chapter and the metabolite data presented in chapter 3 were obtained from the same cell preparation and the relative concentration of metabolites and lipids were measured from similar spectra.

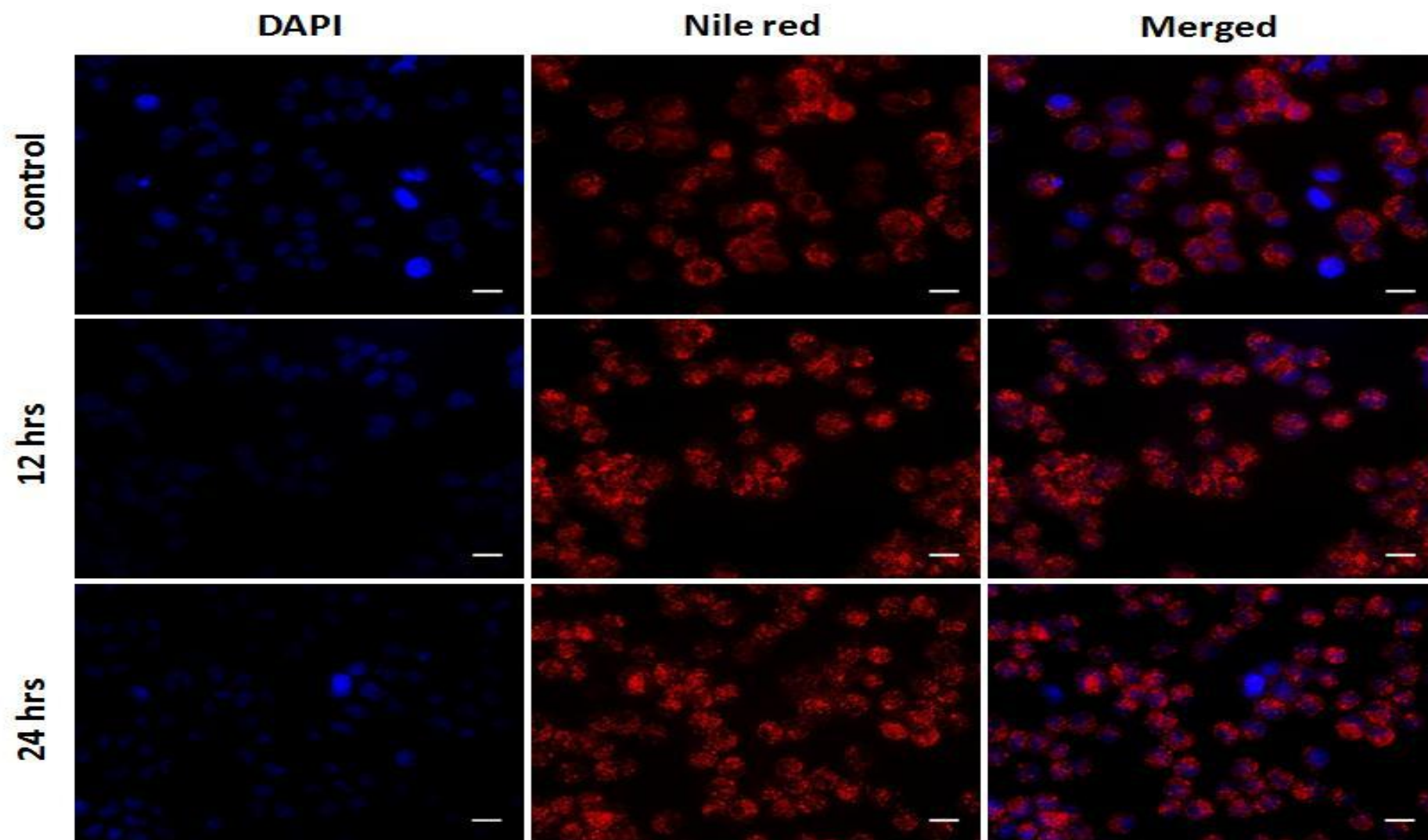
The combination of Nile red and DAPI dye was used to stain BT4C cells of 3 independently prepared samples after each cisplatin exposure time to investigate the source of <sup>1</sup>H HR-MAS NMR visible lipids and to determine the viability of the cells in which lipid alterations occurs. Further evidence on the morphology of cells containing lipid droplets and their viability status was provided by TEM. All assays were carried out on three independently prepared samples for each cisplatin exposure time (figure 3.1).

## **4.3. Results**

### **4.3.1. Nile red and DAPI staining**

Cisplatin exposed cells were co-stained with Nile red and DAPI as described in chapter 2. Nile red was used to investigate the presence of lipid droplets in the cytoplasm of cisplatin exposed cells and to determine the association between cytoplasmic lipid droplet characteristics and the detected  $^1\text{H}$  HR-MAS NMR lipid accumulation using ImageJ software. DAPI dye was combined with Nile red to determine the viability status of the cells containing lipid droplets and to confirm the presence of lipid droplets in morphologically viable cells, determined in the previous chapter to be growth arrested.

Staining with Nile red dye revealed the presence of lipid droplets in the cytoplasm of treated and untreated BT4C cells (figures 4.1.1 and 4.1.2). ImageJ measurements of Nile red stained cells showed substantial increases in the percentage of the cell area occupied by lipid droplets (figure 4.2) and the lipid diameter (figure 4.3). For each time interval 500 random cells of 3 independent samples were measured. In untreated, control cells  $22.2 \pm 3.6\%$  of the cell area was occupied by lipid droplets and the mean diameter of lipid droplets in these cells was  $0.7 \pm 0.02 \mu\text{m}$ . After 12 hours incubation with cisplatin, the area occupied by lipid droplets in each cell increased significantly to  $31.1 \pm 2.4\%$  ( $p < 0.05$ ) and the mean diameter of lipid bodies reached  $0.9 \pm 0.03 \mu\text{m}$  ( $p < 0.001$ ). Within 24 hours exposure the occupied area increased to  $33.2 \pm 3.3\%$  ( $p < 0.05$ ) and the diameter of the lipid droplets increased to  $0.9 \pm 0.032 \mu\text{m}$  ( $p < 0.001$ , compared to untreated cells).



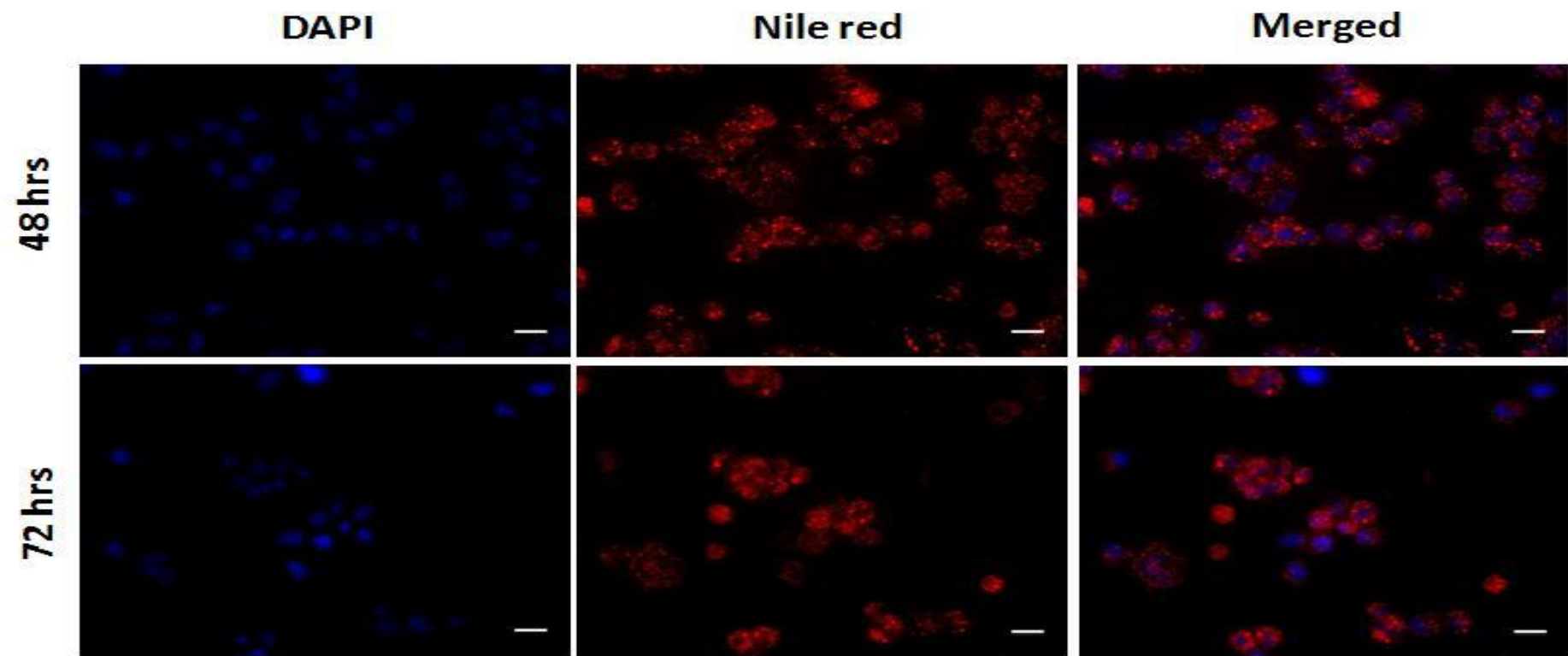


**Figure 4.1.1.** Nile red and DAPI images of cisplatin exposed cells for various times of 12, 24, 48 or 72 hrs. Cells were stained with Nile red and DAPI and images were captured by a Nikon E600 microscope coupled to a SPOT RT KE colour 3 shot CCD camera. Gray scale images were acquired and then images were pseudocoloured red and blue to represent Nile red and DAPI, respectively. Coloured Nile red and DAPI images were then merged (The scale bars represent 20 micrometers).

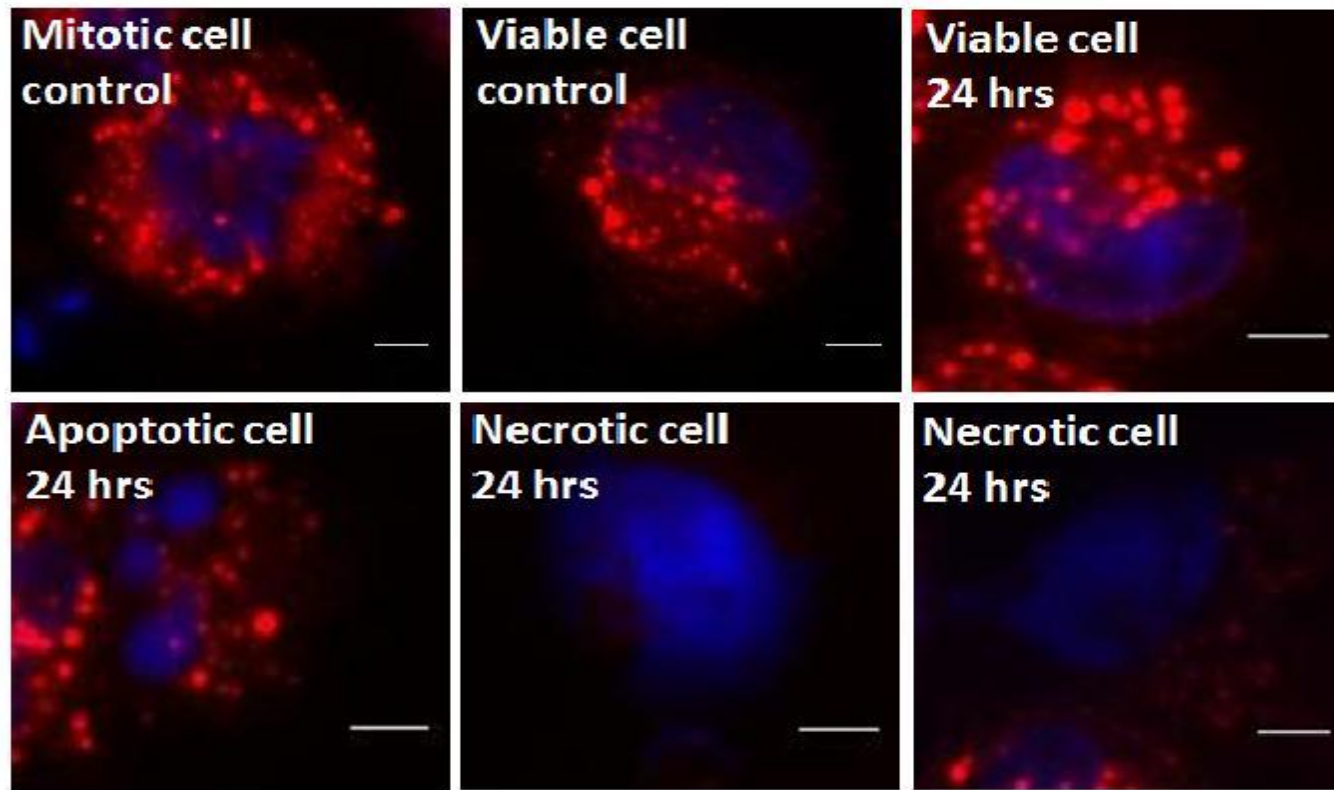


**Figure 4.1.2.** Representative images of mitotic, viable, apoptotic and necrotic cells detected by Nile red and DAPI co-staining (The scale bars represent 5 micrometers).

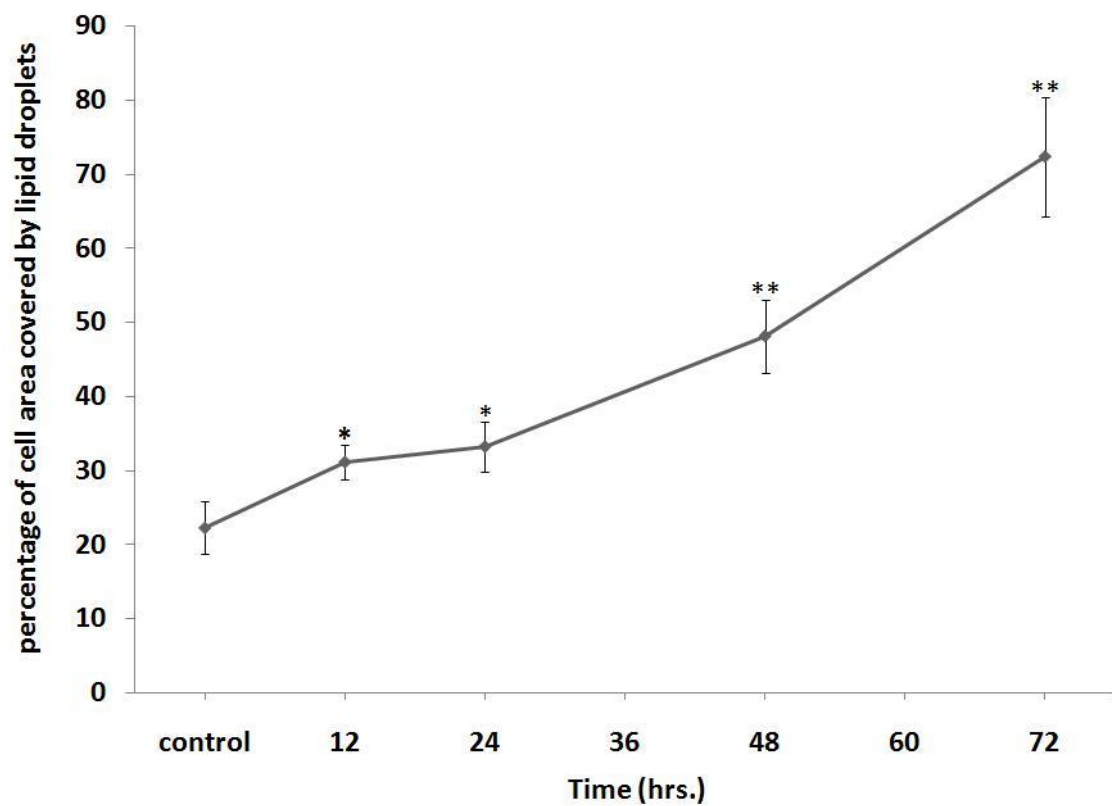


**Figure 4.2.** Mean percentage of cell area covered by lipid droplets in untreated and cisplatin treated samples (12, 24, 48, or 72 hrs) (\* $p < 0.05$ , \*\* $p < 0.001$ ; the error bars are SEM).

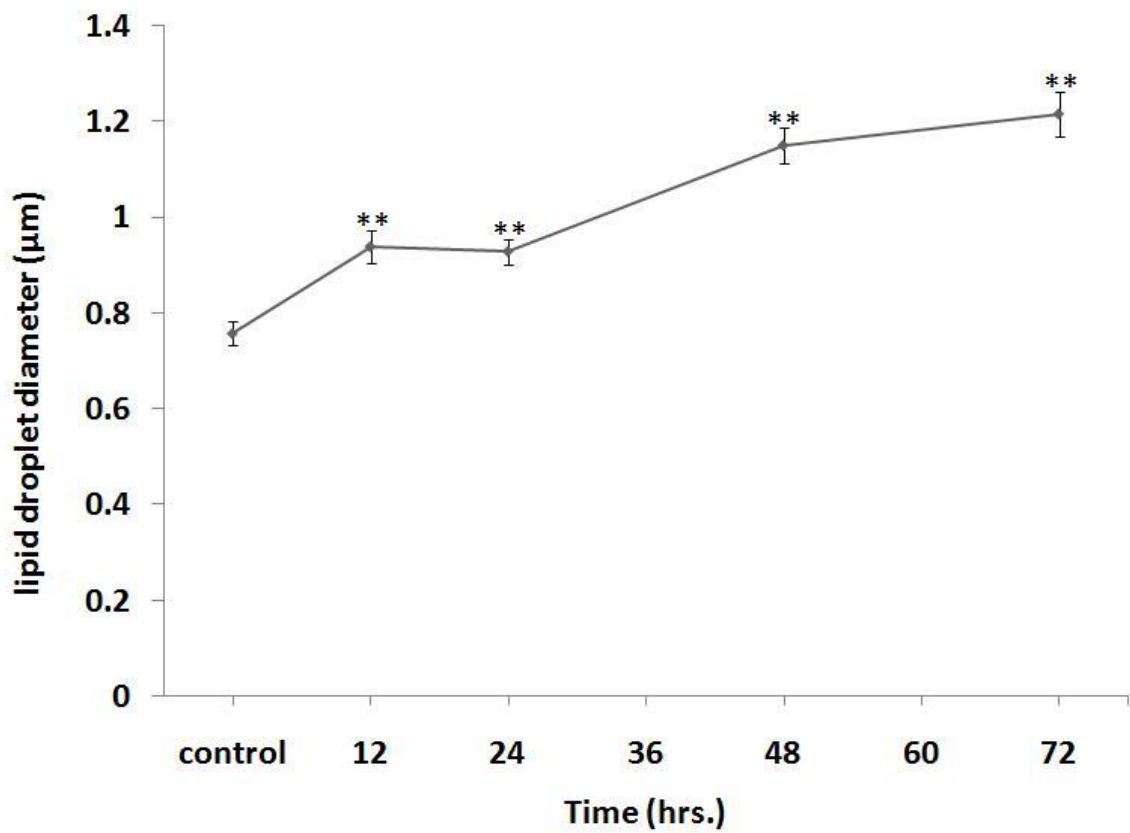


**Figure 4.3.** Lipid droplet diameter of untreated and cisplatin exposed cells (12, 24, 48 or 72 hrs). The results are presented as micrometer ( $\mu\text{m}$ ) ( $*p < 0.05$ ,  $**p < 0.001$ ; the error bars are SEM).

Staining the cells with DAPI revealed small percentages of 9, 10, and 22% dead cells (apoptotic and necrotic cells) in samples incubated with cisplatin for short times of 12, 24, and 48 hours, respectively (figure 4. 4). The combination of Nile red and DAPI revealed that the increase in lipid droplets and their size at earlier exposure times of 12, 24, 48 hours is detectable in cells that are morphologically viable and do not represent any characteristics of apoptosis or necrosis. The percentages of apoptotic and necrotic cells are in agreement with those determined by molecular studies of chapter 3. Therefore, alterations in lipid droplets at 12, 24, and 48 hours occur in growth arrested cells. At later stages of treatment, after 72 hours, the number of dead cells increased significantly to almost 53% ( $p < 0.001$ ). Higher number of apoptotic and necrotic cells at this time point were associated with 3.5 fold significant increase in lipid droplet area and almost 2 fold increase in their diameter reaching  $1.2 \pm 0.04 \mu\text{m}$  ( $p < 0.001$ ).

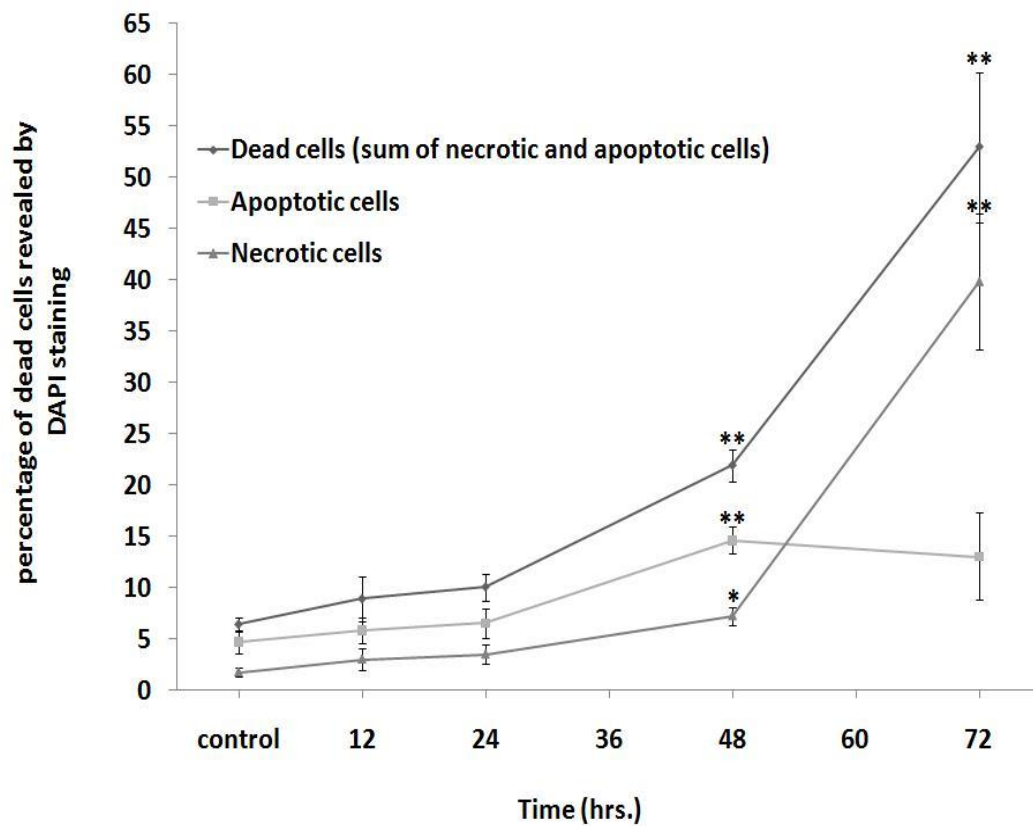


**Figure 4.4.** Percentages of dead cells revealed by DAPI staining in untreated and cisplatin exposed samples of different time points of 12, 24, 48 or 72 hrs (the sum of apoptotic and necrotic cells ◆, apoptotic ■, and necrotic ▲ cells ) (\* $p < 0.05$ , \*\* $p < 0.001$ ; the error bars represent SEM).

### ***4.3.2. Transmission Electron Microscopy Images***

Ultrastructural characteristics of untreated and 24 hours cisplatin exposed cells were studied and compared in more detail with TEM. In untreated samples, the cells represented viable features. They contained intact nuclei with peripheral chromatin, well developed endoplasmic reticulum (ER) and mitochondria were also detected. There were few lipid droplets present in the cell cytoplasm. Most of the treated cells contained features associated with viability such as peripheral chromatin in the nucleus as in untreated cells. However, increasing numbers of vacuoles were also detected in the images. The amount of cytoplasmic lipid droplets increased in cells with viable morphology. Apoptotic cells were also present in the treated samples characterised by condensed and fragmented chromatin in the nuclei. Mitochondria and ER in these cells appeared swollen. Higher numbers of lipid droplets were also detected in the cytoplasm of the apoptotic cells (figure 4.5).

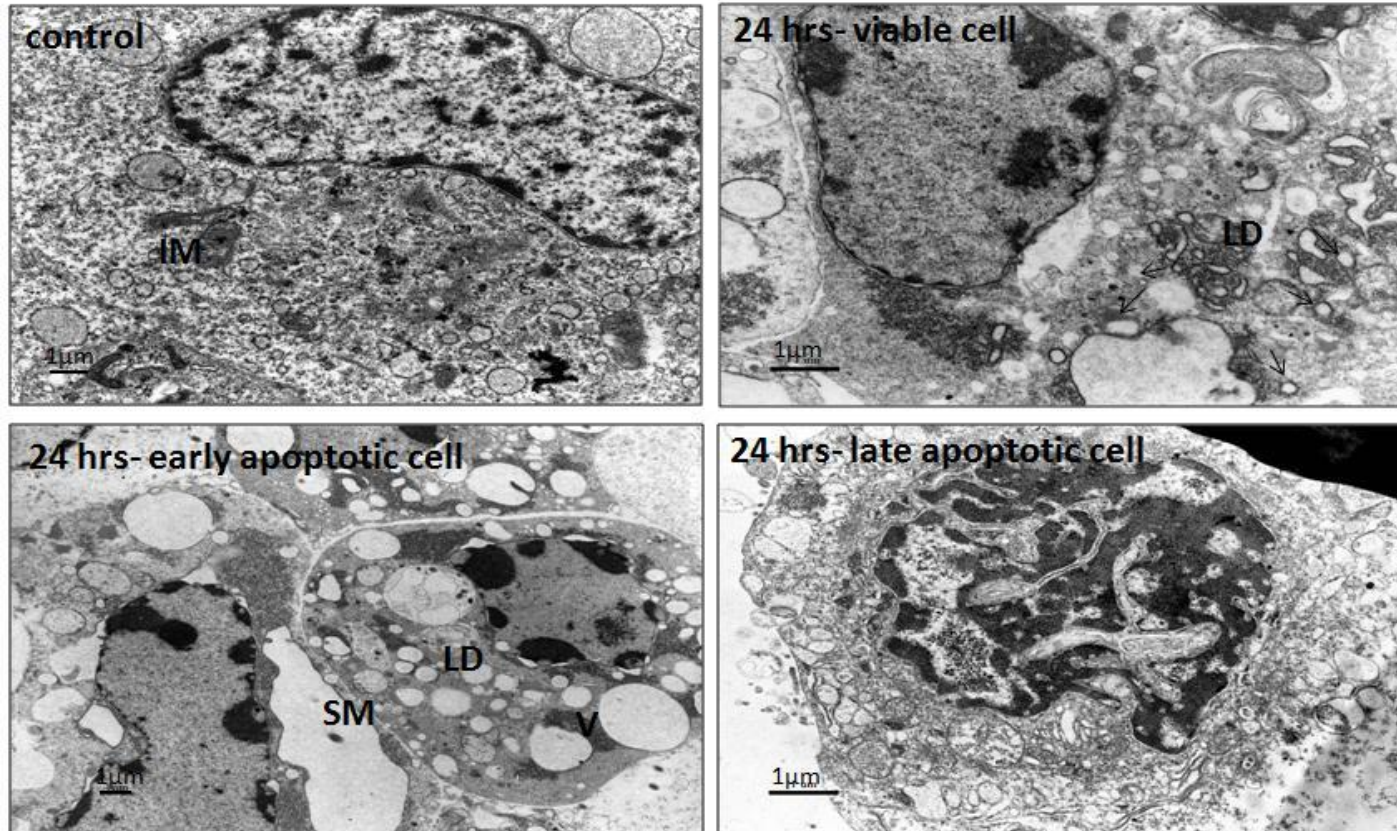


**Figure 4.5.** TEM images of control and 24 hrs cisplatin treated cells (LD- lipid droplets; SM- swollen mitochondria; V- vacuoles; IM- intact mitochondria).

### 4.3.3. $^1\text{H}$ HR-MAS NMR Visible Lipid Alterations

The TARQUIN algorithm was used to assign and quantitate  $^1\text{H}$  HR-MAS NMR visible lipids.  $^1\text{H}$  HR-MAS NMR spectra for different cisplatin exposure times are presented in figure 4.6.

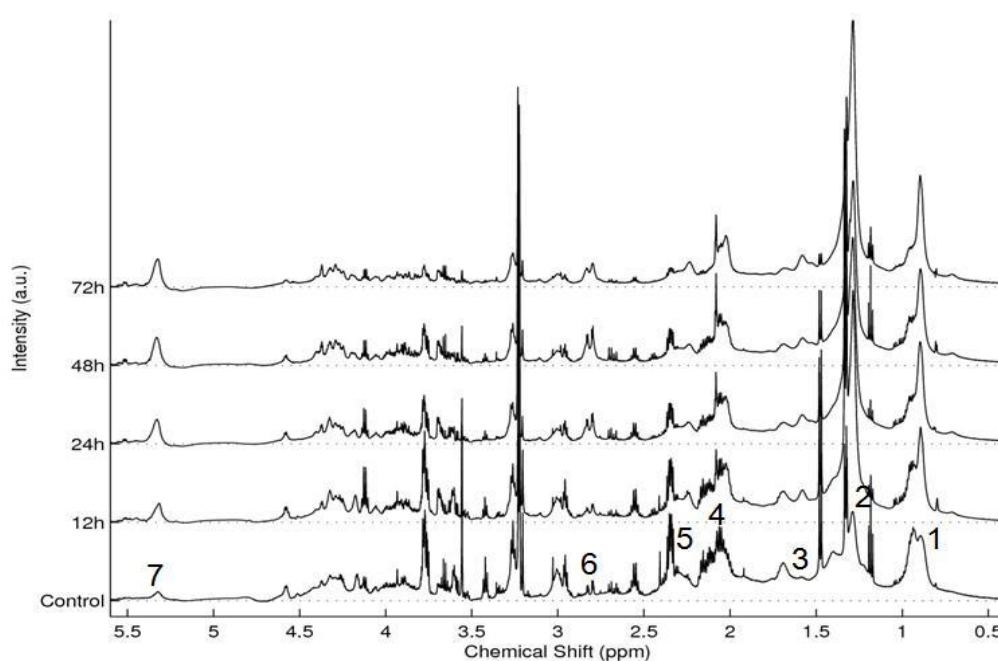


**Figure 4.6.**  $^1\text{H}$  HR-MAS NMR spectra of untreated and cisplatin exposed cells of various time points of 12, 24, 48, or 72 hrs (Lipid signals labelled on the control spectrum are as follows: **1**- 0.89 ppm, **2**- 1.3 ppm, **3**- 1.58 ppm, **4**- 2.02 ppm, **5**- 2.2 ppm, **6**- 2.8 ppm, **7**- 5.4 ppm).

The quantities of lipids were calculated relative to the sum of macromolecule signals at 0.94, 1.68, and 3.00 ppm as described in chapter 2, section 2.4.4. Relative quantities of mobile lipids at different cisplatin exposure times are given in table 4.1.

	Chemical shift (ppm)	Untreated cells	Cisplatin treated cells for different time intervals			
			12h	24h	48h	72h
Saturated and unsaturated Fatty acids	0.89 -CH <sub>3</sub>	0.254±0.055	0.710±0.093*	1.015±0.197*	1.161±0.078**	1.632±0.330*
	1.3 -CH <sub>2</sub> -CH <sub>2</sub> -CH <sub>2</sub> -	1.042±0.095	2.959±0.269*	3.790±0.434*	3.896±0.330*	7.034±1.624*
	1.58 -CH <sub>2</sub> -CH <sub>2</sub> -C=O	0.020±0.007	0.159±0.011**	0.225±0.040*	0.215±0.033*	0.487±0.136*
	2.2 -CH <sub>2</sub> -CH <sub>2</sub> -C=O	0.308±0.047	0.629±0.064*	0.782±0.110*	0.803±0.050**	1.102±0.218*
Unsaturated fatty acids	2.02 -CH <sub>2</sub> -CH <sub>2</sub> -CH=	0.504±0.057	0.873±0.091*	1.061±0.162*	1.185±0.036**	1.650±0.254*
	2.8 =CH-CH <sub>2</sub> -CH=	0.056±0.021	0.143±0.022*	0.329±0.043*	0.449±0.024**	0.486±0.132*
	5.4 =CH	0.118±0.016	0.322±0.036*	0.584±0.101*	0.693±0.034**	1.003±0.237*

**Table 4.1.** Quantities of <sup>1</sup>H HR-MAS NMR visible lipids related to the sum of macromolecule signals at 0.94, 1.68, and 3.00 ppm in untreated and cisplatin exposed cells for different times (12, 24, 48, or 72 hrs). Three samples at each time point were analysed. The results are presented as mean±SD (\**p*<0.05, \*\**p*<0.001, compared to untreated samples).

Peaks at chemical shifts of 0.89, 1.3, 1.58, and 2.2 ppm represent methyl and methylene moieties which arise from saturated and unsaturated fatty acids. After drug exposure the relative concentration of all these peaks increased in intensity and continued to do so as the duration of drug exposure increased. After 12 hours cisplatin exposure, significant increases had occurred in all peaks. By 72 hours exposure to the drug, the lipid signals at 0.89, 1.3, 1.58, and 2.2 ppm showed 6, 7, 24 and 4 fold increases in intensity compared with untreated samples ( $p < 0.05$ ).

Peaks at 2.02, 2.8, and 5.4 ppm arise from unsaturated fatty acids. The relative concentration of these peaks also increased in intensity after drug exposure and continued to increase with longer cisplatin exposure times. After 72 hours cisplatin exposure, the relative concentration of lipid signals at 2.02, 2.8 and 5.4 ppm increased to approximately 3, 9, and 8 fold, respectively, compared with untreated cells ( $p < 0.05$ ).

To investigate the alterations in fatty acid chain length, the ratio of the signals  $-\text{CH}_2-\text{CH}_2-\text{CH}_2-$  and  $-\text{CH}_3$  were calculated (figure 4.7). The ratio of the signals 1.3/0.89 ppm remained unchanged, showing that the mean chain length of the fatty acids was not altered.

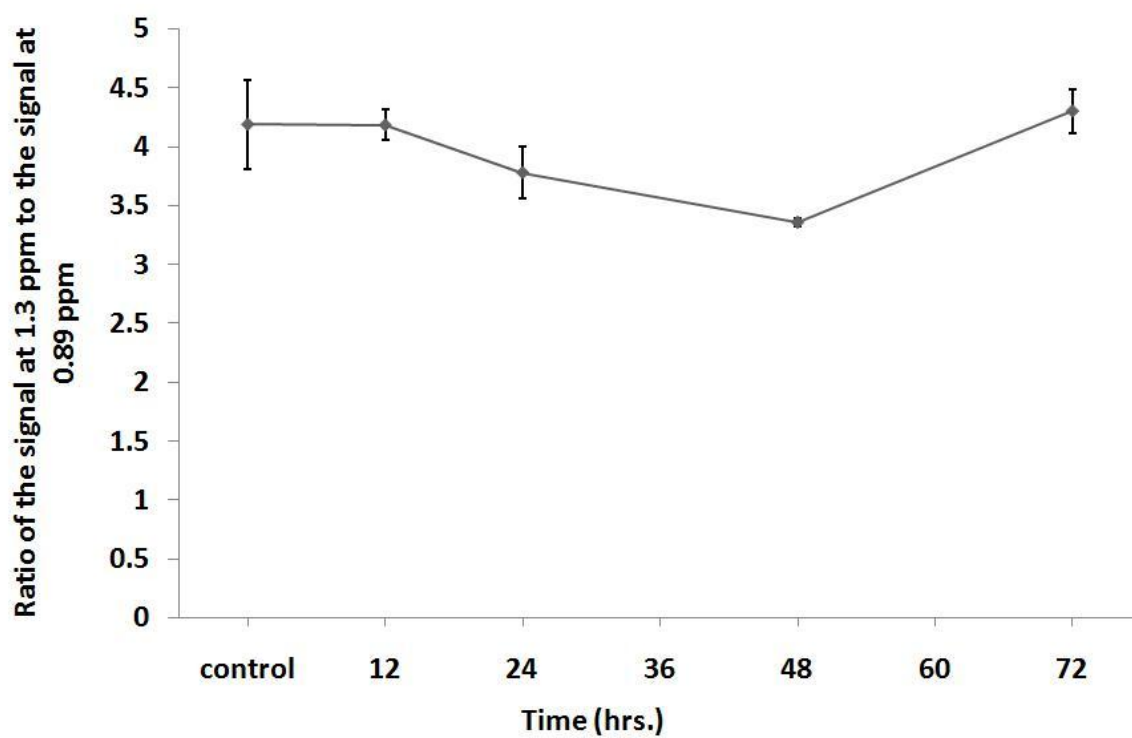


**Figure 4.7.** Ratio of the signals  $-\text{CH}_2-\text{CH}_2-\text{CH}_2-/-\text{CH}_3$  did not alter with longer exposure to cisplatin showing that the mean chain length remains unchanged.

#### ***4.4. Discussion***

It was established in chapter 3 that the  $^1\text{H}$  HR-MAS NMR metabolites alter in response to cisplatin exposure of rat glioma BT4C cells undergoing cell cycle arrest. In this chapter  $^1\text{H}$  HR-MAS NMR visible mobile lipid alterations were investigated in these cells and it was determined that an increase in lipid signals is associated with accumulation of cytoplasmic lipid droplets in morphologically viable cells prior to appearance of cell death indicators.

Nile red staining and subsequent image analysis revealed that an increase in both neutral lipid droplet amount and size within the cytoplasm was the likely source of  $^1\text{H}$  HR-MAS NMR visible lipid accumulation. Combining Nile red and DAPI provided further evidence to the trypan blue and H&E findings described in chapter 3, that after 12, 24, 48 hours treatment the number of apoptotic and necrotic cells are low and the majority of cells are morphologically viable. At these time points, a significant increase in  $^1\text{H}$  HR-MAS NMR visible lipids, lipid droplets and their size was detected indicating that the increase in  $^1\text{H}$  HR-MAS NMR visible lipids is due to lipid accumulation in cells which do not have morphological features of cell death. TEM images of cells treated for 24 hours confirmed that an increase in lipid droplets occurred in cells that contained homogenous chromatin; the characteristic feature of the nucleus in viable cells.

The use of the TARQUIN algorithm to separate fatty acids from macromolecular signals in the  $^1\text{H}$  HR-MAS NMR spectra allowed a more detailed quantitation of the  $^1\text{H}$  HR-MAS NMR lipid signals and this data can be used to explore the composition of the detected fatty acid pool. Increases in the fatty acid signals at 0.89, 1.3, 1.58, and 2.2 ppm with longer exposure to cisplatin demonstrated accumulation of  $-\text{CH}_3$ ,  $-\text{CH}_2-\text{CH}_2-\text{CH}_2-$ ,  $-\text{CH}_2-\text{CH}_2-\text{C}=\text{O}$ , and  $-\text{CH}_2-\text{CH}_2-\text{C}=\text{O}$  moieties, respectively, arising from saturated or

unsaturated fatty acid chains. Contrary to previous studies (55), the ratio of the signals - $\text{CH}_2\text{-CH}_2\text{-CH}_2\text{-CH}_3$  did not alter during treatment implying that there is not a substantial change in the mean chain length of the fatty acids. The difference between this finding and that of previous studies may be explained by the component which arises from the macromolecular signals since the ratio of the combined fatty acid and macromolecular signals 1.3 ppm/0.9 ppm does increase with treatment in these cells. There is a far greater contribution from macromolecules to the feature around 0.9 ppm than the one at 1.3 ppm accounting for the difference. The confounding influence of the macromolecular components around 0.9 ppm and 1.3 ppm implies that the use of these peaks *in vivo* as a marker of treatment response is likely to be tumour dependent.

Unsaturated fatty acid signals were detected at 2.02 ( $-\text{CH}_2\text{-CH}_2\text{-CH=}$ ), 2.8 ( $=\text{CH-CH}_2\text{-CH=}$ ), and 5.4 ppm ( $=\text{CH}$ ). In the control samples, the peak at 2.8 ppm is not readily detectable implying that the small amounts of unsaturated fatty acids present do not contain the polyunsaturated  $=\text{CH-CH}_2\text{-CH=}$ , moiety. Increases in all the unsaturated fatty acid signals were seen after treatment and the ratio of the  $^1\text{H}$  HR-MAS NMR signals at 5.4 ppm/2.8 ppm is close to 2 implying that almost all the unsaturated fatty acids are polyunsaturated and contain a moiety  $-\text{CH}=\text{CH-CH}_2\text{-CH}=\text{CH}-$ . Given this finding, if we assume that each fatty acid has one  $-\text{CH}_3$  group, relative amounts of saturated and unsaturated fatty acid can be estimated. The ratio of the resonances at 0.89 ppm/2.8 ppm is approximately 3 in the treated samples, allowing for proton number, the ratio of the groups  $-\text{CH}_3/=\text{CH-CH}_2\text{-CH=}$  is approximately 2 implying that half of the fatty acids in the treated samples are saturated and the other half are polyunsaturated.

Accumulation of lipids has been detected to occur in the pre-apoptosis phase (44) when lipid synthesis and turnover is taking place (141) and during growth arrest (43, 49, 79,

140). In the study conducted by Hakumaki *et al.*, an increase in polyunsaturated fatty acids was detected after GCV treatment of herpes simplex thymidine kinase transfected BT4C glioma cells and the potential of lipid accumulation as a marker of growth arrest and tumour response to therapy was demonstrated (50). This study on BT4C cell line confirms that such increases in <sup>1</sup>H HR-MAS NMR lipid signals can arise from cytoplasmic lipid droplets in the cell cycle arrested cells.

High phospholipid and PtCho turnover has been associated with the G1 stage of the cell growth cycle (141) and the level of phospholipid breakdown is high in this stage (142). This may explain the accumulation of lipids in cisplatin treated BT4C cells arrested in G1 phase of the cell cycle. However, lipid accumulation was not correlated with growth arrest in Jurkat T-lymphoblasts (44) and transformed murine fibroblast (143). The detected accumulation of lipids was associated with lower proliferation rate (43, 143) and was suggested to provide useful information on tumour proliferation status *in vivo* (43). Holmes *et al.* detected lipid accumulation in stimulated lymphocytes but reducing the proliferation rate by cell cycle blockers did not alter the lipid profile (144). Furthermore Delikatny *et al.* did not detect changes in lipid signals of untreated and partially synchronised human glioma cells accumulated in S-G2/M but detected lipid accumulation in cells exposed to a cell cycle blocker prior to accumulation in G2/M phase. They associated identified lipid alterations to drug-cell interactions (78).

Accumulation of lipids occurs under different circumstances. Increase in lipids has been detected in growth arrested (143), drug treated (145, 146), transformed and activated cells (144, 147-154). Delikatny *et al.* suggested that lipids develop in response to stress caused on the cells. They further suggested that the detected alterations occurring in response to a variety of conditions and treatments may indicate that a common pathway involving

phospholipid metabolism is effected. They proposed if this reaction is general it can be used to investigate cellular response to drugs *in vivo* and *in vitro* (78).

Cyclin dependent protein kinase activity during cell cycle arrest/apoptosis indirectly effects cytidyltransferase and phosphorylation of this enzyme inhibits PtdCho production (22, 141). PtdCho is the most abundant form of membrane phospholipid and is a precursor of two other dominant membrane phospholipids, phosphoethanolamine and sphingomyelin (141). Subsequently cell membrane synthesis and usage of compounds in the assembly of cell membranes is affected by reduced levels of PtdCho production (21). Activation of phospholipase A1, A2, and lysophospholipase have also been suggested as important contributors resulting in release of GPC (22, 78) and production of fatty acids (figure 4.8).

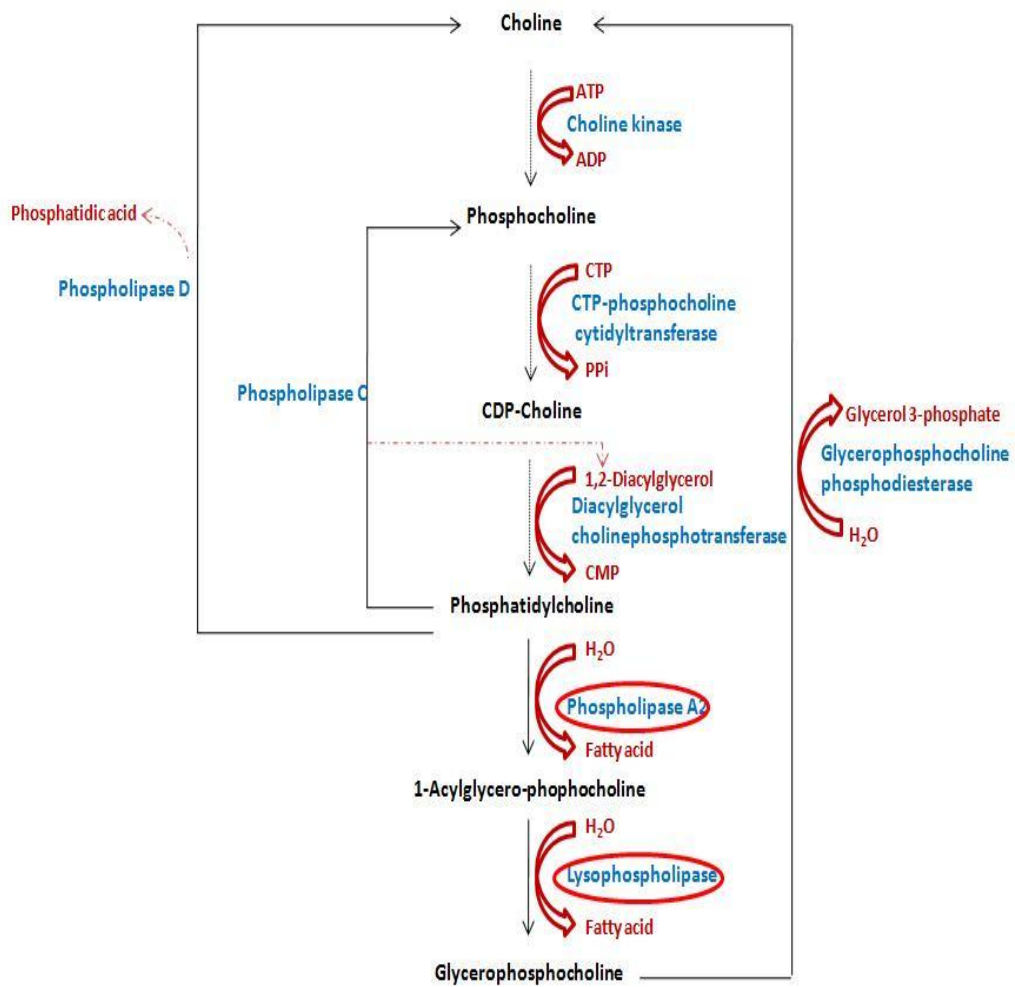


**Figure 4.8.** Phospholipid metabolism. Phospholipase A<sub>2</sub> and lysophospholipase activity result in production of GPC and fatty acids. Fatty acids can be used in production of phospholipids and triglycerides.

Fatty acids can be re-esterified into phospholipids or used with diacylglycerol to produce TGs (48). This causes accumulation of CDP- choline and TG (65, 155) and results in formation of neutral lipid vesicles. The degraded phospholipid compounds such as choline and PC at cell membrane level are transferred freely to the ER for production of PtdCho (156). Diacylglycerol and fatty acids at cell membrane level are actively transported between membranes and the ER. This transport system is in the form of lipid droplets or bodies (156) containing neutral lipids such as TGs and cholesterol esters. In addition, lipid droplets may have proteins and enzymes for lipid metabolism and storage (45). Transformation of diacylglycerol to triacylglycerol (156), and providing compounds for other subcellular structures (45) has been related to the enzymes detected in the structure of these lipid droplets. Also it has been suggested that TG accumulation is an attempt to protect the cell from toxic effects of fatty acids and/or the activated derivatives (48). This may explain accumulation of lipids under various conditions causing stress.

Transport of lipid bodies (156) and their NMR visibility have been associated with the cell cytoskeleton (22). Lipids are more mobile in vesicles than in membranes (21) and this together with an increase in number and size of lipid droplets amplifies their NMR visibility (156).

Various other sources have been suggested and explored as reasons for the detected lipid accumulation. Increase in *de novo* synthesis of fatty acids, decrease in  $\beta$ -oxidation of fatty acids (47, 48), excess release of fatty acids from intracellular storage (22), and/or increased uptake of lipids from exogenous sources such as serum are a few suggested reasons behind lipid accumulation (47, 48). In addition, energy status of the cell (22) and decrease or loss of mitochondrial membrane electrochemical potential during pre-apoptotic stages results in increased mitochondrial membrane permeability and influences the production of lipid

droplets by conversion of citrate to cholesterol and fatty acids (44) and at late stages of apoptosis breakdown of mitochondrial membrane by lysosomal enzymes may influence the level of fatty acids, glycerol and phospholipids (47).

According to the proposal by Quintero *et al.* in normal conditions the lipid droplets are small and therefore are not NMR visible. However in this work the lipid droplets in untreated glioma cells were detectable by fluorescence microscopy and lipid resonances were prominent in the  $^1\text{H}$  HR-MAS NMR spectra which may indicate that the lipid droplets are bigger in the BT4C cell line than in C6 glioma cells, tested by Quintero *et al.* (156). This possibility may arise from the high concentration of TG in BT4C cells, as demonstrated in previous studies by biochemical assays (50).

## ***4.5. Conclusions***

In this chapter,  $^1\text{H}$  HR-MAS NMR detected increases in saturated and unsaturated fatty acids in growth arrested BT4C glioma cells during exposure to cisplatin. Half of the fatty acids in these cells were saturated and the other half unsaturated. Further investigation revealed that the majority of unsaturated fatty acids were polyunsaturated and contain the moiety  $-\text{CH}=\text{CH}-\text{CH}_2-\text{CH}=\text{CH}-$ . Furthermore, the unchanged ratio of  $\text{CH}_2/\text{CH}_3$  indicates constant fatty acid chain length hence the detected increase in this ratio in previous reports are likely due to high macromolecule contribution to the 0.9 ppm signal.

The  $^1\text{H}$  HR-MAS NMR lipid levels detected in BT4C cells were associated with an increase in the diameter and the amount of cytoplasmic lipid droplet. Direct analysis using DAPI and Nile red co-staining techniques confirmed that lipid accumulation occurred in cells which were morphologically viable and growth arrested. Comparison with molecular studies presented in chapter 3 indicated that these cells did not show early markers of apoptosis. Ultra-structural studies using TEM further confirmed that lipid droplets were present in morphologically viable cells.

The findings described in this chapter and the results of other researchers indicate that lipids accumulate under various conditions and the detected increase in neutral lipids is a common feature of the stressed cells. Therefore NMR lipid accumulation shows potential as a general marker of cell stress and in particular treatment response. Their accumulation in malignant tumour cells treated with a cytostatic agent prior to the emergence of early indicators of cell death is particularly attractive for a non-invasive biomarker of treatment monitoring.

In the next chapter, necrosis is induced by starvation in glioma BT4C cells and  $^1\text{H}$  HR-MAS NMR metabolite and lipid alterations are investigated in these cells. The results are compared with the data from cells exposed to cisplatin to investigate the common markers of cell stress and to further examine the potential of lipids as a general marker of stressed cells. In addition, the comparison of cisplatin and cell starvation allows identification of alterations specifically occurring in growth arrested cells or necrotic cells.

**CHAPTER 5**

**<sup>1</sup>H HR-MAS NMR METABOLITE AND LIPID  
ALTERATIONS  
OF STARVATION INDUCED NECROSIS IN  
RAT BT4C CELLS**

## 5.1. Introduction

The ability to continue proliferating and developing resistance to apoptosis is one of the characteristics of tumour cells. Cancer biologists have begun to consider the application of necrosis-inducing methods for effective tumour therapy (9). Currently, various techniques including photodynamic treatment and alkylating DNA-damaging agents and a number of compounds such as lapachone, apoptolidin, and honokil have been reported to cause necrosis in tumour cells (157-160).

Cellular stress caused by nutrient deprivation, results in ATP depletion and continued lack of nutrients and/or growth factors in culture results in necrosis (9, 161). Therefore, in this chapter, substrate starvation of BT4C cells is used as a model of cell necrosis and <sup>1</sup>H HR-MAS NMR lipid and metabolite alterations are investigated in order to identify biomarkers of this type of cell death.

In chapter 4, an increase in saturated and polyunsaturated fatty acids was detected in response to cisplatin exposure and in growth arrested BT4C cells prior to apoptosis. Delikatny *et al.* suggested that lipids develop in response to stress caused in cells. They further suggested that the detected alterations may occur in response to a variety of conditions and treatments. They proposed that, if this reaction is general, it can be used to investigate cellular response to drugs *in vivo* and *in vitro* (78). To further investigate the potential of lipid alterations as markers of cell stress, in this chapter, <sup>1</sup>H HR- MAS NMR lipid changes caused by necrosis due to starvation in BT4C cells is examined.

Furthermore, an increase in lactate and GPC and a decrease in alanine, glycine, glutamate, succinate, and taurine was detected in cisplatin exposed BT4C cells (chapter 3). In this chapter relative metabolite alterations of BT4C cells are further investigated in response to

necrosis induced by starvation and the  $^1\text{H}$  HR-MAS NMR metabolite changes occurring during cell growth arrest and necrosis are compared in order to identify potential biomarkers of cell stress and markers distinguishing cytothasis and necrosis.

## ***5.2. Methods***

Rat BT4C glioma cells were starved by maintaining them in PBS for various time intervals of 4, 6, 12, 18, or 24 hours. Viability of starved cells was investigated by trypan blue dye and the percentages of viable and necrotic cells were determined by H&E and DAPI staining based on morphological characteristics of cell nuclei. To further investigate the morphological alterations of cells due to starvation, TEM images were captured.  $^1\text{H}$  HR-MAS NMR was performed in order to determine the lipid and metabolite profiles and their alterations in starved cells at various examined times. PCA was carried out on the metabolite data to identify alterations in metabolites in response to starvation and with longer substrate deprivation. The source of  $^1\text{H}$  HR-MAS NMR visible lipids was investigated by Nile red staining and ImageJ software was used to determine the association of  $^1\text{H}$  HR-MAS NMR lipid alterations with size and diameter of cytoplasmic lipid droplets. Finally to identify similarities and differences in the metabolite alterations of cisplatin exposed and starved BT4C cells, PCA was performed on the  $^1\text{H}$  HR-MAS NMR metabolite data set of both conditions. In each assay 3 independently prepared samples were tested for the time intervals examined (figure 5.1).

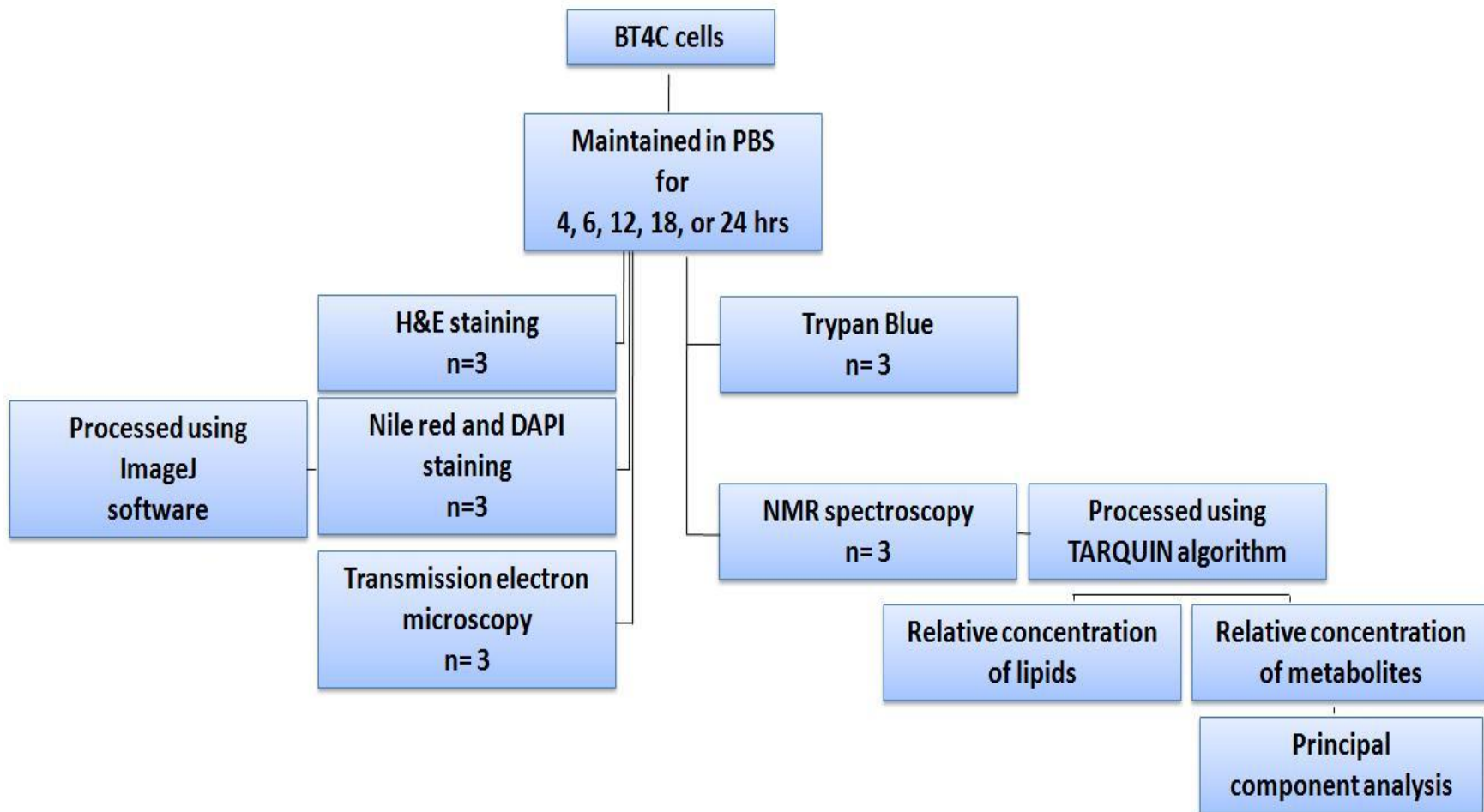


**Figure 5.1.** Flow chart of the methods used in chapter 5.

## **5.3. Results**

### **5.3.1. Trypan Blue and Haematoxylin and Eosin Staining**

Trypan blue and H&E staining were carried out to determine the percentages of viable and necrotic cells in control and PBS maintained cells at various time points (4, 6, 12, 18, and 24 hours). The viability status of 500 random cells was examined in each of the 3 independent samples prepared for each time point. These techniques detected an increase in the number of necrotic cells by longer medium deprivation.

Necrotic cells are unable to prevent trypan blue dye from entering and therefore are stained blue. The percentage of necrotic cells stained with this dye increased significantly from  $5.5 \pm 2.5\%$  in control samples to  $19.8 \pm 3.0\%$  in 6 hours substrate deprived cells. The percentage of necrotic cells continued to increase significantly in samples deprived of substrates for longer, reaching  $39.0 \pm 1.0\%$  and  $59.3 \pm 6.3\%$  after 18 and 24 hours starvation, respectively ( $p < 0.001$ ) (Figure 5.2).

The number of H&E stained cells containing diffused chromatin and red-purple cytoplasm indicating necrotic cells increased in samples with longer incubation in PBS, further confirming the results of trypan blue staining (figure 5.2 and 5.3).

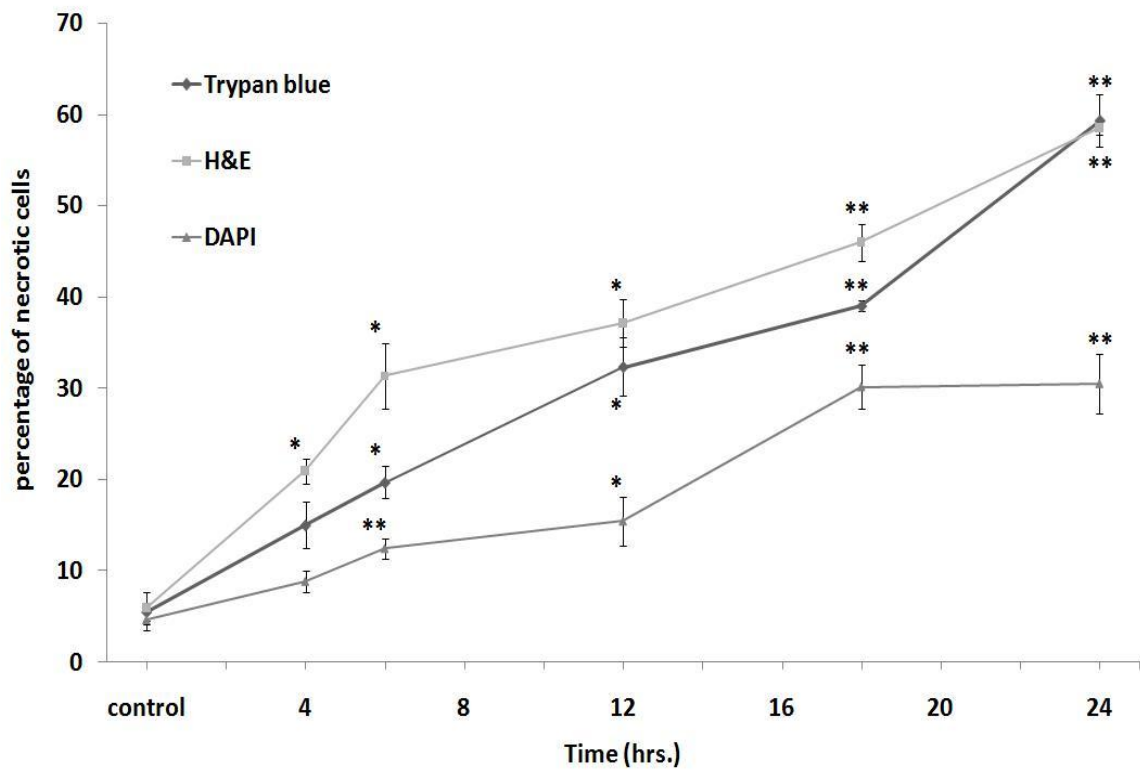


**Figure 5.2.** The percentages of necrotic cells detected by different methods of staining, trypan blue (◆), H&E (■), and DAPI (▲). The error bars are SEM. (\* $p < 0.05$ , \*\* $p < 0.001$ ).

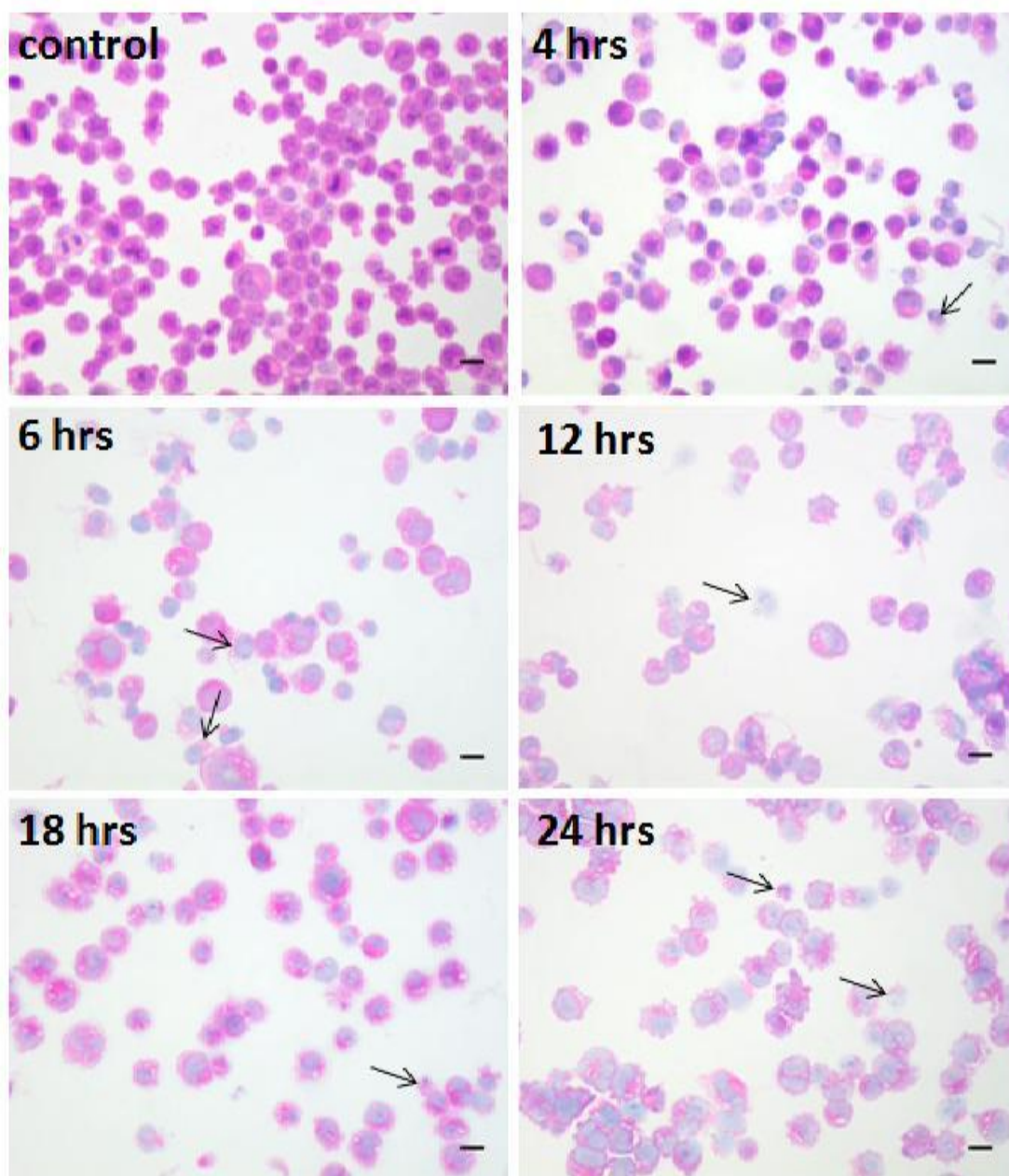


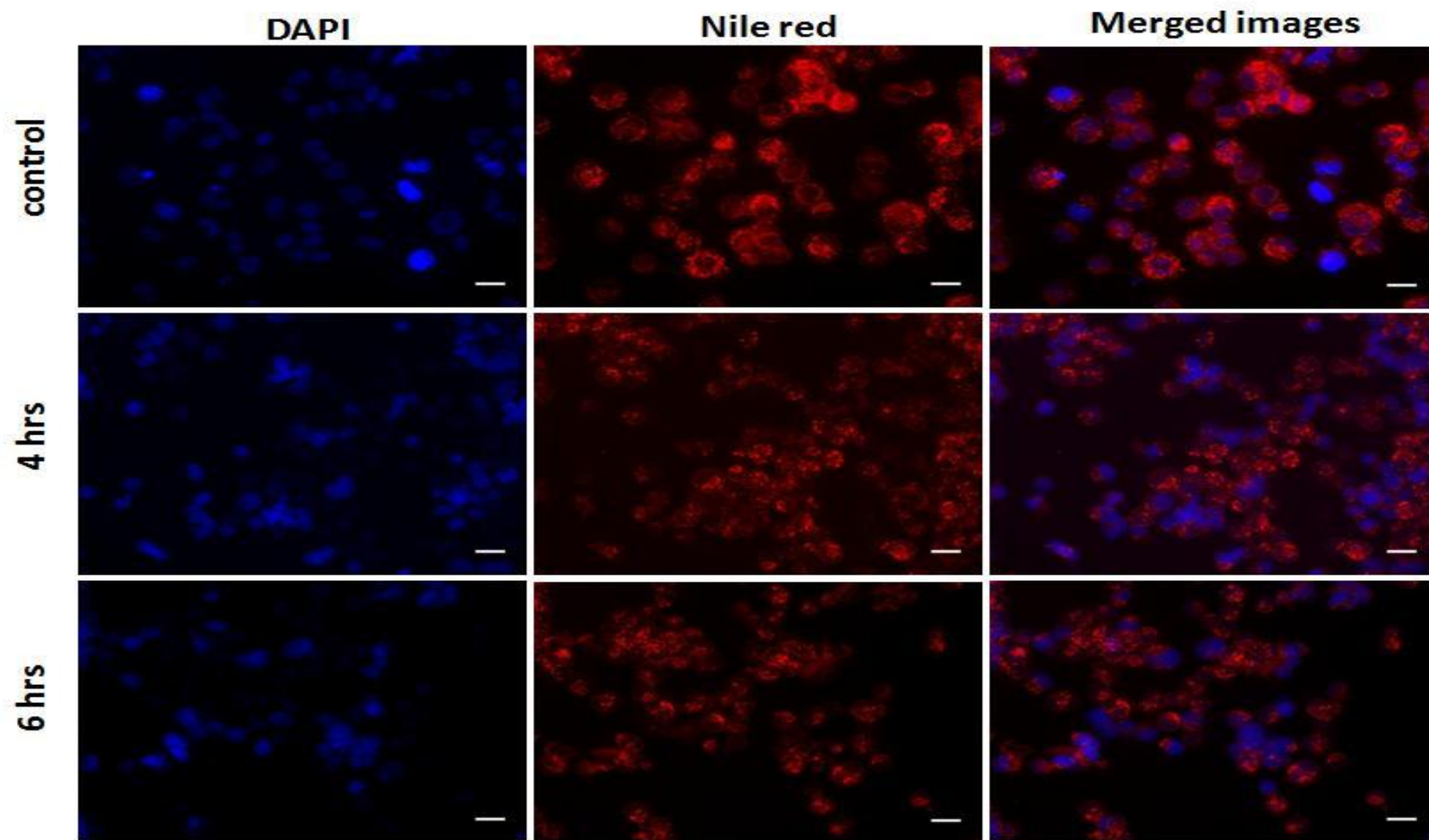
**Figure 5.3.** Images of control and starved cells after various time intervals (4, 6, 12, 18 or 24 hrs), stained with H&E. The arrows are pointing to necrotic cells and the scale bars represent 20 micrometers.

The percentage of necrotic cells detected in H&E stained control samples were  $5.9 \pm 1.6\%$ . This percentage significantly increased to  $20.9 \pm 2.4\%$  in the cells deprived of substrates for 4 hours ( $p < 0.05$ ) and continued to elevate significantly to  $37.1 \pm 4.5\%$  ( $p < 0.05$ ) and  $58.5 \pm 1.4\%$  ( $p < 0.001$ ) after 12 and 24 hours of cell maintenance in PBS, respectively (figure 5.2).

### ***5.3.2. Nile red and DAPI staining***

PBS exposed cells were co-stained with Nile red and DAPI as described in chapter 2. Nile red was used to investigate the presence of lipid droplets in PBS exposed cells and to identify any alterations in the amount and diameter of these lipid bodies with longer substrate deprivation. ImageJ software was used. DAPI was used in order to detect the viability status of the starved cells and to determine the method of cell death in these cells. For each time interval, 500 randomly chosen cells from each of the 3 prepared samples were measured.

Nile red revealed the presence of lipid droplets in the cytoplasm of control and starved cells (figure 5.4). The diameter and the area of the cells covered by lipid bodies increased in stressed or early stage necrotic cells with longer maintenance in PBS (figures 5.5 and 5.6). Morphological characteristics of DAPI stained nuclei of PBS exposed cells revealed that necrosis is the main type of cell death in these samples and the number of necrotic cells increased with longer substrate deprivation (figure 5.4).



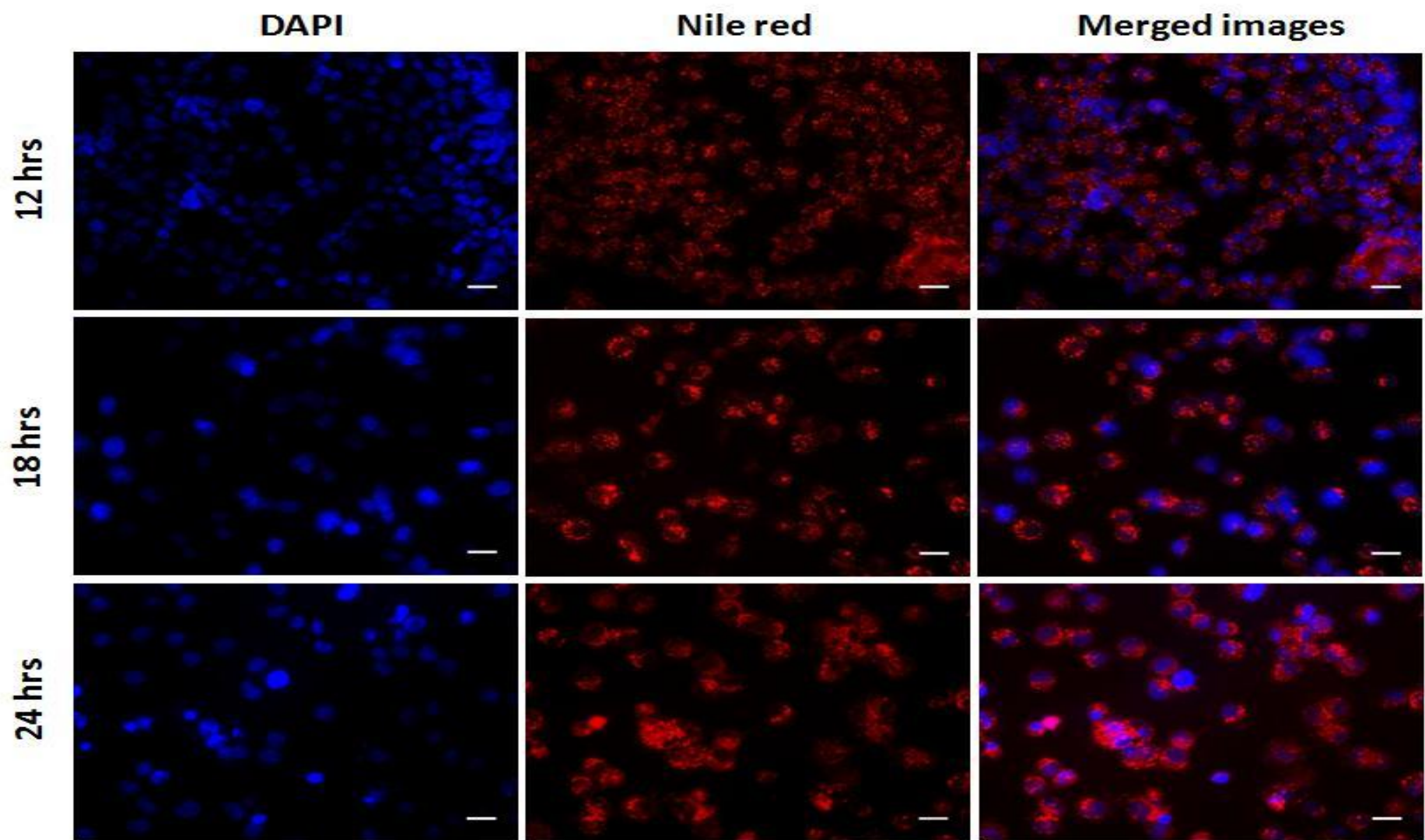


**Figure 5.4.** Nile red and DAPI images of starved cells. Control and starved cells for various times of 4, 6, 12, 18 or 24 hrs were stained with Nile red and DAPI. A Nikon E600 microscope coupled to a SPOT RT KE colour 3 shot CCD camera was used to visualise and capture gray scale images. The images were merged after they were pseudocoloured red and blue to represent Nile red and DAPI, respectively (The scale bars represent 20 micrometer).

The percentage of the cell area covered by lipid droplets showed an increasing trend by longer substrate deprivation. The lipid droplet area elevated significantly from  $22.2 \pm 3.6\%$  in control samples to  $36.5 \pm 2.9\%$  ( $p < 0.05$ ) and  $38.9 \pm 3.03\%$  ( $p < 0.05$ ) in samples incubated in PBS for 18 and 24 hours, respectively (figure 5.5).

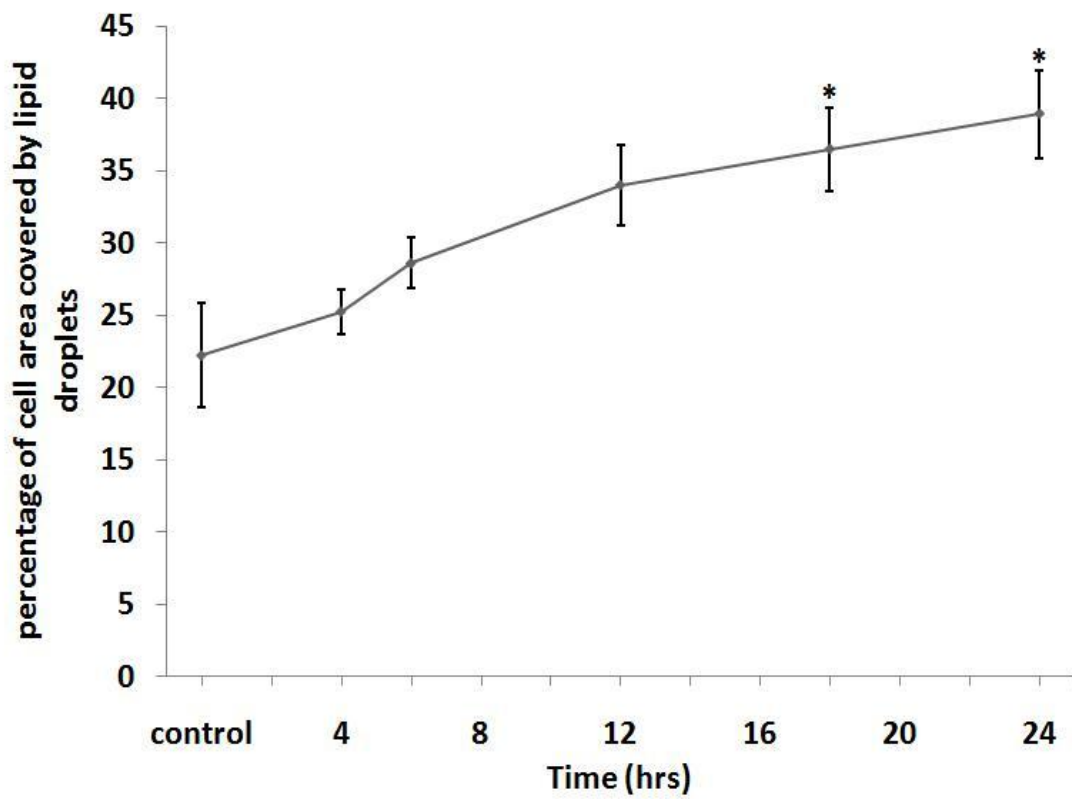


**Figure 5.5.** The mean percentages of cell area covered by lipid droplets in starved cells.

The error bars are SEM ( $*p < 0.05$ ).

The lipid droplet diameter increased significantly ( $p<0.05$ ) from  $0.7\pm 0.02\ \mu\text{m}$  in control samples to  $1.01\pm 0.03\ \mu\text{m}$  and  $1.07\pm 0.02\ \mu\text{m}$  after 4 and 6 hours of starvation, respectively. The lipid droplet diameter continued to increase significantly ( $p<0.001$ ) reaching  $1.1\pm 0.02\ \mu\text{m}$  and  $1.2\pm 0.04\ \mu\text{m}$  after 18 and 24 hours incubation in PBS, respectively (figure 5.6).

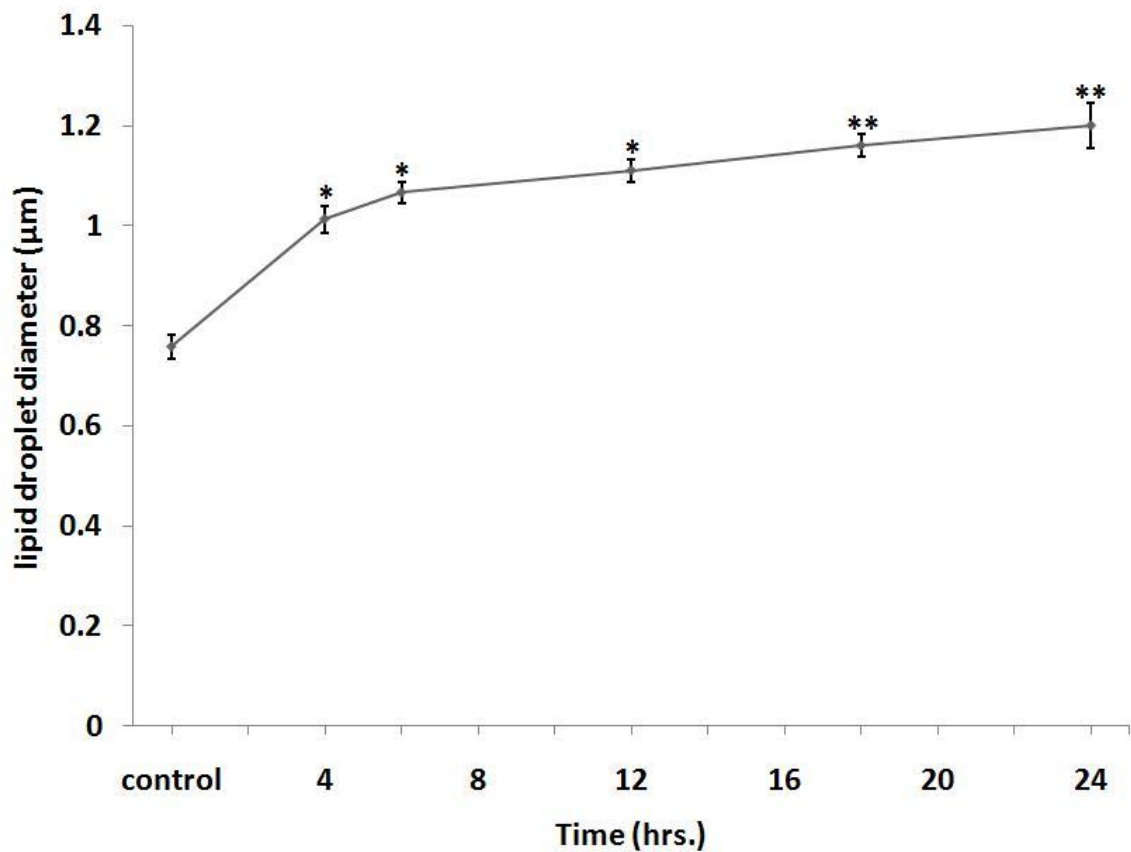


**Figure 5.6.** The diameter of cytoplasmic lipid droplets of starved cells. The error bars are SEM (\* $p<0.05$ , \*\* $p<0.001$ ).

Viable and necrotic cells were distinguished from each other by morphological characteristics of their nuclei after DAPI staining. The percentage of necrotic cells detected by DAPI staining increased significantly ( $p<0.05$ ) to  $12.4\pm 1.2\%$  after 6 hours medium deprivation and continued to increase reaching  $30.1\pm 4.3\%$  and  $30.5\pm 5.7\%$  after 18 and 24 hours maintenance in PBS, respectively ( $p<0.001$ ) (figure 5.2).

Distinguishing stressed, viable cells from cells at early stages of necrosis was difficult due to the similarities between their nuclei features. Consequently the percentages of necrotic cells were underestimated. This emphasised that the results of other assays such as trypan blue or H&E are more reliable.

### ***5.3.3. Transmission Electron Microscopy Images***

The ultrastructural characteristics of substrate deprived cells at various time intervals of 6, 12 or 24 hours were investigated with TEM. The cells maintained in PBS contained swollen mitochondria with condensed matrix. In some mitochondria, the cristae were lost or pushed to the sides forming ring or doughnut like structures. A few autophagic vacuoles and myelinoid bodies were detected in some cells. Lipid droplets were also detected in the cytoplasm of these cells. In some cells the extent of the damage to mitochondria was very severe and a double membrane ghost was seen. Cell membrane rupture and debris were detected confirming the presence of necrosis in these samples (figure 5.7).

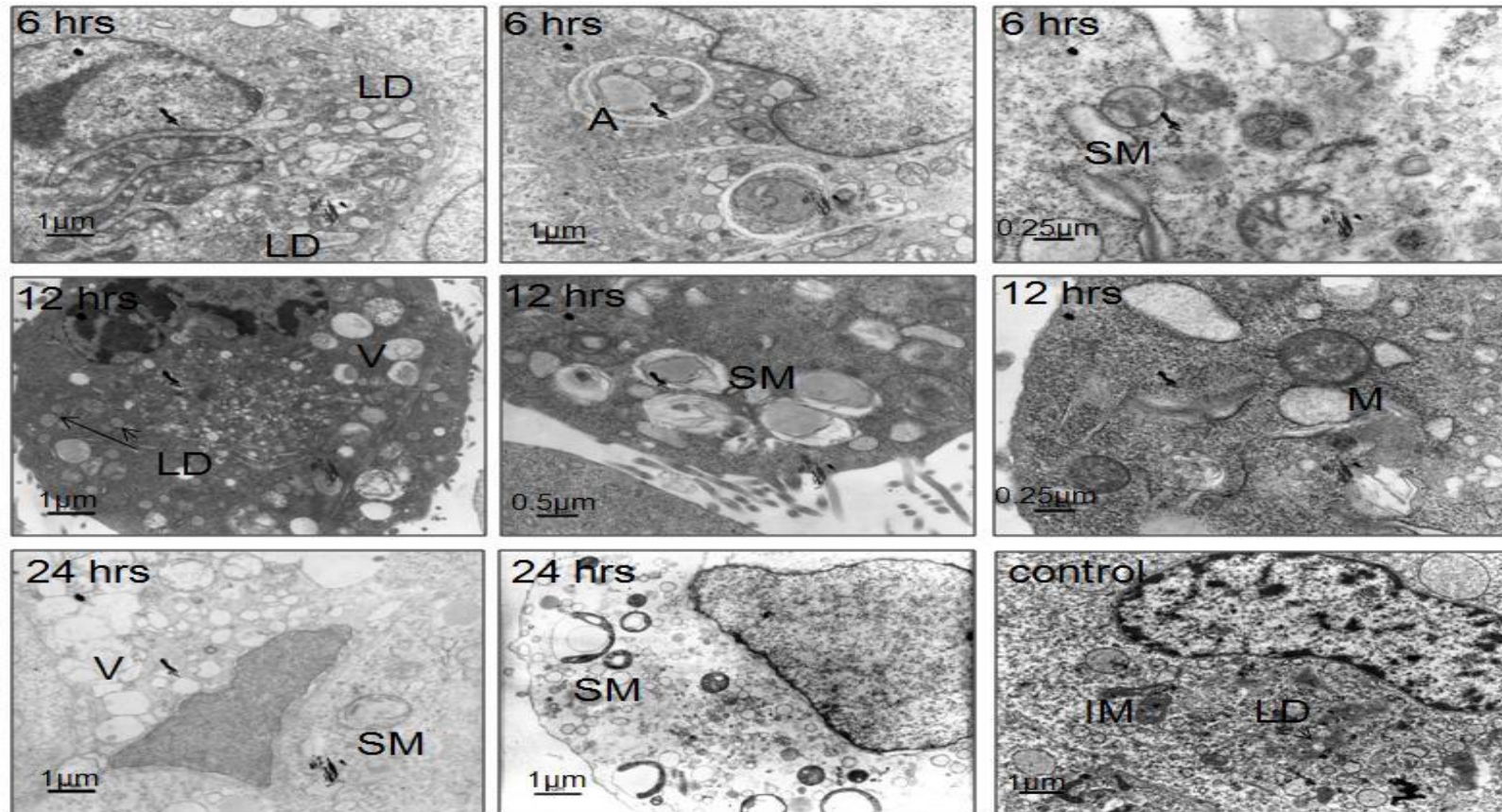


**Figure 5.7.** TEM images of control and starved cells after 6, 12, and 24 hrs (LD- lipid droplets; A- autophagic bodies; SM- swollen mitochondria; M- myelinoid bodies; V- vacuoles; IM- intact mitochondria).

#### **5.3.4. <sup>1</sup>H HR-MAS NMR alterations**

The rat glioblastoma BT4C cells were harvested after 4, 6, 12, 18, and 24 hours of incubation in PBS. <sup>1</sup>H HR-MAS NMR was performed on the prepared samples of each time point as described previously in chapter 2. The spectra are presented in figures 5.8 and 5.9. The lipid, metabolite, and macromolecule signals were assigned and quantitated using the TARQUIN algorithm. The same methods used to measure relative levels of lipids and metabolites in cisplatin exposed BT4C cells (described in chapter 2) were applied here to determine relative concentrations of lipids and metabolites in BT4C cells incubated in substrate free medium.

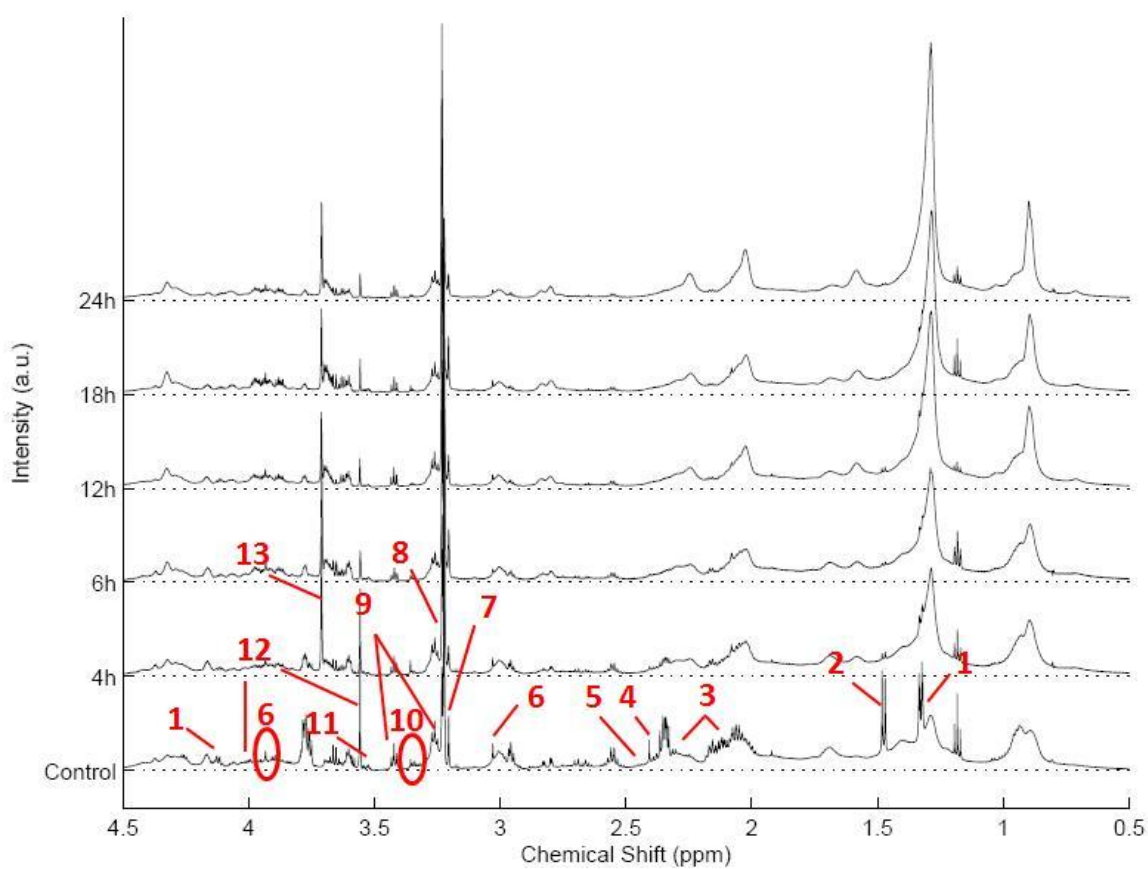


**Figure 5.8.**  $^1\text{H}$  HR-MAS NMR spectra of BT4C cells following substrate starvation. (A) 0.5 to 4.5 ppm region. Metabolites labelled are as follows: **1**- lactate, **2**-alanine, **3**- glutamate, **4**- succinate, **5**- glutamine and aspartate, **6**- creatine, **7**- choline, **8**- GPC and PC, **9**- taurine, **10**- scyllo-inositol, **11**- glycine, **12**- myo-inositol, **13**- guanidinoacetate.

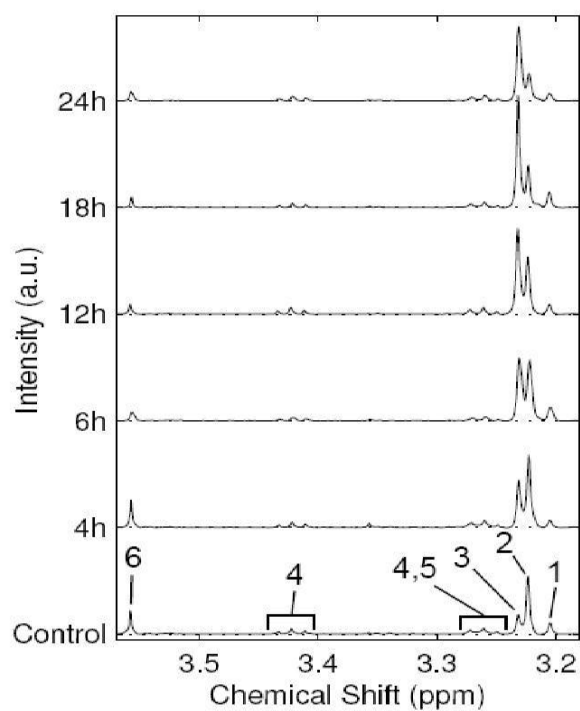


**Figure 5.9.** Choline containing region. metabolites labelled on the control spectrum are as follows: **1-** choline, **2-** phosphocholine, **3-** glycerophosphocholine, **4-** taurine, **5-** phosphatidylcholine **6-** glycine.

### 5.3.4.1. <sup>1</sup>H HR-MAS NMR Visible Lipid Alterations

The sum of macromolecule signals at 0.94, 1.68, and 3.00 ppm were used to calculate relative quantities of lipid signals (table 5.1).

	Chemical shift (ppm)	Untreated cells	Cells incubated with PBS for various time intervals				
			4h	6h	12h	18h	24h
	0.89	0.254±0.055	0.384±0.028*	0.480±0.023*	1.118±0.292*	1.200±0.209*	1.220±0.460*
<b>Saturated and unsaturated Fatty acids</b>	1.3	1.042±0.095	1.765±0.059**	2.032±0.091**	3.978±0.684*	4.597±0.677*	5.113±1.804*
	1.58	0.020±0.007	0.108±0.004**	0.130±0.011**	0.301±0.033**	0.306±0.042*	0.416±0.186*
	2.2	0.308±0.047	0.346±0.022	0.384±0.004	0.690±0.130*	0.731±0.110*	0.791±0.281*
	2.02	0.504±0.057	0.581±0.031	0.625±0.017	1.081±0.199*	1.131±0.153*	1.205±0.383*
<b>Unsaturated fatty acids</b>	2.8	0.056±0.021	0.104±0.007*	1.163±0.008*	0.267±0.036*	0.366±0.107*	0.293±0.073*
	5.4	0.118±0.016	0.177±0.004*	0.213±0.005*	0.534±0.115*	0.651±0.146*	0.652±0.272*

**Table 5.1.** Relative quantities of <sup>1</sup>H HR MAS NMR visible lipids in control, and starved cells. Three samples at each condition were analysed. The results are presented as mean±SD (\**p*<0.05, \*\**p*<0.001, compared to untreated samples).

Saturated and unsaturated moieties of fatty acids contributing to 0.89, 1.3, 1.58, and 2.2 ppm signals and unsaturated fatty acid moieties represented by peaks at 2.02, 2.8, 5.4 ppm

increased following replacement of medium with PBS. The detected lipid signals continued to rise significantly by prolonging the incubation time in PBS.

The signals at 0.89 and 1.3 ppm increased 5 fold ( $p < 0.05$ ) and the peak at 2.2 ppm elevated 3 fold ( $p < 0.05$ ) after 24 hours PBS replacement. The signal at 1.58 ppm increased 15 fold after 12 hours PBS exposure and continued to elevate reaching  $0.4 \pm 0.2$  with a 21 fold increase after 24 hours ( $p < 0.001$  and  $p < 0.05$ ; respectively). The ratio of the signals  $1.3/0.89$  arising from  $-\text{CH}_2-\text{CH}_2-\text{CH}_2-/-\text{CH}_3$  moieties did not change indicating that the mean chain length of fatty acids did not alter by longer maintenance of the cells in PBS.

After 12 hours PBS replacement, the lipid signals at 2.02 and 2.8 ppm increased to approximately 2 and 5 fold, respectively ( $p < 0.05$ ), and the intensity of the 5.4 ppm signal reached  $0.6 \pm 0.1$  after 18 hours PBS replacement with 6 fold increase compared with cells sustained in the substrate containing-medium (control samples) ( $p < 0.05$ ).

Similar results to the cisplatin exposed cells were detected for the ratio of 5.4 ppm/2.8 ppm signals. This ratio is approximately 2 indicating that almost all the unsaturated fatty acids are polyunsaturated containing  $-\text{CH}=\text{CH}-\text{CH}_2-\text{CH}=\text{CH}-$  moiety. The ratio of 0.89 ppm/2.8 ppm ( $-\text{CH}_3/-\text{CH}=\text{CH}-\text{CH}_2-\text{CH}=\text{CH}-$ ) was around 4 in PBS exposed cells. Allowing for the proton number, approximately a third of the fatty acids are polyunsaturated and the rest are saturated.

#### **5.3.4.2. <sup>1</sup>H HR-MAS NMR Metabolite Alterations**

Using the TARQUIN algorithm, several metabolites were identified and quantitated. The relative concentration of each of the metabolites was calculated relative to the sum of all the identified metabolites (table 5.2) and the significant alterations in the pattern of the detected relative metabolites were determined compared to control samples (table 5.3).

Metabolites	Untreated cells	4h	6h	124h	18h	24h
Acetate	8.08E-04±7.04E-04	2.61E-04±4.47E-04	2.53E-04±4.39E-04	4.73E-04±8.19E-04	2.32E-04±4.03E-04	2.09E-04±3.62E-04
Alanine	9.90E-02±4.30E-03	2.18E-02±3.21E-02	1.43E-02±3.44E-03	7.94E-03±2.92E-03	2.80E-03±6.83E-04	1.20E-02±2.07E-02
Aspartate	4.58E-02±6.64E-03	4.33E-02±1.09E-02	4.85E-02±6.35E-03	6.32E-02±2.55E-03	4.69E-02±3.09E-02	4.15E-02±2.10E-02
Choline	1.28E-02±3.09E-03	1.08E-02±8.36E-04	2.24E-02±6.35E-03	2.43E-02±1.20E-03	3.18E-02±8.30E-03	2.59E-02±6.86E-03
Creatine	1.34E-02±3.87E-03	1.65E-02±2.42E-03	1.62E-02±4.94E-04	2.26E-02±1.23E-03	1.80E-02±4.91E-03	1.77E-02±5.22E-03
Glutathione	7.01E-02±3.19E-02	6.31E-02±7.08E-03	5.23E-02±2.29E-03	4.58E-02±3.07E-03	2.61E-02±9.07E-03	3.55E-02±4.48E-03
Glutamate	2.59E-01±2.91E-02	7.64E-02±6.02E-03	1.41E-02±1.19E-02	1.45E-03±1.28E-03	0.00E+00±0.00E+00	6.89E-03±6.26E-03
Glutamine	2.06E-02±6.43E-03	1.18E-03±2.04E-03	5.48E-03±9.50E-03	0.00E+00±0.00E+00	0.00E+00±0.00E+00	5.52E-03±9.55E-03
GPC	3.87E-02±2.11E-02	8.07E-02±8.80E-03	1.43E-01±1.70E-02	1.96E-01±1.86E-02	2.21E-01±4.08E-02	1.93E-01±4.75E-02
Glycine	1.09E-01±2.15E-02	1.03E-01±6.55E-03	6.51E-02±8.05E-03	4.86E-02±5.45E-03	3.89E-02±2.35E-02	7.60E-02±2.84E-02
Lactate	1.06E-01±3.00E-02	7.31E-02±9.92E-03	6.54E-02±5.72E-03	8.90E-02±2.28E-02	6.89E-02±4.75E-03	7.36E-02±8.03E-03
Myo-Inositol	7.79E-03±1.13E-02	0.00E+00±0.00E+00	0.00E+00±0.00E+00	0.00E-00±0.00E+00	0.00E-00±0.00E+00	0.00E+00±0.00E+00
PC	8.38E-02±7.63E-03	1.19E.01±1.63E-02	1.27E-01±5.67E-03	1.29E-01±1.01E-02	8.45E-02±1.61E-02	6.74E-02±5.21E-03
PEth	0.00E+00±0.00E+00	0.00E+00±0.00E+00	0.00E+00±0.00E+00	0.00E+00±0.00E+00	0.00E+00±0.00E+00	0.00E+00±0.00E+00
Scyllo-inositol	3.13E-03±1.38E-03	2.29E-03±9.86E-04	1.27E-03±5.02E-04	2.26E-03±4.60E-04	3.91E-04±6.77E-04	0.00E+00±0.00E+00
Succinate	5.59E-03±2.60E-03	2.17E-03±1.03E-04	1.66E-03±6.96E-04	1.93E-04±1.68E-04	2.70E-04±2.59E-04	6.29E-04±2.37E-04
Taurine	7.82E-02±1.93E-02	6.65E-02±6.53E-03	5.97E-02±6.41E-03	1.01E-01±1.56E-03	6.05E-02±9.96E-03	7.98E-02±2.09E-03
Hypo-Taurine	2.40E-02±5.54E-03	2.65E-02±4.62E-03	2.69E-02±1.70E-03	2.81E-02±5.64E-04	2.47E-02±9.56E-03	3.16E-02±1.21E-02
Guanidioacetate	4.05E-03±4.38E-03	2.70E-01±5.51E-02	3.11E-01±5.70E-02	2.13E-01±2.66E-03	3.55E-01±1.54E-01	3.06E-01±9.97E-02

**Table 5.2.** Relative concentration of  $^1\text{H}$  HR-MAS NMR detectable metabolites in control and starved cells. The results are presented as mean $\pm$ SD. Three samples at each condition were analysed.

Metabolites	Starved cells				
	4h	6h	12h	18h	24h
PC	*↑	**↑	**↑		
GPC		**↑	**↑	**↑	**↑
Choline				**↑	
Alanine	**↓	**↓	**↓	**↓	**↓
Scyllo-Inositol				*↓	*↓
Succinate	*↓	*↓	**↓	**↓	*↓
Glycine			*↓	*↓	
Glutamate	**↓	**↓	**↓	**↓	**↓
Glutathione				*↓	
Guanidinoacetate	*↑	**↑	*↑	**↑	**↑
PC/GPC				*↓	*↓

**Table 5.3.**  $^1\text{H}$  HR-MAS NMR alterations detected in the relative concentration of the metabolites during cell starvation. (↑) represents an increase in relative metabolite levels and (↓) represents a decrease in relative metabolite levels compared to control cells ( $*p<0.05$ ,  $**p<0.001$ ).

The metabolite profile of BT4C cells incubated in PBS changed compared to cells incubated in culture medium and further alterations were detected in samples deprived for longer. An increase in GPC and a decrease in alanine, succinate, and glutamate were detected with longer starvation. PC levels increased up to 12 hours of substrate deprivation

and alteration in the levels of aspartate, lactate, creatine, hypo-taurine, and taurine were not detected. In addition PEth and myo-inositol were not detectable in the samples.

PCA was performed on the relative concentration of metabolites (figure 5.8). The first principal component is the main separation factor of the control and substrate starved cells (figure 5.10.A). This component accounts for approximately 42% of the variance. Starved cells are well separated from cells maintained in culture medium in this principal component. Cells incubated in medium are at the far left of the plot, occupying the negative scores and the positive scores are occupied by PBS maintained cells. Starved samples at various time intervals are close to each other on the PCA score plots. However, they are separated from each other, with the earlier time points skewed towards the negative scores and the longer incubation times occupying increasingly positive scores of the principal component 1 coefficient (figure 5.10.A). According to the principal component 1 loadings (figure 5.10.B) cell starvation lead to lower levels of succinate, glutamate, glutathione, glutamine, scyllo-inositol, acetate, and alanine and higher levels of GPC, creatine, and choline (figure 5.10.B). The PCA results confirm the findings of the one way- ANOVA tests.

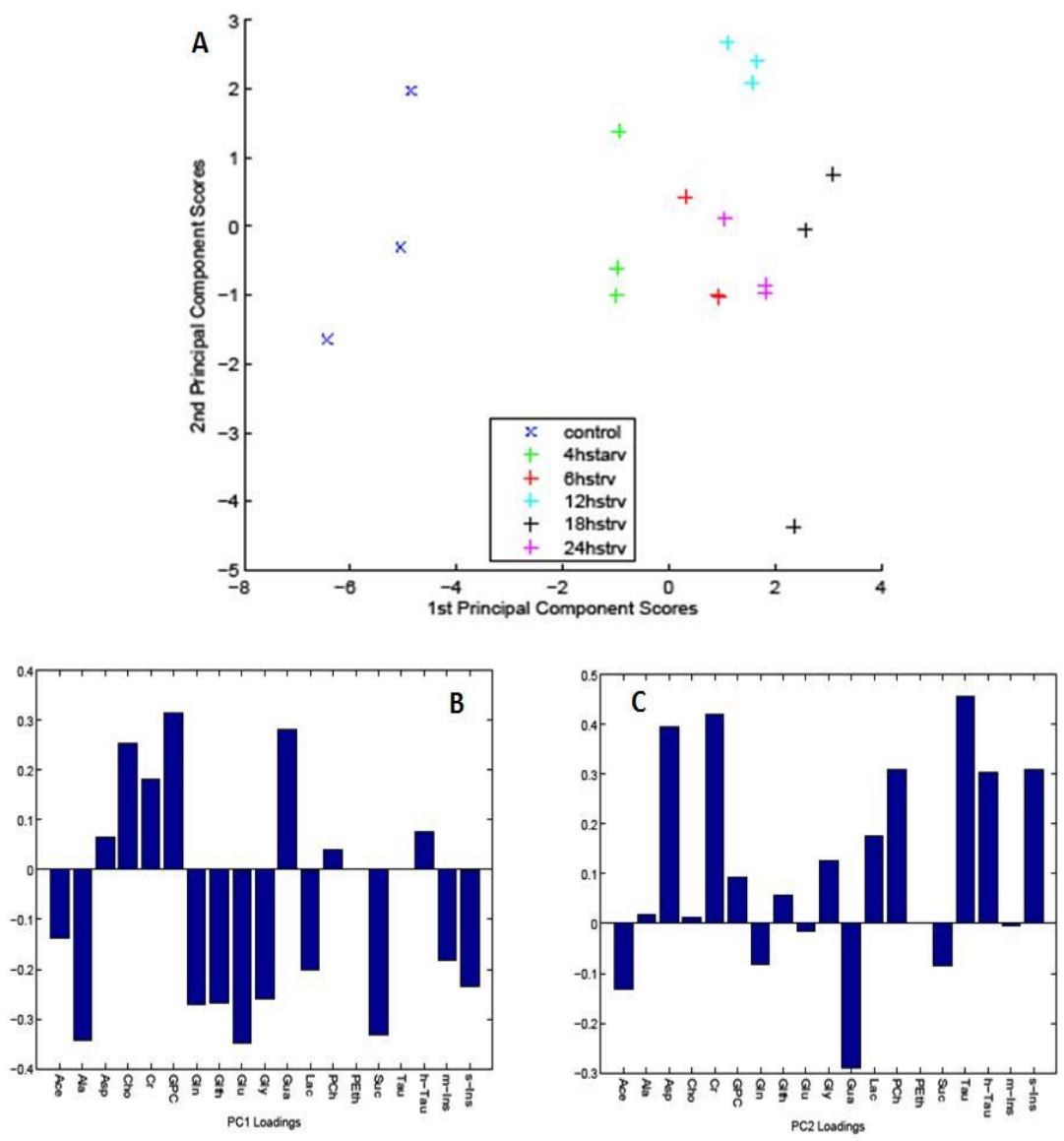


**Figure 5.10.** PCA of  $^1\text{H}$  HR-MAS NMR metabolite profiles for substrate starved cells. (A) Scores plot, (B) Loadings for principal component 1, (C) Loadings for principal component 2.

### ***5.3.5. Principal Component Analysis of Cisplatin Exposed and Substrate Deprived Metabolite Data of BT4C cells***

PCA was performed on the  $^1\text{H}$  HR-MAS NMR metabolite data of cisplatin exposed cells presented in chapter 3 and  $^1\text{H}$  HR-MAS NMR relative metabolite data of starved cells described in this chapter (figure 5.11). Analysis was performed on both sets of data to understand better the relative metabolite alterations due to necrosis and cell growth arrest prior to apoptosis in rat BT4C cells and to identify the similarities and differences between the metabolite alterations caused by these conditions.

The scores plot for the PCA of the metabolite profiles is presented in Figure 5.11.A. Only nutrient starvation is associated with a change in the first principal component and this change occurs early in the time course. A decrease in the second principal component occurs during both cisplatin exposure and nutrient starvation. From the loadings plot for principal component 2 (Figures 5.11.C), both cisplatin exposure and cell starvation are associated with changes in many metabolites, the most prominent changes being decreases in glycine, succinate and glutamate with an increase in GPC. Alterations which were specific to early changes during nutrient starvation can be deduced from the loadings plot for principal component 1 (figure 5.11.B). Again, many metabolites contributed but the largest loadings were associated with decreases in glutamate and alanine.

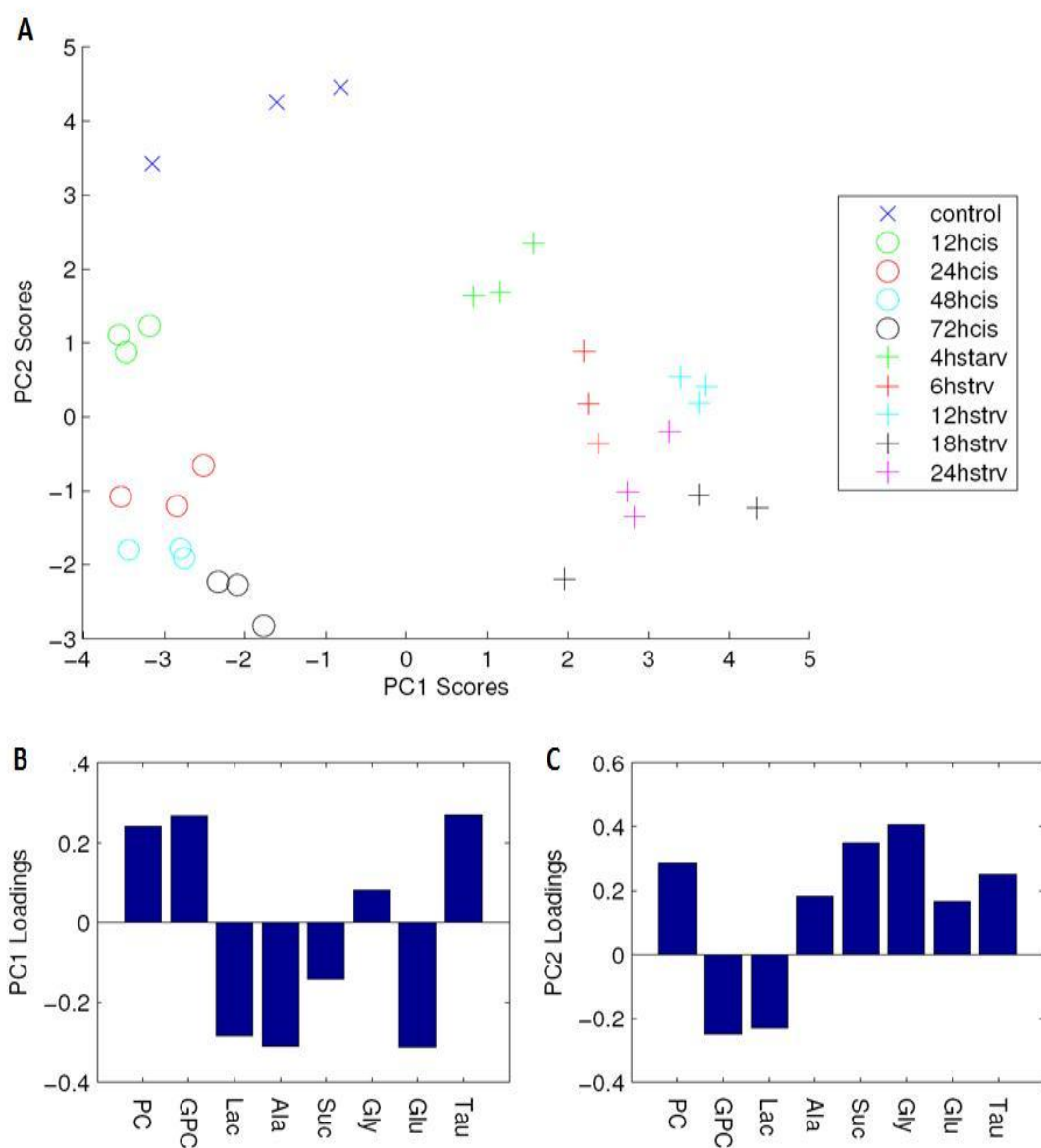


**Figure 5.11.** PCA of  $^1\text{H}$  HR-MAS NMR metabolite profiles for cisplatin exposed and substrate starved cells (A) scores plot, (B) loadings for principal component 1, (C) loadings for principal component 2.

## 5.4. Discussion

Microscopic analysis of various staining techniques including DAPI, trypan blue, and H&E revealed that with longer substrate deprivation the number of necrotic cells increased. Large vacuoles were identified by H&E staining in cells incubated with PBS. Further by using TEM necrosis was confirmed as the type of cell death and the presence of cytoplasmic vacuoles and swollen mitochondria was revealed in these cells. In addition, some of the cells contained autophagic and myelinoid bodies in their cytoplasm.

Increases in the diameter and the cell area occupied by lipid droplets were observed in necrotic and viable, stressed cells. This implies that the cytoplasmic lipid droplets are the source of the detected increase in lipid signals by  $^1\text{H}$  HR-MAS NMR. Saturated and unsaturated moieties of fatty acids at 0.89, 1.3, 1.58, and 2.2 ppm and unsaturated fatty acids represented by peaks at 2.02, 2.8, 5.4 ppm increased with longer substrate deprivation.

Increase in  $^1\text{H}$  HR-MAS NMR visible lipids in necrotic regions of tumours has been identified previously (42, 46, 110, 162). Mobile lipid signals were detected *in vivo* by  $^1\text{H}$  MRS in necrotic and perinecrotic regions of C6 rat brain glioma and they were associated with accumulation of lipid droplets (42, 46). Kuesel *et al.* also ascribed the increase in mobile lipid resonances detected by *in vivo*  $^1\text{H}$  MRS to the necrotic foci of several high grade astrocytomas (56). A correlation was also detected between lipid droplets and  $^1\text{H}$  MRS lipid signals in human brain tumour biopsy samples. The lipid droplets were detected in non-necrotic regions of grade II and III astrocytomas and in higher levels in necrotic regions of grade IV astrocytoma. It was suggested that lipid droplets in high grade astrocytoma accumulate during the transition from hypoxia to necrosis. This finding

indicated that lipid droplets are formed prior to necrosis (110). The presence of lipid droplets in viable, stressed BT4C cells in substrate deprived medium is in agreement with previous findings and demonstrates the formation of lipid droplets prior to necrosis. The detected alterations in <sup>1</sup>H HR-MAS NMR visible lipids and the identified source of lipid increase in starved cells were similar to the results found in cisplatin exposed cells of various time points described in chapter 4.

In addition to lipid alterations, relative concentrations of metabolites were altered with longer substrate deprivation. In these samples, an increase in choline and GPC and a decrease in the levels of alanine, glycine, glutamate, succinate, and scyllo-inositol were noticed. The detected levels of lactate, aspartate, creatine, taurine, and hypo-aurine did not alter during longer periods of substrate deprivation. In addition, PEth and myo-inositol were not detectable in the samples and PC levels were decreased after an initial increase up to 12 hours substrate deprivation.

Necrosis cell death is a regulated event and consists of serial steps (9, 86, 87). Morphological characteristics are the best method to identify and distinguish necrosis from apoptosis cell death. Swelling of organelles such as mitochondria and loss of membrane integrity are associated with necrosis. In addition, necrosis does not require energy and the production of bioenergetic compounds are impaired in this process.

Nutrient deprivation causes necrosis in cells by ensuring a drastic decrease in cellular energy. Impaired bioenergetic status causes decreased activity of ATP-dependent ion pumps situated in the cell membrane. Consequently ion homeostasis is altered affecting mitochondria and ATP production through oxidative phosphorylation (9). Cells try to

survive by autophagy and by consuming cell resources such as macromolecules (9, 161, 163), however if the nutrients are not replaced cells progress to necrosis (161).

Oxidative phosphorylation is a more efficient pathway of ATP production compared to glycolysis. However, ATP production via glycolysis occurs at a faster rate and it is the main source of energy production in tumour cells (122). The rate of glycolysis depends on glucose availability and lactate clearance (9). Therefore, absence of glucose in the medium causes a decrease in bioenergetic compounds in tumour cells. Reduced energy levels results in necrosis followed by impaired mitochondria and oxidative phosphorylation. As the BT4C cells were incubated in substrate free medium, amino acids such as alanine, glycine, and glutamate and the TCA cycle intermediates such as succinate and scyllo-inositol may have entered pathways resulting in ATP generation in an attempt to survive. Hence, a decrease was detected in the relative level of these metabolites in starved BT4C cells (figure 5.12).

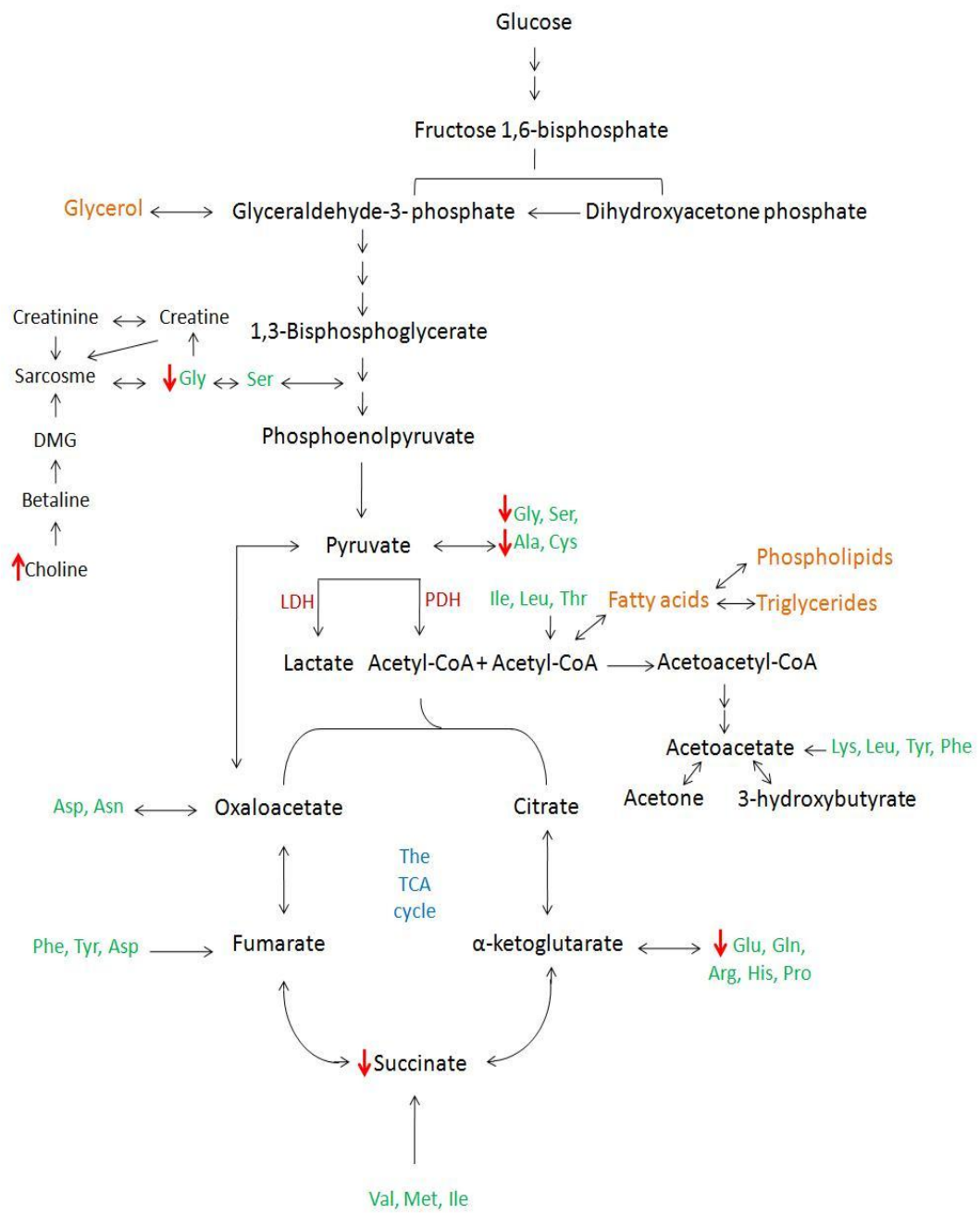


**Figure 5.12.** The relevant metabolite pathways in starved BT4C cells. In this diagram, the metabolites with red arrows altered significantly with longer substrate deprivation (Ala. alanine, Arg. Arginine, Asn. asparagine, Asp. aspartate, Cys. cysteine, Glu. glutamate, Gln. glutamine, Gly. glycine, His. histidine, Ile. isoleucine, Leu. leucine, Lys. lysine, Met. methionine, Phe. phenylalanine, Pro. proline, Ser. serine, Thr. threonine, Trp. tryptophan, Tyr. tyrosine, Val. Valine).

An increase in  $^1\text{H}$  HR-MAS NMR visible lipids and lipid droplets containing neutral lipids as well as elevated levels of GPC and PC indicate the possibility of phospholipid catabolism as the underlying mechanism of the detected alterations (78).

An increase in MRS visible lipids was detected in human breast cell line HBL-100 treated with cationic lipophilic agents. In these necrotic cells, swollen mitochondria with disordered cristae and myelinoid bodies were identified. The degradation of damaged mitochondria by lysosomal enzymes was suggested as the reason behind the detected alterations (47). Lysosomal enzymes such as sphingomyelinase and phospholipase A1, A2, and C process phospholipids and produce fatty acids, glycerol, and phosphodiester. Fatty acids and glycerol are exported from the lysosome and TGs are produced from the fatty acids (47, 164) (described in chapter 4). There is a possibility that in necrotic BT4C cells lysosomal enzymes catabolise PLs and degrade them to fatty acids, resulting in the detected increase in  $^1\text{H}$  HR-MAS NMR lipids and cytoplasmic lipid droplets.

Furthermore, the detected increase in PC and GPC levels is in agreement with the suggested PL degradation mechanism and the previous findings associating an increase in membrane substrates with cell death (165).

It has been suggested that phospholipase D (PLD) is specifically activated in response to TNF-induced necrosis *vs.* apoptosis resulting in production of choline. Mitochondrial damage during the necrosis process results in formation of reactive oxygen species and damage to the membrane by lipid peroxidation. PLD activity perhaps is a mechanism to repair the damage caused to the cell (166).

The increase in PC levels up to 12 hours into substrate deprivation indicates activation of PLC and catabolism of membrane PtCho. It has been suggested that PLA2 is activated

during the late stages of necrosis (166). Activation of PLC during early stages and PLA2 during late stages of substrate deprivation would explain the high level of PC at early stages and an increase in GPC level at later stages of necrosis in BT4C cells.

#### ***5.4.1. Cell Growth Arrest Leading to Apoptosis vs. Necrosis***

The current study shows that drug-induced cell growth arrest and starvation-induced necrotic cell death cause both common and distinct changes in cellular metabolites. Both challenges result in increases in GPC and decreases in alanine, glutamate, glycine and succinate. Decreases in amino acids such as alanine, glutamate, glycine and the TCA cycle intermediates, such as succinate, in growth arrested cells prior to apoptosis and in necrotic cells indicate a redirection of metabolites to energy production rather than consumption through synthesis pathways. Lactate and alanine can also be linked to energy metabolism and although there have been fewer reports related to the levels of succinate and glutamate, these are also closely involved with energy metabolism. The trend detected is similar under both conditions. However, the extent of the alterations caused by cell cycle arrest or necrosis differs.

High levels of glycine, taurine and glutamate have all been seen in highly malignant tumours and have been proposed as biomarkers of malignancy (128). It is therefore of interest that relative levels of these metabolites decrease with drug response. The detected decrease in taurine levels in growth arrested cells (chapter 3) and the lack of significant taurine alterations in necrotic cell emphasises that this metabolite is not associated with all forms of cell stress or cell death and further investigation of its role in tumour cells is required.

Combined levels of GPC, PC and Choline are usually measured in *in vivo*  $^1\text{H}$  MRS due to the poor spectral resolution. The tCho level relative to the total metabolite concentration decreased with longer substrate deprivation indicating altered levels of metabolites contributing to tCho. However, tCho was not altered relative to the total metabolite concentration when the cells were treated with cisplatin. With significant alterations in the levels of PC and GPC in cisplatin treated cells, this work emphasises the risk of using a combined quantity for treatment monitoring when the components are affected differently by treatment.

## ***5.5. Conclusion***

Increases in saturated and unsaturated fatty acids were detected in starved cells by  $^1\text{H}$  HR-MAS NMR spectroscopy. Almost one third of the fatty acids detected were unsaturated, mainly polyunsaturated fatty acids. Investigations revealed that cytoplasmic lipid droplets are the source of lipid accumulation and the likely source of lipids detected by  $^1\text{H}$  HR-MAS NMR. DAPI and Nile red co-staining revealed the presence of lipid droplets in early necrotic and viable, stressed cells, indicating the early formation of lipid droplets in stressed cells. Accumulation of  $^1\text{H}$  HR-MAS NMR lipids in stressed or necrotic cells provided further evidence on the potential of NMR lipids as markers of cell stress.

Energy metabolism was affected in starved BT4C cells and decreased levels of amino acids such as glycine, glutamate, and alanine and the TCA cycle intermediates such as succinate were detected. Unlike growth arrested cells, taurine levels did not alter in necrotic BT4C cells, demonstrating the potential of taurine in distinguishing necrosis from cell cycle arrest. Both GPC and PC levels increased initially in starved BT4C cells. The contrast between the PC pattern of growth arrested cells and necrotic cells may represent different patterns of activity in phospholipase in response to the mode of cell death and the stimuli.

Although the time-dependency and magnitude of the alterations were different in cisplatin exposed cells and starved cells, PCA revealed two patterns of metabolite changes, one which was common to both types of cell stress and another which was specific for necrosis induced by cell starvation. Glycine, alanine and glutamate may provide new biomarkers of cell stress and cell death whilst taurine may distinguish between cyto-stasis and necrosis.

**CHAPTER 6**

**CONCLUSIONS**

## 6.1. Summary and Conclusions

Early detection of tumour therapy response is a powerful indicator of outcome and by identifying unsuccessful therapy at early stages of treatment alternative therapy can be selected and the patient's quality of life can be improved.

Glioma is the most common form of primary brain tumour of the CNS in humans and has a poor prognosis. Identifying markers of treatment efficacy non-invasively may influence the clinical management of this tumour.

In this work, rat BT4C cell line was used as a model for glioma and  $^1\text{H}$  HR-MAS NMR spectroscopy was used to identify metabolite and lipid alterations in response to cell cycle arrest or necrosis.

Compared with *in vivo* MRS studies, *in vitro* experiments have better spectral resolution and have the advantage of revealing higher number of metabolites and lipids. In addition, in *in vivo* settings the surrounding tissue influences tumour metabolite and lipid profiles. In contrast, the experimental conditions can be more controlled in *in vitro* and the effects of various factors on lipid and metabolite profiles can be investigated.

Using cells rather than extracts provides a closer system to *in vivo* models and enables study of lipids and metabolites simultaneously. In addition, by using whole cells minimum sample preparation on a small number of cells is required. During performance of MRS the cells remain viable for a period of time. This provides the opportunity to use the samples for further investigations. However, due to inhomogeneity of the cells MRS spectra may have poor resolution and low signal to noise ratio. During  $^1\text{H}$  HR-MAS NMR

spectroscopy, cells are spun at a specific angle. This reduces the effects of decoupling and chemical shift anisotropy, resulting in improved spectral resolution from inhomogeneous samples within a short time.

In chapter 3 trypan blue and H&E dyes were used and in chapter 4 cells were stained with DAPI to investigate viability of rat glioma BT4C cells exposed to 50  $\mu$ M cisplatin after various times of 12, 24, 48, or 72 hours. In chapter 3, the occurrence of DNA fragments on gel electrophoresis were used to determine the presence of apoptosis in cisplatin exposed cells and flow cytometry of annexin V-FITC labelled and PI stained cells were used to determine the percentages of viable, necrotic, and apoptotic cells. Further investigations using flow cytometry and PI dye were carried out to identify cell distribution in different stages of growth cycle.

In chapter 4 TEM was used to further confirm the type of cell death in cisplatin exposed cells. Combination of Nile red and DAPI staining were used to investigate the presence of lipid droplets in the cytoplasm of viable, growth arrested cells.

Finally,  $^1\text{H}$  HR-MAS NMR spectroscopy was performed on cisplatin exposed cells of various times to identify metabolite and lipid alterations in response to treatment. Metabolite changes were described in chapter 3 and lipid alterations were explained in chapter 4 (figure 3.1).

Morphological and molecular analysis showed that the majority of cisplatin exposed BT4C cells were viable and small numbers were undergoing apoptosis or necrosis and that the morphologically viable cells were growth arrested.

<sup>1</sup>H HR-MAS NMR revealed increased relative levels of saturated and unsaturated lipids in these cells with longer cisplatin exposure. Direct examination of these cells using Nile red and DAPI co-staining associated the detected <sup>1</sup>H HR-MAS NMR lipid increase with the alterations in the amount and size of cytoplasmic lipid droplets in the cell cycle arrested cells. <sup>1</sup>H HR-MAS NMR metabolite alterations revealed a decrease in relative levels of PC and an increase in relative concentrations of GPC by exposure to cisplatin and PC/GPC ratio reduced in these cells. A decrease in PC levels has been identified in response to chemotherapy and has been proposed as an early marker of treatment efficacy (63). The detected decrease in PC/GPC level is in agreement with previous findings of cell cycle arrest studies and may indicate growth arrest prior to apoptosis (50). The relative levels of glycine, glutamate, alanine and succinate decreased by longer cisplatin exposure. Reduced relative levels of these amino acids along with increased relative levels of lactate indicate altered energy metabolism pathways in cisplatin exposed cells and provide potential novel biomarkers for early treatment response in gliomas.

In chapter 5 cell stress and necrosis was induced by maintaining the rat glioma BT4C cells in PBS for different time intervals of 4, 6, 12, 18, or 24 hours. Cell viability was examined using trypan blue dye and the percentages of necrotic and viable cells were identified by H&E and DAPI staining. TEM was used to confirm the viability status of PBS maintained cells and to study the ultrastructure of these cells. Nile red and DAPI dyes were used to

investigate the presence of lipid droplets in cytoplasm of stressed and necrotic cells (figure 5.1).

Morphological analysis of BT4C cells maintained in substrate free medium revealed the presence of stressed and necrotic cells. An increase in relative levels of saturated and unsaturated fatty acids was detected by  $^1\text{H}$  HR-MAS NMR. Nile red and DAPI co-staining associated this increase with the presence of cytoplasmic lipid droplets in viable, stressed cells and necrotic cells.  $^1\text{H}$  HR-MAS NMR metabolite investigations revealed an initial increase in PC and continual increase in GPC relative levels. In addition decreases in amino acids such as alanine, glycine, glutamate, and TCA cycle intermediates such as succinate were identified.

$^1\text{H}$  HR-MAS NMR lipid accumulation following induction of cytostasis or necrosis and the presence of associated cytoplasmic lipid droplets in stressed, growth arrested or necrotic cells shows that lipid accumulation is a general indicator of cell stress and occurs early in the process. Lipid accumulation and the presence of cytoplasmic lipid droplets in both conditions show that alterations in phospholipid metabolism are prominent in cell stress.

The alterations in phospholipid metabolism pathway and the activity of phospholipase enzymes have been previously suggested to influence the levels of lipid droplets in stressed cells (78). Activation of phospholipases A1, A2, and lysophospholipase result in production of fatty acids (22, 78). The produced fatty acids can be re-esterified to generate phospholipids such as PtdCho or in the presence of DAG can produce TAG (48). DAG and fatty acids are actively transported between membranes in form of lipid droplets (156). In

growth arrested cells PhtCho is not used in membrane synthesis and it is degraded to choline and fatty acids. This results in accumulation of lipid droplets. During early stages of starvation induced necrosis, cell membranes and other cellular components are degraded in order to provide substrates for cell survival (161).

Alterations in PC and GPC levels provide further evidence for altered phospholipid metabolism. The difference in the detected pattern of PC alterations in growth arrested or necrotic cells implies that there is not a single common mechanism for altered choline metabolism and that the activities of various phospholipase enzymes differ following initiation of cytostasis or necrosis. For example phospholipase D activity has been detected in TNF-induced necrosis (166).

The level of tCho remained constant by longer exposure to cisplatin. However, the individual metabolites contributing to tCho altered and the detected changes were different in cisplatin exposed and starved cells. In cisplatin exposed cells GPC relative levels decreased and PC relative levels increased by exposure to cisplatin and in starved cells the relative concentrations of PC and GPC increased. This further highlights the potential of the individual tCho metabolites as biomarkers of tumour response and emphasises the importance of separating these metabolites *in vivo*.

A decrease in the levels of amino acids (alanine, glycine, glutamate) and TCA cycle intermediates (succinate) following induction of cell cycle arrest or necrosis indicates

alteration in the energy metabolism pathways. Increase in relative levels of lactate in growth arrested cells show that the effected pathways are different in necrotic and cell cycle arrested cells. Previous studies have shown an association between high levels of glycine, glutamate, taurine with malignancy (116, 128, 129). As the levels of alanine, glycine and taurine are high in malignant cells, decreased relative levels of these metabolites provide early biomarkers of cell stress and cell death.

Taurine levels decreased in growth arrested cells and remained constant in necrotic cells. This shows that alterations in taurine levels are not representative of all types of cell stress or cell death. Perhaps release of taurine and other osmolytes in growth arrested cells prior to apoptosis are indicative of progression to apoptosis and cell shrinkage (138- 139). High levels of taurine in primitive neuroectodermal tumours with high proliferation levels were detected (137). Reduced taurine levels in growth arrested cells may have the potential to identify growth arrest prior to apoptosis and may have the potential to be used in distinguishing different types of cell death.

A number of detected metabolite alterations were common in growth arrested cells and necrotic cells. An increase in saturated and unsaturated fatty acids, a decrease in amino acids and TCA cycle intermediates have been identified during cytostasis and cell death. Therefore, these metabolites may have the potential to be used as indicators of cell stress. A group of metabolites altered differently in growth arrested and necrotic cells. The changes in individual choline containing metabolites and taurine relative levels were

different in growth arrested cells prior to apoptosis and in necrotic cells and may have the potential to distinguish between cytotostasis and necrosis.

## **6.2. Future Work**

The work carried out here investigated relative alterations of lipids and metabolites in one cell line and in response to cisplatin exposure or substrate deprivation. Future work on other cell lines using different stimuli is required to confirm the potential of the detected alterations as general markers of cell stress and to investigate their ability to distinguish cytostasis from necrosis.

Different animal and human glioma cell lines are required to be examined in order to confirm the changes detected previously in response to treatment in gliomas. Perhaps examination of other cell types would provide general markers of cell stress and cytostasis. Further examining the metabolite profiles of cell extracts would confirm the spectra achieved from MRS of the whole cells and may provide further information.

Although there are advantages in working with cell lines, a monolayer culture does not reflect all properties of tumours and as the ultimate goal is to use the detected metabolite alterations as markers of treatment efficacy in clinical settings, *in vivo* applicability of these *in vitro* biomarkers require investigations. The next step would be to examine animal models. In addition more information can be gained from comparing the MRS spectra of patients at diagnosis and throughout treatment.

Cell death mainly apoptosis and necrosis can be induced in cells via different stimuli. Metabolite profiling after induction of cell death by different methods of treatment such as chemotherapy, photodynamic or gene therapy may provide useful information and assist in identifying general markers of treatment efficacy. The biochemical pathways of apoptosis and necrosis are different. Therefore, dissimilarities can be identified in their metabolite profiles. Separating apoptotic and necrotic cells by methods such as flow cytometric cell

sorting may provide the opportunity to investigate specific MRS markers of each type of cell death.

The use of other techniques such as mass spectrometry will provide additional information and identifying changes in metabolites not detected by NMR will help to reveal the altered pathways and to better understand the changes occurring in tumour cells. A comparison with studies of molecular quantities and gene expression of the tumours will further help to elucidate the molecular pathways.

Investigations are required to identify the role of lipid droplets in stressed cells. Identifying the composition of the lipid bodies may be useful in achieving this purpose. Currently our team is extracting the lipid droplets from treated cells. The alteration in properties of the extracted lipid droplets in response to treatment are being studied by Nile red dye and fluorescence microscopy. In addition the nature of these lipid bodies will be investigated by MRS.

Novel biomarkers such as glycine, glutamate, and taurine warrant further investigation. High levels of glycine, glutamate, taurine, and alanine were associated with high malignancy. Reduced levels of these metabolites in response to treatment, reveals their potential as markers of treatment. However, further work is required to examine the profile of these metabolites in response to treatment in *in vivo* settings. Currently further work is being carried out to further assess the potential of glycine as a biomarker in clinical settings.

The work carried out here and previous studies show the vast potential of MRS in treatment evaluation. MRS has also shown possible applications in tumour diagnosis and prognosis. However, further work and robust multi-centre trials are required to explore and validate the potential of MRS and increase its utility in clinical settings.

## References

1. Morse DL, Raghunand N, Sadarangani P, Murthi S, Job C, Day S, et al. Response of choline metabolites to docetaxel therapy is quantified *in vivo* by localized  $^{31}\text{P}$  MRS of human breast cancer xenografts and *in vitro* by high-resolution  $^{31}\text{P}$  NMR spectroscopy of cell extracts. *Magn Reson Med*. 2007 Aug;58(2):270-80.
2. Robinson SP, Barton SJ, McSheehy PM, Griffiths JR. Nuclear magnetic resonance spectroscopy of cancer. *Br J Radiol*. 1997 Nov;70 Spec No:S60-9.
3. Griffin JL, Shockcor JP. Metabolic profiles of cancer cells. *Nat Rev Cancer*. 2004 Jul;4(7):551-61.
4. Oliver SG. Functional genomics: lessons from yeast. *Philos Trans R Soc Lond B Biol Sci*. 2002 Jan 29;357(1417):17-23.
5. Boudreau CR, Yang I, Liau LM. Gliomas: advances in molecular analysis and characterization. *Surg Neurol*. 2005 Oct;64(4):286-94; discussion 94.
6. Brandes AA, Tosoni A, Franceschi E, Reni M, Gatta G, Vecht C. Glioblastoma in adults. *Crit Rev Oncol Hematol*. 2008 Aug;67(2):139-52.
7. Evelhoch JL, Gillies RJ, Karczmar GS, Koutcher JA, Maxwell RJ, Nalcioglu O, et al. Applications of magnetic resonance in model systems: cancer therapeutics. *Neoplasia*. 2000 Jan-Apr;2(1-2):152-65.

8. Lutz NW. From metabolic to metabolomic NMR spectroscopy of apoptotic cells  
*Metabolomics* 2005;1(3):251-68.
9. Zong WX, Thompson CB. Necrotic death as a cell fate. *Genes Dev.* 2006 Jan 1;20(1):1-15.
10. Williams SR, Crockard HA, Gadian DG. Cerebral ischaemia studied by nuclear magnetic resonance spectroscopy. *Cerebrovasc Brain Metab Rev.* 1989 Summer;1(2):91-114.
11. Bezabeh T, Mowat MR, Jarolim L, Greenberg AH, Smith IC. Detection of drug-induced apoptosis and necrosis in human cervical carcinoma cells using  $^1\text{H}$  NMR spectroscopy. *Cell Death Differ.* 2001 Mar;8(3):219-24.
12. Shulman RG, Rothman DL, Blamire AM. NMR studies of human brain function. *Trends Biochem Sci.* 1994 Dec;19(12):522-6.
13. Kauppinen RA, Nissinen T, Karkkainen AM, Pirttila TR, Palvimo J, Kokko H, *et al.* Detection of thymosin beta 4 in situ in a guinea pig cerebral cortex preparation using  $^1\text{H}$  NMR spectroscopy. *J Biol Chem.* 1992 May 15;267(14):9905-10.
14. Sibtain NA, Howe FA, Saunders DE. The clinical value of proton magnetic resonance spectroscopy in adult brain tumours. *Clin Radiol.* 2007 Feb;62(2):109-19.

15. McBride DQ, Miller BL, Nikas DL, Buchthal S, Chang L, Chiang F, *et al.* Analysis of brain tumors using  $^1\text{H}$  magnetic resonance spectroscopy. *Surg Neurol.* 1995 Aug;44(2):137-44.
16. Kugel H, Heindel W, Ernestus RI, Bunke J, du Mesnil R, Friedmann G. Human brain tumors: spectral patterns detected with localized  $^1\text{H}$  MR spectroscopy. *Radiology.* 1992 Jun;183(3):701-9.
17. Govindaraju V, Young K, Maudsley AA. Proton NMR chemical shifts and coupling constants for brain metabolites. *NMR Biomed.* 2000 May;13(3):129-53.
18. Kinoshita Y, Kajiwara H, Yokota A, Koga Y. Proton magnetic resonance spectroscopy of astrocytic tumors: an *in vitro* study. *Neurol Med Chir (Tokyo).* 1993 Jun;33(6):350-9.
19. Andronesi OC, Blekas KD, Mintzopoulos D, Astrakas L, Black PM, Tzika AA. Molecular classification of brain tumor biopsies using solid-state magic angle spinning proton magnetic resonance spectroscopy and robust classifiers. *Int J Oncol.* 2008 Nov;33(5):1017-25.
20. Griffin JL, Blenkiron C, Valonen PK, Caldas C, Kauppinen RA. High-Resolution Magic Angle Spinning  $^1\text{H}$  NMR Spectroscopy and Reverse Transcription-PCR Analysis of Apoptosis in a Rat Glioma. *Analytical Chemistry.* 2006;78(5):1546-52.

21. Griffin JL, Lehtimäki KK, Valonen PK, Grohn OH, Kettunen MI, Ylä-Herttuala S, *et al.* Assignment of  $^1\text{H}$  nuclear magnetic resonance visible polyunsaturated fatty acids in BT4C gliomas undergoing ganciclovir-thymidine kinase gene therapy-induced programmed cell death. *Cancer Res.* 2003 Jun 15;63(12):3195-201.
22. Hakumäki JM, Kauppinen RA.  $^1\text{H}$  NMR visible lipids in the life and death of cells. *Trends Biochem Sci.* 2000 Aug;25(8):357-62.
23. Castillo M, Smith JK, Kwock L. Correlation of myo-inositol levels and grading of cerebral astrocytomas. *AJNR Am J Neuroradiol.* 2000 Oct;21(9):1645-9.
24. Bruhn H, Frahm J, Gyngell ML, Merboldt KD, Hanicke W, Sauter R, *et al.* Noninvasive differentiation of tumors with use of localized  $^1\text{H}$  MR spectroscopy *in vivo*: initial experience in patients with cerebral tumors. *Radiology.* 1989 Aug;172(2):541-8.
25. Wilken B, Dechent P, Herms J, Maxton C, Markakis E, Hanefeld F, *et al.* Quantitative proton magnetic resonance spectroscopy of focal brain lesions. *Pediatr Neurol.* 2000 Jul;23(1):22-31.
26. Shimizu H, Kumabe T, Tominaga T, Kayama T, Hara K, Ono Y, *et al.* Noninvasive evaluation of malignancy of brain tumors with proton MR spectroscopy. *AJNR Am J Neuroradiol.* 1996 Apr;17(4):737-47.

27. Gill SS, Thomas DG, Van Bruggen N, Gadian DG, Peden CJ, Bell JD, *et al.* Proton MR spectroscopy of intracranial tumours: *in vivo* and *in vitro* studies. *J Comput Assist Tomogr.* 1990 Jul-Aug;14(4):497-504.
28. Negendank W. Studies of human tumors by MRS: a review. *NMR Biomed.* 1992 Sep-Oct;5(5):303-24.
29. Williams SR, Gadian DG. Tissue metabolism studied *in vivo* by nuclear magnetic resonance. *Q J Exp Physiol.* 1986 Jul;71(3):335-60.
30. Kondziolka D, Lunsford L, Martinez A. Unreliability of contemporary neurodiagnostic imaging in evaluating suspected adult supratentorial (low-grade) astrocytoma. *J Neurosurg.* 1993;Oct; 79(4):533- 6.
31. Howe FA, Opstad KS. <sup>1</sup>H MR spectroscopy of brain tumours and masses. *NMR Biomed.* 2003 May;16(3):123-31.
32. Castillo M, Kwock L. Clinical applications of proton magnetic resonance spectroscopy in the evaluation of common intracranial tumors. *Top Magn Reson Imaging.* 1999 Apr;10(2):104-13.
33. Jackson EF. *In vivo* magnetic resonance spectroscopy in humans: a brief review. *Am J Physiol Imaging.* 1992 Jul-Dec;7(3-4):146-54.

34. Sapunar F, Smith IE. Neoadjuvant chemotherapy for breast cancer. *Ann Med.* 2000 Feb;32(1):43-50.
35. Astrakas LG, Zurakowski D, Tzika AA, Zarifi MK, Anthony DC, De Girolami U, *et al.* Noninvasive magnetic resonance spectroscopic imaging biomarkers to predict the clinical grade of pediatric brain tumors. *Clin Cancer Res.* 2004 Dec 15;10(24):8220-8.
36. Nelson SJ, Cha S. Imaging glioblastoma multiforme. *Cancer J.* 2003 Mar-Apr;9(2):134-45.
37. Mountford CE, Wright LC, Holmes KT, Mackinnon WB, Gregory P, Fox RM. High-resolution proton nuclear magnetic resonance analysis of metastatic cancer cells. *Science.* 1984 Dec 21;226(4681):1415-8.
38. Veale MF, Roberts NJ, King GF, King NJC. The Generation of  $^1\text{H}$ -NMR-Detectable Mobile Lipid in Stimulated Lymphocytes: Relationship to Cellular Activation, the Cell Cycle, and Phosphatidylcholine-Specific Phospholipase C. *Biochemical and Biophysical Research Communications.* 1997;239(3):868-74.
39. Mackinnon WB, Dyne M, Holmes KT, Mountford CE, Gupta RS. Further evidence that the narrow  $^1\text{H}$  magnetic resonance signals from malignant cells do not arise from intracellular lipid droplets. *NMR Biomed.* 1989 Nov;2(4):161-4.

40. Mountford CE, Grossman G, Reid G, Fox RM. Characterization of transformed cells and tumors by proton nuclear magnetic resonance spectroscopy. *Cancer Res.* 1982 Jun;42(6):2270-6.
41. Hakumaki JM, Poptani H, Puumalainen AM, Loimas S, Paljarvi LA, Yla-Herttuala S, *et al.* Quantitative  $^1\text{H}$  nuclear magnetic resonance diffusion spectroscopy of BT4C rat glioma during thymidine kinase-mediated gene therapy *in vivo*: identification of apoptotic response. *Cancer Res.* 1998 Sep 1;58(17):3791-9.
42. Remy C, Fouilhe N, Barba I, Sam-Lai E, Lahrech H, Cucurella MG, *et al.* Evidence that mobile lipids detected in rat brain glioma by  $^1\text{H}$  nuclear magnetic resonance correspond to lipid droplets. *Cancer Res.* 1997 Feb 1;57(3):407-14.
43. Barba I, Cabanas ME, Arus C. The relationship between nuclear magnetic resonance-visible lipids, lipid droplets, and cell proliferation in cultured C6 cells. *Cancer Res.* 1999 Apr 15;59(8):1861-8.
44. Di Vito M, Lenti L, Knijn A, Iorio E, D'Agostino F, Molinari A, *et al.*  $^1\text{H}$  NMR-visible mobile lipid domains correlate with cytoplasmic lipid bodies in apoptotic T-lymphoblastoid cells. *Biochimica et Biophysica Acta (BBA) - Molecular and Cell Biology of Lipids.* 2001;1530(1):47-66.
45. Ferretti A, Knijn A, Iorio E, Pulciani S, Giambenedetti M, Molinari A, *et al.* Biophysical and structural characterization of  $^1\text{H}$ -NMR-detectable mobile lipid

- domains in NIH-3T3 fibroblasts. *Biochim Biophys Acta*. 1999 Jun 10;1438(3):329-48.
46. Zoula S, Herigault G, Ziegler A, Farion R, Decorps M, Remy C. Correlation between the occurrence of  $^1\text{H}$ -MRS lipid signal, necrosis and lipid droplets during C6 rat glioma development. *NMR Biomed*. 2003 Jun;16(4):199-212.
47. Delikatny EJ, Cooper WA, Brammah S, Sathasivam N, Rideout DC. Nuclear magnetic resonance-visible lipids induced by cationic lipophilic chemotherapeutic agents are accompanied by increased lipid droplet formation and damaged mitochondria. *Cancer Res*. 2002 Mar 1;62(5):1394-400.
48. Milkevitch M, Shim H, Pilatus U, Pickup S, Wehrle JP, Samid D, *et al*. Increases in NMR-visible lipid and glycerophosphocholine during phenylbutyrate-induced apoptosis in human prostate cancer cells. *Biochim Biophys Acta*. 2005 May 1;1734(1):1-12.
49. Callies R, Sri-Pathmanathan RM, Ferguson DY, Brindle KM. The appearance of neutral lipid signals in the  $^1\text{H}$  NMR spectra of a myeloma cell line correlates with the induced formation of cytoplasmic lipid droplets. *Magn Reson Med*. 1993 Apr;29(4):546-50.
50. Hakumaki JM, Poptani H, Sandmair AM, Yla-Herttuala S, Kauppinen RA.  $^1\text{H}$  MRS detects polyunsaturated fatty acid accumulation during gene therapy of

- glioma: implications for the *in vivo* detection of apoptosis. *Nat Med.* 1999 Nov;5(11):1323-7.
51. Mountford CE, Grossman G, Gatenby PA, Fox RM. High-resolution proton nuclear magnetic resonance: application to the study of leukaemic lymphocytes. *Br J Cancer.* 1980 Jun;41(6):1000-3.
  52. May GL, Wright LC, Holmes KT, Williams PG, Smith IC, Wright PE, *et al.* Assignment of methylene proton resonances in NMR spectra of embryonic and transformed cells to plasma membrane triglyceride. *J Biol Chem.* 1986 Mar 5;261(7):3048-53.
  53. Williams PG, Helmer MA, Wright LC, Dyne M, Fox RM, Holmes KT, *et al.* Lipid domain in cancer cell plasma membrane shown by  $^1\text{H}$  NMR to be similar to a lipoprotein. *FEBS Lett.* 1985 Nov 11;192(1):159-64.
  54. Blankenberg FG, Storrs RW, Naumovski L, Goralski T, Spielman D. Detection of apoptotic cell death by proton nuclear magnetic resonance spectroscopy. *Blood.* 1996 Mar 1;87(5):1951-6.
  55. Blankenberg FG, Katsikis PD, Storrs RW, Beaulieu C, Spielman D, Chen JY, *et al.* Quantitative analysis of apoptotic cell death using proton nuclear magnetic resonance spectroscopy. *Blood.* 1997 May 15;89(10):3778-86.

56. Kuesel AC, Sutherland GR, Halliday W, Smith IC.  $^1\text{H}$  MRS of high grade astrocytomas: mobile lipid accumulation in necrotic tissue. *NMR Biomed.* 1994 May;7(3):149-55.
57. Jagannathan NR, Kumar M, Seenu V, Coshic O, Dwivedi SN, Julka PK, *et al.* Evaluation of total choline from *in-vivo* volume localized proton MR spectroscopy and its response to neoadjuvant chemotherapy in locally advanced breast cancer. *Br J Cancer.* 2001 Apr 20;84(8):1016-22.
58. Meisamy S, Bolan PJ, Baker EH, Bliss RL, Gulbahce E, Everson LI, *et al.* Neoadjuvant chemotherapy of locally advanced breast cancer: predicting response with *in vivo*  $^1\text{H}$  MR spectroscopy- a pilot study at 4 T. *Radiology.* 2004 Nov;233(2):424-31.
59. Mori N, Glunde K, Takagi T, Raman V, Bhujwala ZM. Choline Kinase Down-regulation Increases the Effect of 5-Fluorouracil in Breast Cancer Cells. *Cancer Res.* 2007 December 1;67(23):11284-90.
60. Madhu B, Waterton JC, Griffiths JR, Ryan AJ, Robinson SP. The response of RIF-1 fibrosarcomas to the vascular-disrupting agent ZD6126 assessed by *in vivo* and *ex vivo*  $^1\text{H}$  magnetic resonance spectroscopy. *Neoplasia.* 2006 Jul;8(7):560-7.
61. Lehtimaki KK, Valonen PK, Griffin JL, Vaisanen TH, Grohn OH, Kettunen MI, *et al.* Metabolite changes in BT4C rat gliomas undergoing ganciclovir-thymidine

- kinase gene therapy-induced programmed cell death as studied by  $^1\text{H}$  NMR spectroscopy *in vivo*, *ex vivo*, and *in vitro*. *J Biol Chem*. 2003 Nov 14;278(46):45915-23.
62. Valonen PK, Griffin JL, Lehtimäki KK, Liimatainen T, Nicholson JK, Grohn OH, *et al*. High-resolution magic-angle-spinning  $^1\text{H}$  NMR spectroscopy reveals different responses in choline-containing metabolites upon gene therapy-induced programmed cell death in rat brain glioma. *NMR Biomed*. 2005 Jun;18(4):252-9.
63. Podo F. Tumour phospholipid metabolism. *NMR Biomed*. 1999 Nov;12(7):413-39.
64. Brindle KM. Detection of apoptosis in tumors using magnetic resonance imaging and spectroscopy. *Adv Enzyme Regul*. 2002;42:101-12.
65. Williams SN, Anthony ML, Brindle KM. Induction of apoptosis in two mammalian cell lines results in increased levels of fructose-1,6-bisphosphate and CDP-choline as determined by  $^{31}\text{P}$  MRS. *Magn Reson Med*. 1998 Sep;40(3):411-20.
66. Podo F, Carpinelli G, Di Vito M, Giannini M, Proietti E, Fiers W, *et al*. Nuclear magnetic resonance analysis of tumor necrosis factor-induced alterations of phospholipid metabolites and pH in Friend leukemia cell tumors and fibrosarcomas in mice. *Cancer Res*. 1987 Dec 15;47(24 Pt 1):6481-9.

67. Ronen SM, DiStefano F, McCoy CL, Robertson D, Smith TA, Al-Saffar NM, *et al.* Magnetic resonance detects metabolic changes associated with chemotherapy-induced apoptosis. *Br J Cancer*. 1999 Jun;80(7):1035-41.
68. Chung YL, Troy H, Kristeleit R, Aherne W, Jackson LE, Atadja P, *et al.* Noninvasive magnetic resonance spectroscopic pharmacodynamic markers of a novel histone deacetylase inhibitor, LAQ824, in human colon carcinoma cells and xenografts. *Neoplasia*. 2008 Apr;10(4):303-13.
69. Lutz NW, Tome ME, Cozzone PJ. Early changes in glucose and phospholipid metabolism following apoptosis induction by IFN-gamma/TNF-alpha in HT-29 cells. *FEBS Lett*. 2003 Jun 5;544(1-3):123-8.
70. Aboagye EO, Bhujwala ZM, Shungu DC, Glickson JD. Detection of Tumor Response to Chemotherapy by <sup>1</sup>H Nuclear Magnetic Resonance Spectroscopy: Effect of 5-Fluorouracil on Lactate Levels in Radiation-induced Fibrosarcoma 1 Tumors. *Cancer Res*. 1998 March 1, 1998;58(5):1063-7.
71. Poptani H, Bansal N, Graham RA, Mancuso A, Nelson DS, Glickson JD. Detecting early response to cyclophosphamide treatment of RIF-1 tumors using selective multiple quantum spectroscopy (SelMQC) and dynamic contrast enhanced imaging. *NMR Biomed*. 2003 Apr;16(2):102-11.

72. Wahl RL, Zasadny K, Helvie M, Hutchins GD, Weber B, Cody R. Metabolic monitoring of breast cancer chemohormonotherapy using positron emission tomography: initial evaluation. *J Clin Oncol*. 1993 Nov;11(11):2101-11.
73. Harris LM, Davies NP, Macpherson L, Lateef S, Natarajan K, Brundler MA, *et al*. Magnetic resonance spectroscopy in the assessment of pilocytic astrocytomas. *Eur J Cancer*. 2008 Nov;44(17):2640-7.
74. Opstad KS, Bell BA, Griffiths JR, Howe FA. Taurine: a potential marker of apoptosis in gliomas. *Br J Cancer*. 2009;100(5):789-94.
75. Hickman JA. Apoptosis induced by anticancer drugs. *Cancer Metastasis Rev*. 1992 Sep;11(2):121-39.
76. Thompson CB. Apoptosis in the pathogenesis and treatment of disease. *Science*. 1995 Mar 10;267(5203):1456-62.
77. Hakumaki JM, Brindle KM. Techniques: Visualizing apoptosis using nuclear magnetic resonance. *Trends Pharmacol Sci*. 2003 Mar;24(3):146-9.
78. Delikatny EJ, Jeitner TM. The accumulation of <sup>1</sup>H MR-visible lipid in human glioma cells is independent of the cell cell cycle. *Internatonal Journal of Oncology*. 1997;11:543-50.

79. Hirakawa T, Maruyama K, Kohl NE, Kodama T, Ruley HE. Massive accumulation of neutral lipids in cells conditionally transformed by an activated H-ras oncogene. *Oncogene*. 1991 Feb;6(2):289-95.
80. Bogin L, Papa MZ, Polak-Charcon S, Degani H. TNF-induced modulations of phospholipid metabolism in human breast cancer cells. *Biochim Biophys Acta*. 1998 Jun 15;1392(2-3):217-32.
81. Wyllie AH, Kerr JF, Currie AR. Cell death: the significance of apoptosis. *Int Rev Cytol*. 1980;68:251-306.
82. Okada H, Mak TW. Pathways of apoptotic and non-apoptotic death in tumour cells. *Nat Rev Cancer*. 2004 Aug;4(8):592-603.
83. de Bruin EC, Medema JP. Apoptosis and non-apoptotic deaths in cancer development and treatment response. *Cancer Treat Rev*. 2008 Dec;34(8):737-49.
84. Kerr JF, Winterford CM, Harmon BV. Apoptosis. Its significance in cancer and cancer therapy. *Cancer*. 1994 Apr 15;73(8):2013-26.
85. Nelson DA, White E. Exploiting different ways to die. *Genes & Development*. 2004 June 1;18(11):1223-6.

86. Danial NN, Korsmeyer SJ. Cell death: critical control points. *Cell*. 2004 Jan 23;116(2):205-19.
87. Proskuryakov SY, Konoplyannikov AG, Gabai VL. Necrosis: a specific form of programmed cell death? *Exp Cell Res*. 2003 Feb 1;283(1):1-16.
88. Kerr JF, Wyllie AH, Currie AR. Apoptosis: a basic biological phenomenon with wide-ranging implications in tissue kinetics. *Br J Cancer*. 1972 Aug;26(4):239-57.
89. Majno G, Joris I. Apoptosis, oncosis, and necrosis. An overview of cell death. *Am J Pathol*. 1995 Jan;146(1):3-15.
90. Kerr JF. Shrinkage necrosis: a distinct mode of cellular death. *J Pathol*. 1971 Sep;105(1):13-20.
91. Mizushima N. Autophagy: process and function. *Genes Dev*. 2007 Nov 15;21(22):2861-73.
92. Mizushima N. The pleiotropic role of autophagy: from protein metabolism to bactericide. *Cell Death Differ*. 2005 Nov;12 Suppl 2:1535-41.
93. Levine B. Cell biology: autophagy and cancer. *Nature*. 2007 Apr 12;446(7137):745-7.

94. Lodish H, Berk A, Matsudaira P, Kaiser C, Krieger M, Scott M, *et al.* Molecular cell biology 5<sup>th</sup> ed. New York: W.H. Freeman; 2004.
95. Kubista M, Akerman B, Norden B. Characterization of interaction between DNA and 4',6-diamidino-2-phenylindole by optical spectroscopy. *Biochemistry*. 1987 Jul 14;26(14):4545-53.
96. McGahon AJ, Martin SJ, Bissonnette RP, Mahboubi A, Shi Y, Mogil RJ, *et al.* The end of the (cell) line: methods for the study of apoptosis *in vitro*. *Methods Cell Biol*. 1995;46:153-85.
97. Apoptosis, cell death and cell proliferation manual., Roche Applied Sciences., [www.roche-applied-science.com](http://www.roche-applied-science.com).
98. Connor J, Pak CH, Zwaal RF, Schroit AJ. Bidirectional transbilayer movement of phospholipid analogs in human red blood cells. Evidence for an ATP-dependent and protein-mediated process. *J Biol Chem*. 1992 Sep 25;267(27):19412-7.
99. Bretscher MS. Asymmetrical lipid bilayer structure for biological membranes. *Nat New Biol*. 1972 Mar 1;236(61):11-2.
100. van Engeland M, Nieland LJ, Ramaekers FC, Schutte B, Reutelingsperger CP. Annexin V-affinity assay: a review on an apoptosis detection system based on phosphatidylserine exposure. *Cytometry*. 1998 Jan 1;31(1):1-9.

101. Andree HA, Reutelingsperger CP, Hauptmann R, Hemker HC, Hermens WT, Willems GM. Binding of vascular anticoagulant alpha (VAC alpha) to planar phospholipid bilayers. *J Biol Chem*. 1990 Mar 25;265(9):4923-8.
102. Koopman G, Reutelingsperger CP, Kuijten GA, Keehnen RM, Pals ST, van Oers MH. Annexin V for flow cytometric detection of phosphatidylserine expression on B cells undergoing apoptosis. *Blood*. 1994 Sep 1;84(5):1415-20.
103. Gonzalez VM, Fuertes MA, Alonso C, Perez JM. Is cisplatin-induced cell death always produced by apoptosis? *Mol Pharmacol*. 2001 Apr;59(4):657-63.
104. Barry MA, Behnke CA, Eastman A. Activation of programmed cell death (apoptosis) by cisplatin, other anticancer drugs, toxins and hyperthermia. *Biochem Pharmacol*. 1990 Nov 15;40(10):2353-62.
105. Qin LF, Ng IO. Induction of apoptosis by cisplatin and its effect on cell cycle-related proteins and cell cycle changes in hepatoma cells. *Cancer Lett*. 2002 Jan 10;175(1):27-38.
106. Mares V, Giordano PA, Mazzini G, Lisa V, Pellicciari C, Scherini E, *et al*. Influence of cis-dichlorodiamineplatinum on glioma cell morphology and cell cycle kinetics in tissue culture. *Histochem J*. 1987 Apr;19(4):187-94.

107. Andrews PA, Howell SB. Cellular pharmacology of cisplatin: perspectives on mechanisms of acquired resistance. *Cancer Cells*. 1990 Feb;2(2):35-43.
108. Perez RP. Cellular and molecular determinants of cisplatin resistance. *Eur J Cancer*. 1998 Sep;34(10):1535-42.
109. Reynolds G, Wilson M, Peet A, Arvanitis TN. An algorithm for the automated quantitation of metabolites in *in vitro* NMR signals. *Magn Reson Med*. 2006 Dec;56(6):1211-9.
110. Opstad KS, Bell BA, Griffiths JR, Howe FA. An investigation of human brain tumour lipids by high-resolution magic angle spinning  $^1\text{H}$  MRS and histological analysis. *NMR Biomed*. 2008 Aug;21(7):677-85.
111. Tree Star Inc., [www.flowjo.com](http://www.flowjo.com).
112. Fowler SD, Greenspan P. Application of Nile red, a fluorescent hydrophobic probe, for the detection of neutral lipid deposits in tissue sections: comparison with oil red O. *J Histochem Cytochem*. 1985 Aug;33(8):833-6.
113. Greenspan P, Mayer EP, Fowler SD. Nile red: a selective fluorescent stain for intracellular lipid droplets. *J Cell Biol*. 1985 Mar;100(3):965-73.
114. Mathworks Inc., [www.mathworks.com](http://www.mathworks.com).

115. Peet AC, Arvanitis TN, Auer DP, Davies NP, Hargrave D, Howe FA, *et al.* The value of magnetic resonance spectroscopy in tumour imaging. *Arch Dis Child.* 2008 Sep;93(9):725-7.
116. Wilson M, Davies NP, Brundler MA, McConville C, Grundy RG, Peet AC. High resolution magic angle spinning  $^1\text{H}$  NMR of childhood brain and nervous system tumours. *Mol Cancer.* 2009;8:6.
117. Poptani H, Puumalainen AM, Grohn OH, Loimas S, Kainulainen R, Yla-Herttuala S, *et al.* Monitoring thymidine kinase and ganciclovir-induced changes in rat malignant glioma *in vivo* by nuclear magnetic resonance imaging. *Cancer Gene Ther.* 1998 Mar-Apr;5(2):101-9.
118. Sharma U, Jagannathan NR. Biochemical characterization of breast tumors by *in vivo* and *in vitro* magnetic resonance spectroscopy (MRS). *Biophys Rev.* 2009;1:21-6.
119. Newton HB, Page MA, Junck L, Greenberg HS. Intra-arterial cisplatin for the treatment of malignant gliomas. *J Neurooncol.* 1989 May;7(1):39-45.
120. Nelson DL, Cox MM. *Lehninger principles of biochemistry* 4th ed. New York: W.H. Freeman; 2005.

121. Warburg O. On the origin of cancer cells. *Science*. 1956 Feb 24;123(3191):309-14.
122. Pfeiffer T, Schuster S, Bonhoeffer S. Cooperation and competition in the evolution of ATP-producing pathways. *Science*. 2001 Apr 20;292(5516):504-7.
123. Dang CV, Semenza GL. Oncogenic alterations of metabolism. *Trends Biochem Sci*. 1999 Feb;24(2):68-72.
124. Gatenby RA, Gillies RJ. Why do cancers have high aerobic glycolysis? *Nat Rev Cancer*. 2004 Nov;4(11):891-9.
125. Mazurek S, Eigenbrodt E. The tumor metabolome. *Anticancer Res*. 2003 Mar-Apr;23(2A):1149-54.
126. Bauer DE, Harris MH, Plas DR, Lum JJ, Hammerman PS, Rathmell JC, *et al*. Cytokine stimulation of aerobic glycolysis in hematopoietic cells exceeds proliferative demand. *FASEB J*. 2004 Aug;18(11):1303-5.
127. Berger NA, Sims JL, Catino DM, Berger SJ. Poly(ADP-ribose) polymerase mediates the suicide response to massive DNA damage: studies in normal and DNA-repair defective cells. *Princess Takamatsu Symp*. 1983;13:219-26.

128. Davies NP, Wilson M, Harris LM, Natarajan K, Lateef S, Macpherson L, *et al.* Identification and characterisation of childhood cerebellar tumours by *in vivo* proton MRS. *NMR Biomed.* 2008 Oct;21(8):908-18.
129. Davies NP, Wilson M, Natarajan K, Lateef S, Macpherson L, Brundler M-A, *et al.* Non-invasive detection of glycine as a biomarker of malignancy in childhood brain tumours using *in vivo*  $^1\text{H}$  MRS at 1.5 Tesla and *ex vivo* high resolution magic angle spinning NMR. *NMR in Biomedicine*. Submitted May 2009.
130. Carapella CM, Carpinelli G, Knijn A, Raus L, Caroli F, Podo F. Potential role of *in vitro*  $^1\text{H}$  magnetic resonance spectroscopy in the definition of malignancy grading of human neuroepithelial brain tumours. *Acta Neurochir Suppl.* 1997;68:127-32.
131. Carpinelli G, Carapella CM, Palombi L, Raus L, Caroli F, Podo F. Differentiation of glioblastoma multiforme from astrocytomas by *in vitro*  $^1\text{H}$  MRS analysis of human brain tumors. *Anticancer Res.* 1996 May-Jun;16(3B):1559-63.
132. Kinoshita Y, Yokota A. Absolute concentrations of metabolites in human brain tumors using *in vitro* proton magnetic resonance spectroscopy. *NMR Biomed.* 1997 Jan;10(1):2-12.
133. Roda JM, Pascual JM, Carceller F, Gonzalez-Llanos F, Perez-Higueras A, Solivera J, *et al.* Nonhistological diagnosis of human cerebral tumors by  $^1\text{H}$  magnetic

- resonance spectroscopy and amino acid analysis. *Clin Cancer Res.* 2000 Oct;6(10):3983-93.
134. Lehnhardt FG, Bock C, Rohn G, Ernestus RI, Hoehn M. Metabolic differences between primary and recurrent human brain tumors: a  $^1\text{H}$  NMR spectroscopic investigation. *NMR Biomed.* 2005 Oct;18(6):371-82.
135. Lehnhardt FG, Rohn G, Ernestus RI, Grune M, Hoehn M.  $^1\text{H}$ - and  $^{31}\text{P}$ -MR spectroscopy of primary and recurrent human brain tumors *in vitro*: malignancy-characteristic profiles of water soluble and lipophilic spectral components. *NMR Biomed.* 2001 Aug;14(5):307-17.
136. Gyngell ML, Hoehn-Berlage M, Kloiber O, Michaelis T, Ernestus RI, Horstmann D, *et al.* Localized proton NMR spectroscopy of experimental gliomas in rat brain *in vivo*. *NMR Biomed.* 1992 Nov-Dec;5(6):335-40.
137. Kovanlikaya A, Panigrahy A, Krieger MD, Gonzalez-Gomez I, Ghugre N, McComb JG, *et al.* Untreated pediatric primitive neuroectodermal tumor *in vivo*: quantitation of taurine with MR spectroscopy. *Radiology.* 2005 Sep;236(3):1020-5.
138. Friis MB, Friborg CR, Schneider L, Nielsen M-B, Lambert IH, Christensen ST, *et al.* Cell shrinkage as a signal to apoptosis in NIH 3T3 fibroblasts. *The Journal of Physiology.* 2005 September 1, 2005;567(2):427-43.

139. Moran J, Hernandez-Pech X, Merchant-Larios H, Pasantes-Morales H. Release of taurine in apoptotic cerebellar granule neurons in culture. *Pflugers Arch*. 2000 Jan;439(3):271-7.
140. Fox JC, Hay RV. Eicosapentaenoic acid inhibits cell growth and triacylglycerol secretion in McA-RH7777 rat hepatoma cultures. *Biochem J*. 1992 Aug 15;286 ( Pt 1):305-12.
141. Jackowski S. Cell cycle regulation of membrane phospholipid metabolism. *J Biol Chem*. 1996 Aug 23;271(34):20219-22.
142. Jackowski S. Coordination of membrane phospholipid synthesis with the cell cycle. *J Biol Chem*. 1994 Feb 4;269(5):3858-67.
143. Delikatny EJ, Lander CM, Jeitner TM, Hancock R, Mountford CE. Modulation of MR-visible mobile lipid levels by cell culture conditions and correlations with chemotactic response. *Int J Cancer*. 1996 Jan 17;65(2):238-45.
144. Holmes KT, Lean CL, Hunt NH, King NJ. Development of the "activated" high resolution  $^1\text{H}$  MR spectrum in murine T cells and B cells occurs in G1 phase of the cell cycle. *Magn Reson Med*. 1990 Oct;16(1):1-8.

145. Delikatny EJ, Roman SK, Hancock R, Jeitner TM, Lander CM, Rideout DC, *et al.* Tetraphenylphosphonium chloride induced MR-visible lipid accumulation in a malignant human breast cell line. *Int J Cancer*. 1996 Jul 3;67(1):72-9.
146. Le Moyec L, Tatoud R, Degeorges A, Calabresse C, Bauza G, Eugene M, *et al.* Proton nuclear magnetic resonance spectroscopy reveals cellular lipids involved in resistance to adriamycin and taxol by the K562 leukemia cell line. *Cancer Res*. 1996 Aug 1;56(15):3461-7.
147. Dingley AJ, King NJ, King GF. An NMR investigation of the changes in plasma membrane triglyceride and phospholipid precursors during the activation of T-lymphocytes. *Biochemistry*. 1992 Sep 22;31(37):9098-106.
148. Dingley AJ, Veale MF, King NJ, King GF. Two-dimensional  $^1\text{H}$  NMR studies of membrane changes during the activation of primary T lymphocytes. *Immunomethods*. 1994 Apr;4(2):127-38.
149. King NJ, Delikatny EJ, Holmes KT.  $^1\text{H}$  magnetic resonance spectroscopy of primary human and murine cells of the myeloid lineage. *Immunomethods*. 1994 Apr;4(2):188-98.
150. King NJ, Ward MH, Holmes KT. Magnetic resonance studies of murine macrophages. Proliferation is not a prerequisite for acquisition of an 'activated' high resolution spectrum. *FEBS Lett*. 1991 Aug 5;287(1-2):97-101.

151. May GL, Sztelma K, Paul ML, Sorrell TC. Proton magnetic resonance spectroscopy of polymorphonuclear leukocytes from patients with serious bacterial infections. *J Infect Dis.* 1993 Aug;168(2):386-92.
152. Mountford CE, Mackinnon WB. Proton magnetic resonance spectroscopy of lymphocytes: an historical perspective. *Immunomethods.* 1994 Apr;4(2):98-112.
153. Rutter A, Mackinnon WB, Huschtscha LI, Mountford CE. A proton magnetic resonance spectroscopy study of aging and transformed human fibroblasts. *Exp Gerontol.* 1996 Nov-Dec;31(6):669-86.
154. Veale MF, Dingley AJ, King GF, King NJ. <sup>1</sup>H-NMR visible neutral lipids in activated T lymphocytes: relationship to phosphatidylcholine cycling. *Biochim Biophys Acta.* 1996 Oct 18;1303(3):215-21.
155. Anthony ML, Zhao M, Brindle KM. Inhibition of phosphatidylcholine biosynthesis following induction of apoptosis in HL-60 cells. *J Biol Chem.* 1999 Jul 9;274(28):19686-92.
156. Quintero M, Cabañas ME, Arús C. A possible cellular explanation for the NMR-visible mobile lipid (ML) changes in cultured C6 glioma cells with growth. *Biochimica et Biophysica Acta (BBA) - Molecular and Cell Biology of Lipids.* 2007;1771(1):31-44.

157. Bai X, Cerimele F, Ushio-Fukai M, Waqas M, Campbell PM, Govindarajan B, *et al.* Honokiol, a small molecular weight natural product, inhibits angiogenesis *in vitro* and tumor growth *in vivo*. *J Biol Chem.* 2003 Sep 12;278(37):35501-7.
158. Li YZ, Li CJ, Pinto AV, Pardee AB. Release of mitochondrial cytochrome C in both apoptosis and necrosis induced by beta-lapachone in human carcinoma cells. *Mol Med.* 1999 Apr;5(4):232-9.
159. Salomon AR, Voehringer DW, Herzenberg LA, Khosla C. Understanding and exploiting the mechanistic basis for selectivity of polyketide inhibitors of F(0)F(1)-ATPase. *Proc Natl Acad Sci U S A.* 2000 Dec 19;97(26):14766-71.
160. Tagliarino C, Pink JJ, Dubyak GR, Nieminen AL, Boothman DA. Calcium is a key signaling molecule in beta-lapachone-mediated cell death. *J Biol Chem.* 2001 Jun 1;276(22):19150-9.
161. Lum JJ, DeBerardinis RJ, Thompson CB. Autophagy in metazoans: cell survival in the land of plenty. *Nat Rev Mol Cell Biol.* 2005 Jun;6(6):439-48.
162. Lahrech H, Zoula S, Farion R, Remy C, Decorps M. *In vivo* measurement of the size of lipid droplets in an intracerebral glioma in the rat. *Magn Reson Med.* 2001 Mar;45(3):409-14.

163. Rathmell JC, Vander Heiden MG, Harris MH, Frauwirth KA, Thompson CB. In the absence of extrinsic signals, nutrient utilization by lymphocytes is insufficient to maintain either cell size or viability. *Mol Cell*. 2000 Sep;6(3):683-92.
164. Johnson WJ, Warner GJ, Yancey PG, Rothblat GH. Lysosomal metabolism of lipids. *Subcell Biochem*. 1996;27:239-93.
165. Griffin JL, Kauppinen RA. A metabolomics perspective of human brain tumours. *FEBS J*. 2007 Mar;274(5):1132-9.
166. De Valck D, Vercammen D, Fiers W, Beyaert R. Differential activation of phospholipases during necrosis or apoptosis: a comparative study using tumor necrosis factor and anti-Fas antibodies. *J Cell Biochem*. 1998 Dec 1;71(3):392-9.
167. Peet AC, McConville C, Wilson M, Levine BA, Reed M, Dyer SA, et al., <sup>1</sup>H MRS identifies specific metabolite profiles associated with MYCN-amplified and non-amplified tumour subsets of neuroblastoma cell line. *NMR Biomed*. 2007 May; 20(7):692-700.

## List of Conference Abstracts

Below is the list of accepted conference abstracts that stem from data collected during the course of postgraduate study.

- Mirbahai, L., Wilson, M., Shaw, C.S., McConville, C., Malcomson, R.D.G., Kauppinen, R.A., Peet, A.C.,  $^1\text{H}$  MAS NMR spectroscopy of metabolites and lipids during cell growth arrest induced by cisplatin in cultured rat glioma, 17<sup>th</sup> Annual meeting of ISMRMB, Hawaii, April 2009.
- Mirbahai, L., Wilson, M., Shaw, C.S., McConville, C., Malcomson, R.D.G., Kauppinen, R.A., Peet, A.C., Lipid alterations detected by  $^1\text{H}$  MAS NMR spectroscopy in rat glioma cells (BT4C) during cisplatin exposure provide early biomarkers of treatment efficacy, 25<sup>th</sup> Annual meeting of ESMRMB, Valencia, Spain, October 2008.
- Mirbahai, L., Wilson, M., McConville, C., Peet, A.C., Kauppinen, R.A., Nucleotide breakdown products detected by  $^1\text{H}$  NMR in rat brain glioma cells during cell death induced by cisplatin, 17<sup>th</sup> Annual NMR symposium, University of Sheffield, March 2008.
- Mirbahai, L., Wilson, M., McConville, C., Peet, A.C., Kauppinen, R.A., Biomarkers of cell death in glioblastoma and neuroblastoma as detected by  $^1\text{H}$  NMR spectroscopy, 16<sup>th</sup> Annual NMR symposium, University of Oxford, March 2007
- Mirbahai, L., Wilson, M., McConville, C., Peet, A.C., Kauppinen, R.A., Accumulation of  $^1\text{H}$  MRS visible lipids in rat glioma cells during cell death

induced by cisplatin, 13<sup>th</sup> Annual Meeting of the British Chapter of the International Society for Magnetic Resonance in Medicine, University of Birmingham, September 2006.